Responses to Referees

The authors wish to thank both reviewers for their useful suggestions and thoughtful comments on means to improve and strengthen the paper. Below are our point-by-point responses to each of the reviewer's comments. Corresponding modifications are reflected in the manuscript and Supplementary Information (SI).

Referee #1

Reviewer's comment: *Consider subdividing and reorganizing the Introduction into further subsections, e.g. "Background," "Motivation," "Previous work," etc. to improve structural clarity.*

Authors' response: This is a good suggestion. We now add three subsection titles (i.e., 1.1. Background – Page 22048 Line 20; 1.2. State of the art of IN measurement techniques – Page 22049 Line 28; 1.3. Objectives – Page 22052 Line 27).

Reviewer's comment: *Page 22054, Line 5-13: The sentences before "In this study" should be part of the introduction, not in the Methods section.*

Authors' response: The following sentences now appear at the end of the first paragraph in the Introduction section (i.e., Page 22049 Line 2).

"In particular, yearly emission rates of soil dust are 1000 to 4000 teragrams, accounting for a major proportion of both the dust component and the total particle loading in the atmosphere (*Boucher et al*., 2013). The resulting radiative forcing directly exerted by mineral dust is estimated to range from -0.3 to +0.1 W m^{-2}. Therefore, dust slightly contributes to the direct cooling effect of aerosols. However, our understanding of the influence of the dust burden upon overall climate forcing, including its secondary effect on cloud albedo, remains highly uncertain, in part due to the absence of accurate INP representations in atmospheric models. Thus, the effective radiative forcing effect of airborne dust on current climate predictions remains unresolved."

Reviewer's comment: *Page 22055, Line 22-24: The sentence "The influence of dust washing..." seems to suggest that differences in IN propensity were measured for of washed and unwashed particles. However, it seems that in Welti et al., (2014), IC was used to confirm the presence of soluble material, but no experiments were actually performed to test for differences in IN propensity of washed and unwashed samples (rather, these tests are proposed as future work). Please verify that this sentence reflects the actual findings in the cited paper or include references that support this sentence.*

Authors' response: The reviewer is right in pointing out that *Welti et al*. (2014) 'proposed' (did not 'measure') the influence of soluble impurities from kaolinite rich minerals on ice nucleation (IN) propensity. As per the reviewer's suggestion, we have modified and updated the sentence in Page 22055 Lines 22-24.

Original: "The influence of dust washing and discharge of soluble materials on IN propensity has been previously reported (*Welti et al*., 2014)."
→
Modified: "The influence of dust washing and discharge of soluble materials on IN propensity has been previously proposed (*Welti et al*., 2014). More specifically, the authors postulated two different scenarios at different temperatures based on their observations. At temperatures below ~ -38 ºC, the washed dust component may have enhanced water condensation below water saturation, and a formed liquid layer presumably may have stabilized the subcritical ice embryo entrapped inside the liquid. The authors

proposed this capillary condensation process as a part of condensation freezing or homogeneous nucleation based on the previous observation (*Christenson*, 2013) and the theoretical framework (*Marcolli*, 2013). Above ~ -38 ºC, on the other hand, heterogeneous nucleation might have been suppressed because the liquid layer derived from the deliquescence of soluble impurities from individual particles may have diminished accessibility of water vapor to active sites (e.g., localized surface features such as cracks and edges), originally proposed by *Koehler et al*. (2010), preventing the ice embryo formation. In this study, suspended samples…"

Newly added reference:

Koehler, K. A., Kreidenweis, S. M., DeMott, P. J., Petters, M. D., Prenni, A. J., and Möhler, O.: Laboratory investigations of the impact of mineral dust aerosol on cold cloud formation, Atmos. Chem. Phys., 10, 11955–11968, doi:10.5194/acp-10-11955-2010, 2010.

Reviewer's comment: *Page 22061, Line 15-28: The explanation for why the DLS value for S_{total}/M_{total} is preferred over the TSI-OPS value needs to be clearer and more concise. It might make intuitive sense to use an SSA value that matches $n_{s,geo}$ for suspension and dry-dispersed measurements, but choosing one over the other need to be better justified. First of all, why is there such a large difference in the S_{total}/M_{total} values reported by DLS and TSI-OPS? Could there be a physical reason that suspended particles (through their interactions with and processing by water) actually have a significantly different S_{total}/M_{total} than dry particles?*

Authors' response: This difference in the S_{total}/M_{total} values is presumably due to the fact that dry-dispersed particles are typically prone to agglomeration (i.e., Sect. 3.1) with more pronounced variation compared to suspended-particles.

As discussed in Page 22061 Lines 17-20, the 'representativeness' of our S_{total}/M_{total} highly depends on the degree of agglomeration, and it could vary up to a factor of 13 based on our size distribution comparisons. Since we do not have size distribution measurements and associated S_{total}/M_{total} for each suspension measurement, DLS-SSA is used for the data evaluation for the measurements with polydispersed suspended particles throughout this study. Nevertheless, the usage of DLS-SSA is reasonable because the presence of fewer agglomerates in suspended particles has been demonstrated with hematite particles and shown in Fig. 1 of *Hiranuma et al*. (2014b). We presume such a similarity might remain true for the illite NX particles. Furthermore, the use of DLS-SSA ($= 6.54\ m^2\ g^{-1}$) is reasonable because the conversion factor ranged for size-selected particle diameters from 200 to 1000 nm (as discussed in Page 22061 Lines 3-6) is similar to DLS-SSA (also similar to AIDA-SSA; i.e., Fig. 2b). We also note that the discussion of the potential effect of agglomerates is separately given in Sect. 4.4. The text in the manuscript is slightly changed (see modified Page 22061-22062 Lines 10-3; discussed below).

Reviewer's comment: *Shouldn't the text say $0.49\ m^2\ g^{-1}$ is 13 times smaller than $6.54\ m^2\ g^{-1}$?*

Authors' response: Corrected (Page 22061 Line 18). Thank you.

Reviewer's comment: *It is unclear whether it is fair to say "$n_{s,BET}$ is especially representative of measurements with suspended samples because minimal corrections..." Yes, the resulting value is based on a relatively simple correction, but how does this make it "especially representative" of measurements if it is strongly dependent on the choice of S_{total}/M_{total}? Granted, the resulting value may indeed be representative of the measurements (though removing the "especially" qualifier would be more appropriate), but a stronger case needs to be made about the appropriate choice for S_{total}/M_{total}. Since using $n_{m,sus}$ requires an additional assumption than using $n_{m,geo}$, the latter does seem to be a better option,*

given a better explanation for the choice of S_{total}/M_{total}. Changing "where the latter..." to "so the latter..." would greatly improve the clarity.

Authors' response: Discussed above (Page 2). For clarity, the authors have modified Pages 22061-22062 Lines 10-3. This section now reads:

"...in which, $n_{m,sus}$ is the IN active mass for suspension measurements, α represents the ice activated fraction (= N_{ice}/N_{total}), which is the direct measurement of suspension experiments and some of the dry-dispersed particle methods. With an assumption of a uniform BET-SSA, the resulting $n_{s,BET}$ may be representative of measurements with suspended samples because minimal corrections (only α and θ) are involved when compared to that with dry-dispersed particles. Owing to internal surface area and surface roughness, BET-SSA may be greater than DLS-SSA (*O'Sullivan et al*., 2014).

Alternatively, we can also convert ice-nucleating mass derived from suspension measurements, $n_{m,sus}$, to $n_{s,geo}$ using DLS-SSA to provide a reasonable comparison to dry-dispersed particle measurements. However, this process requires one more step than when using $n_{s,BET}$ (with an additional assumption of constant size distribution for all suspensions) and two more steps than when using n_m. For our inter-comparison study, we used both $n_{s,BET}$ and $n_{s,geo}$. Because fewer conversion factors are involved, $n_{s,BET}$ may be best suited for suspension measurements, and $n_{s,geo}$ may be best suited for dry-dispersed particle measurements (Eqn. 3 to 4 or vice versa).

The usage of DLS-SSA for the calculation of S_{total}/M_{total} of suspension measurements appears to be reasonable, as this leads to $n_{s,geo}$ for suspension measurements nearly equivalent to $n_{s,geo}$ for dry-dispersed particles. When S_{total}/M_{total} is derived based on TSI-OPS measurements, a value of 0.49 m^2 g^{-1} is obtained, which is smaller by a factor of about thirteen compared to DLS-SSA. This difference may be mainly due to the fact that dry-dispersed particles are typically prone to agglomeration (discussed below, i.e., Sect. 3.1) compared to the measurements with suspended particles. The presence of fewer agglomerates in suspended particles is shown in Fig. 1 of *Hiranuma et al*. (2014b). Since the size distribution of a suspended sample for each experiment was not measured, DLS-SSA was used for the data evaluation for suspension measurements throughout this study."

In addition, we removed "especially" according to the reviewer's suggestion.

Reviewer's comment: *Page 22064, Line 4-15: Could there be aspects of the measurement techniques themselves (or differences in calibrations, corrections, etc.) that could contribute to the differences seen in the SA distributions in Figure 2? How might differences in optical, aerodynamic, and mobility sizing techniques contribute to the differences observed?*

Authors' response: Yes, the different types of dispersion methods, impactors and size segregating instruments used in the present work can contribute to the different degree of agglomeration and the differences in surface area distributions as discussed in Sect. 4.4 (Page 22084 Lines 1-3). See also the Supplement Table S1 for further details. However, we cannot quantitatively compare the effect of measurement techniques themselves on the observed differences in particle size distribution (though all particle sizing instruments have been calibrated well). This is beyond the scope of the current work. Hence, a continued investigation to obtain further insights into consistencies or discrepancies of particle dispersion and size distribution characterization as well as IN measurement techniques, perhaps by assembling and comparing them using identical test dust samples over similar thermodynamic conditions as demonstrated in ICIS-2007, is important (i.e., Page 22092 Lines 5-13).

It should also be noted that all size distribution measurements with dry particles are converted and evaluated in volume equivalent diameter (as inferred in Page 22056 Line 16, Page 22057 Lines1, 13 and 23), and the consistency between DLS-based hydrodynamic diameter and AIDA-based volume equivalent

diameter has been demonstrated in our previous study with hematite particles (Fig. 1 from *Hiranuma et al*., 2014b).

Reviewer's comment: *These (and perhaps other) possibilities should also be mentioned here as potential explanations for the observed differences in addition to possible agglomeration. A more detailed discussion should then appear in Section 4.*

Authors' response: We agreed and modified Page 22064 Lines 4-15. Now this part reads, "The surface area distribution of the DLS hydrodynamic diameter-based measurement (Fig. 2a) agreed well with *in situ* measurements from the AIDA chamber (Fig. 2b), suggesting the size distributions of dry illite NX particles during AIDA experiments were similar to those of suspension measurements. This observation is consistent with results presented in *Hiranuma et al*. (2014b). Briefly, the authors found agreement between the DLS-based hydrodynamic diameter and the AIDA-derived volume equivalent diameter of hematite particles. As opposed to the AIDA observation, the wider distributions and the shift in the mode diameters in the MRI-DCECC measurements towards a larger size (0.62 μm, Fig. 2c) when compared to Fig. 2a and b may indicate a higher degree of particle agglomeration as a result of different degrees of pulverization during the particle generation processes or particle coagulation at the high aerosol number concentration used for these measurements. A more pronounced agglomeration effect was observed by the TSI-OPS measurements (Fig. 2d), such that a surface area distribution of supermicron-sized particles was obtained. Thus, different types of dry particle dispersion methods can contribute to varying degrees of agglomeration and the observed differences in surface area distributions. Though all size segregating instruments used in the present study are well calibrated, we cannot rule out the effect of measurement techniques themselves on the observed differences in particle size distribution. In Sect. 4.4 we discuss whether agglomeration has an effect on the IN activity.".

Reviewer's comment: *Page 22068, Line 10-15: No results are discussed here for CU-RMCS. Include a brief summary here like for the other instruments.*

Authors' response: Page 22068 Lines 11-12 now reads, "The University of Colorado (CU)-RMCS examined the freezing abilities of droplets containing 1.0 wt% illite NX. CU-RMCS detected the warmest immersion freezing of illite NX particles at about -23 °C under the experimental conditions used in the present work (see the Supplementary Methods for further details).".

Reviewer's comment: *Page 22075-6, Line 25-1: Is the presence of agglomerates directly measured or just inferred from the results? If the latter is the case, it would be more appropriate for this sentence to say "...may have been carried out in the presence..."*

Authors' response: We thank the reviewer for this suggestion. Page 22075-6 Line 25-1 now reads, "We note that MRI-DCECC experiments may have been carried out in the presence of a high degree of agglomeration (Fig. 2c and d).".

Reviewer's comment: *Page 22083, Line 16-17: "agglomerated-fractions based on a relative comparison to D_{95}" implicitly assumes that differences in D_{95} are a result of agglomerations, rather than discussing the possibility of other contributing factors, such as differences in the hydrodynamic size-based, volume equivalent diameter-based, and optical size-based results.*

Authors' response: Discussed above (hydrodynamic vs. volume equivalent). The presence of larger D_{95} fraction is indicative of the presence of agglomerates.

Reviewer's comment: *Figure 10: In all other figures, $n_{s,geo}$ is the left column. Please change this figure to match the rest.*

Authors' response: No, the panel based on $n_{s,BET}$ is the left column throughout (Figs. 6, 7 and 8). The figure caption is modified.

"Figure 10. Examination of mode dependency of heterogeneous ice nucleation of illite NX particles. A comparison of FRIDGE (default) and FRIDGE (imm.mode) in $n_{s,BET}$ and $n_{s,geo}$ are shown in (a) and (b), respectively. (c) and (d) show a comparison between EDB (contact), EDB (imm.), ZINC, IMCA-ZINC, and PNNL-CIC data in $n_{s,BET}$ and $n_{s,geo}$, respectively."

Reviewer's comment: *As a general technical comment, the authors are advised to check the consistency of past and present tenses used in the manuscript. Some specific examples are included below, but the flow of the text is sometimes interrupted by unexpected tense changes. Consider using the present tense whenever possible, especially when discussing work done for this study.*

Authors' response: Thank you. Corrected.

Reviewer's comment: *Another general technical comment, there are often missing spaces before and after mathematical expressions and symbols. Many are pointed out below, but the authors are advised to verify that all such cases are fixed.*

Authors' response: All fixed.

Reviewer's comment: *Page 22047, Line 27: Consider rewording "Only instruments making measurements with wet suspended samples were able to measure..."*

Authors' response: Reworded.

Reviewer's comment: *Page 22048, Line 3: Put a space between "to" and "n_s".*

Authors' response: Corrected.

Reviewer's comment: *Page 22048, Line 9: Remove comma after "spectra"*

Authors' response: Removed.

Reviewer's comment: *Page 22048, Line 16: Remove "an"*

Authors' response: Removed.

Reviewer's comment: *Page 22048, Line 17: Remove ",thereby,"*

Authors' response: Removed.

Reviewer's comment: *Page 22049, Line 23: Replace "towards immersion freezing properties" with "for immersion freezing".*

Authors' response: Replaced.

Reviewer's comment: *Page 22050, Line 3: remove ", which".*

Authors' response: Removed.

Reviewer's comment: *Page 22050, Line 6-9: For clarity, change to "Supersaturated conditions with respect to water and ice, as a function of temperature, were created in the simulation chamber vessel by a rapid pressure drop caused by mechanical expansion and subsequent cooling."*

Authors' response: Changed.

Reviewer's comment: *Page 22052, Line 28: Change "was" to "is"*

Authors' response: Changed.

Reviewer's comment: *Page 22053, Line 6-7: The meaning of "The dataset constitutes a function of..."is unclear. Consider rewording as "This dataset captures the functional dependence of... nucleation time on illite NX immersion freezing properties" or something similar.*

Authors' response: Thank you. For clarity, the sentence now reads, "The dataset captures the functional dependence of various experimental parameter variables, such as particle concentration, particle size, droplet size, temperature, cooling rate and nucleation time, on the immersion freezing properties of illite NX particles.".

Reviewer's comment: *Page 22053, Line 16: Is the hyphen between parameterization and approach necessary?*

Authors' response: Thank you. The hyphen is now removed.

Reviewer's comment: *Page 22055, Line 2: Consider using "irregular" rather than "deformed."*

Authors' response: Corrected.

Reviewer's comment: *Page 22057, Line 12: Replace "about 2" with "~2"*

Authors' response: Replaced.

Reviewer's comment: *Page 22057, Line 21: "is" is inconstant with the tense of the rest of the paragraph.*

Authors' response: Rephrased to "was".

Reviewer's comment: *Page 22058, Line 2: "in the table" should specify the table number.*

Authors' response: Rephrased to "As seen in Table 1,…".

Reviewer's comment: *Page 22059, Line 11-14: As this sentence is currently written, it seems to say that* $n_{s,geo}$ *represents the geometrically determined surface area (instead of the IN active surface-site density based on geometric size).*

Authors' response: We modified the sentence.

Original: "We now describe a method to parameterize surface area-scaled immersion freezing activities using the size equivalent ice nucleation active surface-site density (Connolly et al., 2009; Niemand et al., 2012; Hoose and Möhler, 2012), relating it to the geometrically determined surface area, $n_{s,geo}$."

→
Modified: "We now describe a method to parameterize surface area-scaled immersion freezing activities using the size equivalent ice nucleation active surface-site density based on geometric size ($n_{s,geo}$; *Connolly et al*., 2009; *Niemand et al*., 2012; *Hoose and Möhler*, 2012)."

Reviewer's comment: *Page 22060, Line 7: Consider replacing "under water suspended conditions" with "for experiments using suspended particles."*

Authors' response: No, $n_{s,BET}$ is applicable to both dry and suspension measurements. We now modify Page 22060 Lines 6-7.

"In addition, the IN efficiency can be related to the BET-SSA to estimate BET-inferred ice nucleation surface-site density, $n_{s,BET}$."

Reviewer's comment: *Page 22060, Line 12: Replace ", therefore S_{total}" with "; therefore, S_{total}.*

Authors' response: Corrected.

Reviewer's comment: *Page 22060, Line 15-17: Since you are not actually describing a list of steps, consider changing to "...$n_{s,BET}$, the geometric size-based ice nucleating mass, $n_{m,geo}$ (g^{-1}), was first calculated..."*

Authors' response: Corrected.

Reviewer's comment: *Page 22060, Line 17: Change S_{total}-to-M_{total} to S_{total}/M_{total} here and throughout for consistency with mathematical notation for the size-selected case.*

Authors' response: This is a good suggestion. Thank you. All corrected (Page 22061 Line 2; Page 22061 Line 17).

Reviewer's comment: *Page 22061, Line 6: Changing "Lastly" to "Therefore" would provide consistency with the change on Page 22060, Line 15-17.*

Authors' response: Corrected.

Reviewer's comment: *Page 22061, Line 25: Remove comma after "technique"*

Authors' response: Corrected.

Reviewer's comment: *Page 22061, Line 27-28: Consider rewording "it is one step further when compared to $n_{s,BET}$ (with an additional assumption of constant size distribution for all suspensions) and two steps further compared to nm" as "this process requires one more step than when using $n_{s,BET}$ (with an additional assumption of constant size distribution for all suspensions) and two more steps than when using nm" for clarity.*

Authors' response: Thank you. Reworded.

Reviewer's comment: *Page 22062, Line 2-3: Either specify "$n_{s,BET}$ is more representative for suspensions than... and $n_{s,geo}$ is better for for dry-dispersed particle measurements than..." or simply say something like "$n_{s,BET}$ is suited for suspensions, and $n_{s,geo}$ is suited for dry-dispersed particle measurements."*

Authors' response: Thank you. We modified the sentence.

"Because fewer conversion factors are involved, $n_{s,BET}$ may be best suited for suspension measurements, and $n_{s,geo}$ may be best suited for dry-dispersed particle measurements (Eqn. 3 to 4 or vice versa)."

Reviewer's comment: *Page 22062, Line 20-22: Change "wt '%" to "wt %'s" or "abundances" and "was measured" to "were measured."*

Authors' response: We thank the referee for this suggestion. We reworded "wt%" and "was measured" to "abundances" and "were measured", respectively.

Reviewer's comment: *Page 22063, Line 2: Consider changing "published elsewhere" to "previously published."*

Authors' response: Corrected.

Reviewer's comment: *Page 22063, Line 17: Change "suggests" to 'suggest."*

Authors' response: Corrected.

Reviewer's comment: *Page 22063, Line 20-23: For clarity consider rewording, e.g. "Since illite NX particles have significant internal surface area, BET-derived surface areas can be expected to be larger than those derived from the laser diffraction technique. Supporting this notion, ..."*

Authors' response: Thank you for a good suggestion. We modified the sentences according to the reviewer's suggestion.

Reviewer's comment: *Page 22063, Line 28: Change "These" to "this."*

Authors' response: Corrected.

Reviewer's comment: *Page 22064, Line 12: Change "discusses" to "discuss."*

Authors' response: Corrected.

Reviewer's comment: *Page 22065, Line 4: Would be clearer as "$n_s(T)$, (m_{-2} as a function of ºC)."*

Authors' response: Corrected.

Reviewer's comment: *Page 22066, Line 14: Change "500 nm mobility diameter size" to "500 nm mobility diameter size-selected" for consistency.*

Authors' response: Corrected.

Reviewer's comment: *Page 22066, Line 23-24: Consider changing "with droplets of volume from micro-liter to pico-liter" to "using droplets with volumes in the micro-liter to pico-liter range."*

Authors' response: Corrected to "using droplets with volumes in the microliter to picoliter range".

Reviewer's comment: *Page 22067, Line 1: Replace "; with the highest temperatures attained" with ". The highest temperatures are attained."*

Authors' response: Corrected.

Reviewer's comment: *Page 22067, Line 2: Add a comma before "which."*

Authors' response: Corrected.

Reviewer's comment: *Page 22067, Line 5: "$n_s(T)$" should be written in math mode.*

Authors' response: Corrected.

Reviewer's comment: *Page 22067, Line 23: Replace "to allow" with "that allows" for consistency.*

Authors' response: Corrected.

Reviewer's comment: *Page 22068, Line 20-21: Consider rewording "within previously reported uncertainties for immersion freezing experiments" as "for immersion freezing experiments, within previously reported uncertainties" for clarity.*

Authors' response: Corrected.

Reviewer's comment: *Page 22069, Line 4-6: Consider changing to "As demonstrated in DeMott et al. (2014), higher RH_w values were required for full expression of immersion freezing in the CFDC. The use of 105 % RH_w in CSU- CFDC does not capture INP activity for many natural dusts, up to a factor of three." for clarity.*

Authors' response: Changed.

Reviewer's comment: *Page 22069, Line 14: Remove "available" for clarity.*

Authors' response: Removed.

Reviewer's comment: *Page 22070, Line 7: Remove "one"*

Authors' response: Removed.

Reviewer's comment: *Page 22071, Line 5-6: It is unclear what is meant by "and, with a slightly better agreement, a time-dependent treatment." Please provide a clearer explanation.*

Authors' response: For clarity, the authors updated the text as, " The results from both instruments agreed well with each other from a data evaluation based on n_s, and this agreement was even improved when the different residence times in LACIS and the CSU-CFDC were accounted for (i.e., when nucleation rate coefficients were compared).".

Reviewer's comment: *Page 22071, Line 12: Change "from" to "than."*

Authors' response: Changed.

Reviewer's comment: *Page 22071, Line 14-15: Why is "(i.e., MRI-DCECC)" included? Also, replace ", which is N_{ice} of" with "of N_{ice} ="*

Authors' response: Thanks for pointing out this error. We deleted (i.e., MRI-DCECC) and replaced ", which is N_{ice} of" with "of N_{ice} = "as per the reviewer's suggestion.

Reviewer's comment: *Page 22071, Line 17: Change "their" to "the."*

Authors' response: Corrected.

Reviewer's comment: *Page 22071, Line 20: Replace "therefore" with "so" or use a semicolon to separate the clauses.*

Authors' response: Now the text reads, "…particles; therefore, an OPC threshold…".

Reviewer's comment: *Page 22071-2, Line 25-1: Replace "resulting in the data from PINC being in agreement with LACIS..." with "resulting in agreement between the data from PINC and data from LACIS..." for clarity.*

Authors' response: Corrected.

Reviewer's comment: *Page 22072, Line 9: Replace the comma with a semicolon to separate independent clauses.*

Authors' response: Corrected.

Reviewer's comment: *Page 22073, Line 21: Put a space between "in" and "n_s."*

Authors' response: Corrected.

Reviewer's comment: *Page 22074, Line 6-8: Consider changing ", whereas" to ". However," and placing a comma before "which" to avoid a run-on sentence.*

Authors' response: Corrected.

Reviewer's comment: *Page 22074, Line 15: Change "its" to "the."*

Authors' response: Corrected. This sentence is now moved to Page 22068 Lines 11-12, and it now reads, "CU-RMCS detected the warmest immersion freezing of illite NX particles at about -23 °C under the experimental conditions used in the present work (see the Supplementary Methods for further details).".

Reviewer's comment: *Page 22075, Line 22: Change "well agreed" to "agreed well."*

Authors' response: Corrected.

Reviewer's comment: *Page 22075, Line 24: Is "unique" necessary here?*

Authors' response: No. Deleted.

Reviewer's comment: *Page 22076, Line 2-4: A space is required before "n_s."*

Authors' response: Corrected.

Reviewer's comment: *Page 22077, Line 21: "axs" should be "axes."*

Authors' response: Corrected.

Reviewer's comment: *Page 22077, Line 24: Again, "especially" in this context is an unnecessary qualifier?*

Authors' response: The reviewer is correct. Deleted.

Reviewer's comment: *Page 22080, Line 21: Consider removing "to control of the conditions leading to" for clarity.*

Authors' response: We agree. It is not necessary and has been removed.

Reviewer's comment: *Page 22084, Line 13: Replace "be of" with "have."*

Authors' response: Corrected.

Reviewer's comment: *Page 22085, Line 1: Replace "shows" with "show"*

Authors' response: Corrected.

Reviewer's comment: *Page 22085, Line 16: Remove "of" for consistency.*

Authors' response: Corrected.

Reviewer's comment: *Page 22086, Line 11: Commas are unnecessary.*

Authors' response: Commas are now deleted.

Reviewer's comment: *Page 22086, Line 12-14: Consider changing "...PNNL-CIC and IMCA-ZINC both of which measured condensation/immersion and purely immersion mode freezing efficiency of particles, respectively, are in reasonable..." to "...PNNL-CIC and IMCA-ZINC measured condensation/immersion and purely immersion mode freezing efficiency of particles, respectively, and are in reasonable..." for clarity.*

Authors' response: Corrected.

Reviewer's comment: *Page 22087, Line 6-7: Change "K-feldspar and" and "orthoclase which" to "K-feldspar, and" and "orthoclase, which."*

Authors' response: Corrected.

Reviewer's comment: *Page 22088, Line 26: Change "the function" to "a function."*

Authors' response: Corrected.

Reviewer's comment: *Page 22089, Line 8: Change "the function" to "a function."*

Authors' response: Corrected.

Reviewer's comment: *Page 22089, Line 15: Change "(Garimella et al., 2014)" to "Garimella et al., (2014)."*

Authors' response: Corrected.

Additional revision: In addition to addressing the reviewers' comments, other editorial corrections (major ones) were made as below.

- Page 22047-22048 Lines 23-18: This paragraph now starts with a more general statement of how the different datasets compare and then discuss the possible difference between the dry-dispersed and suspended measurements further down in the paragraph. This paragraph now reads, "In general, the seventeen immersion freezing measurement techniques deviate, within a range of about 8 ˚C in terms of temperature, by three orders of magnitude with respect to n_s. In addition, we show evidence that the immersion freezing efficiency expressed in n_s of illite NX particles is relatively independent of droplet size, particle mass in suspension, particle size and cooling rate during freezing. A strong temperature dependence and weak time- and size dependence of the immersion freezing efficiency of illite rich clay mineral particles enabled the n_s parameterization solely as a function of temperature. We also characterized the $n_s(T)$ spectra and identified a section with a steep slope between -20 and -27 ˚C, where a large fraction of active sites of our test dust may trigger immersion freezing. This slope was followed by a region with a gentler slope at temperatures below -27 ˚C. While the agreement between different instruments was reasonable below ~ -27 ˚C, there seemed to be a different trend in the temperature-dependent ice nucleation activity from the suspension and dry-dispersed particle measurements for this mineral dust, in particular at higher temperatures. For instance, the ice nucleation activity expressed in n_s was smaller for the average of the wet suspended samples and higher for the average of the dry-dispersed aerosol samples between about -27 and -18 ˚C. Only instruments making measurements with wet suspended samples were able to measure ice nucleation above -18 ˚C. A possible explanation for the deviation between -27 and -18 ˚C is discussed. Multiple exponential distribution fits in both linear and log space for both specific surface area and geometric surface area are provided. These new fits, constrained by using identical reference samples, will help to compare IN measurement methods that are not included in the present study and IN data from future IN instruments.".

- The authors have realized that the averaging/fitting procedure in the linear space in Fig. 7 would bias the fit to higher n_s values. Therefore, we have added the fit in the log space in Fig. 7 and associated fit expressions in Table 3. We also present T-binned $n_{s,\mathrm{BET}}(T)$ and $n_{s,\mathrm{geo}}(T)$ spectra averaged in the log space in Fig. S3 (see the current version of SI Lines 724-741) in a similar way to Fig. 8. As can be seen in both Fig. S3 and Fig. 8, there seems a different trend between suspension and dry-dispersed particle measurements for this mineral dust. Thus, the choice of averaging procedure does not influence our data interpretation of this deviation (i.e., n_s from dry-dispersed methods > n_s from suspension methods) in this study.

  Accordingly, we have also modified the following texts to clarify the use of linear or log space:

  Page 22048 Lines 12-15 now reads, "Multiple exponential distribution fits in both linear and log space for both specific surface area and geometric surface area are provided.".

  Pages 22077-22078 Lines 27-1 now reads, "We also report the absolute values of $\Delta\log(n_s)/\Delta T$ for four T-segregated segments based on T-binned Lin. Avg. (multiple exponential distribution fit to

the *T*-binned average data in the linear space), *T*-binned Max. (fit to the *T*-binned maxima in the linear space) and *T*-binned Min. (fit to the *T*-binned minima in the linear space) in Fig. 7 (i.e., T_1 to T_4).".

Page 22078 Lines 12-14 now reads, "In this figure, panels i, ii and iii show *T*-binned data averaged in the linear space of all seventeen instruments, all suspension type measurements, and all measurements that involved dry particles, respectively, while panel iv shows a comparison between suspension and dry-particle measurements.".

Table 3 legend now reads, "Table 3. List of the Gumbel cumulative distribution fit parameters to the $n_{s,BET}$ and $n_{s,geo}$ for *T*-binned ensemble dataset fitted in the linear space [All (lin)], ensemble dataset fitted in the log space [All (log)], ensemble maximum values (All_{max}), ensemble minimum values (All_{min}), suspension subset fitted in the linear space [Sus (lin)], suspension subset fitted in the log space [Sus (log)], dry-dispersed particle subset fitted in the linear space [Dry (lin)] and dry-dispersed particle subset fitted in the log space [Dry (log)]. Note that All_{max} and All_{min} are fitted in the linear space.".

Figure 7 caption now reads, "The multiple exponential distribution fit in the linear space (*T*-binned Lin. Avg.) is expressed as $n_{s,BET}(T) = \exp(23.82 \times \exp(-\exp(0.16 \times (T + 17.49))) + 1.39)$ or $n_{s,geo}(T) = \exp(25.75 \times \exp(-\exp(0.13 \times (T + 17.17))) + 3.34)$. The same fit in the log space (*T*-binned Log. Avg.) is expressed as $n_{s,BET}(T) = \exp(22.00 \times \exp(-\exp(0.16 \times (T + 20.07))) + 3.00)$ or $n_{s,geo}(T) = \exp(22.93 \times \exp(-\exp(0.16 \times (T + 20.31))) + 5.72)$.".

Figure 8 caption now reads, "*T*-binned $n_{s,geo}$ (a) and $n_{s,BET}$ (b). *T*-binned data (i.e., average in the linear space with 1 ˚C bins for -37 ˚C < *T* < -11 ˚C) of $n_s(T)$ spectra are presented for…".

- We replaced MΩ with MΩ cm. MΩ was the wrong unit (Page 22055 Line 25; SI Line 66 and 190).

- The first sentence in 3.2.8 (Page 22069 Line 1) now reads, "This CFDC provided data for condensation/immersion freezing at around -21.2, -25.1 and -29.7 ℃ (a total of eight data points with two, two and four points at around each temperature, respectively), which extends to a warmer region than the AIDA measurements.". All data points are now presented in Figs. 4, 5 and 6.

- PINC provided data for immersion freezing at around -25.4, -30.2 and -34.6 °C (a total of nine data points with one, four and four points at around each temperature, respectively). This distribution of data points results in the black fit curve-shape (see black dotted line named 'old interpolated data' in the figure below). To obtain a more representative fit, we grouped/averaged those four data points at the averaged T and performed the same polynomial interpolation with only three data points (at -25.4, -30.2 and -34.6 °C) for -35 °C < T < -26 °C. New interpolated data fits the data better than the previous one and gives much better trace on the $\log(n_{s,ind.})/\log(n_{s,fit})$ data as shown in the Figs. S4-S8. Accordingly, the fit parameters (i.e., expressions in Table 3) as well as data representations (Figs. 4, 5, 7 and 8) have changed but only slightly.

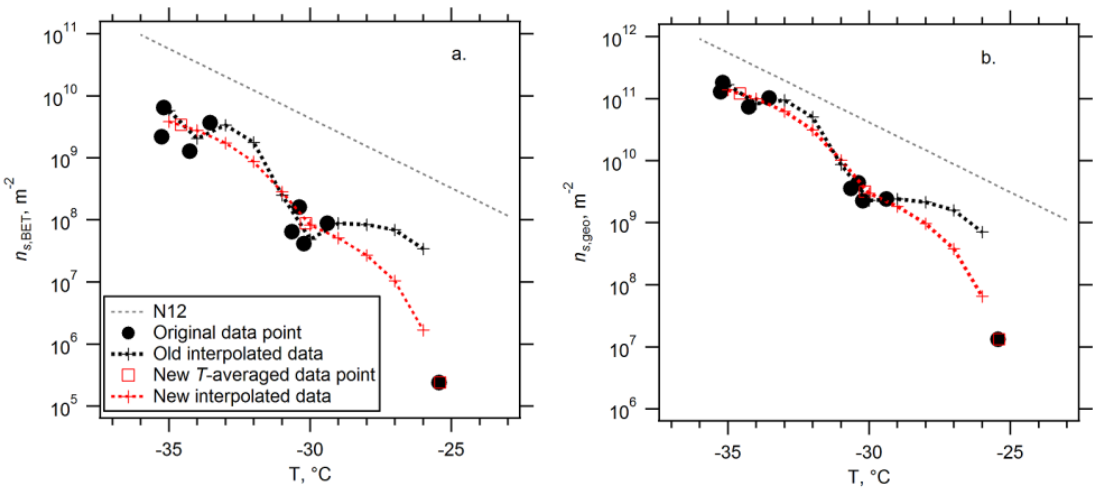

Extra Figure. *T*-binned interpolated $n_s(T)$ data (black and red cross markers) for PINC based on the BET (a) and geometric (b) surface areas. Note that the interpolation is valid for -35 ˚C < *T* < -26 ˚C with 1 ˚C bins. Literature results (N12) are also shown.

Additionally, the authors added a new sentence in Page 22071 Line 17.

"PINC provided data for immersion freezing at around -25.4, -30.2 and -34.6 °C (a total of nine data points with one, four and four points at around each temperature, respectively).".

- The authors found the recent publication showing the IN activity of supermicron particles of mineral dust (i.e., *Wheeler et al*., 2014). We added this new reference in Page 22083 Lines 18-20.

  "Since dry aggregates can have large 'supermicron' sizes, they may have different IN propensities and efficiencies (*Wheeler et al*., 2014)…"

  Since we examined the size dependency by comparing only submicron range diameters vs. bulk throughout this study, we modified Page 22066 Lines 16- for clarity.

  "The results suggest size independence of n_s within the experimental uncertainties (a combination of binomial sampling error and the uncertainty of conversion of aerodynamic particle diameter to mass) for the range of examined size (500 nm vs. bulk) and mass concentrations…"

  We also modified another sentence in Page 22073 Lines 5-7.

  Original: "Specifically, a number of instruments (AIDA, LACIS, MRI-DCECC, PINC, PNNL-CIC and IMCA-ZINC) have shown size-independent *n*s values for dry-dispersed particles."
  →
  Modified: "Specifically, AIDA and MRI-DCECC have shown size-independent n_s values for submicron dry-dispersed particles."

  New Reference: Wheeler, M. J., Mason, R. H., Steunenberg, K., Wagstaff, M., Chou, C. and Bertram, A. K.: Immersion freezing of supermicron mineral dust particles: freezing results, testing different schemes for describing ice nucleation, and ice nucleation active site densities, J. Phys. Chem. A, Article ASAP, doi: 10.1021/jp507875q, 2014.

- For clarity, we added the following sentence in Page 22086 Line 20.

  "As described in the Supplementary Methods, immersion mode experiments were performed for the droplets, which were not activated via contact freezing."

- We modified the following sentence in Page 22087 Lines 26-27.

  Original: "…acid processing of K-feldspar which deactivated kaolinite samples."
  →
  Modified: "…acid processing of K-feldspar which deactivated Fluka-kaolinite."

  We also added another sentence in Page 22087 Line 28.

  "More quantitative investigations of the acid processing of both reference and atmospherically relevant materials and its influence on their immersion mode ice nucleation efficiencies are needed."

- Figure 2 now shows the surface area distributions normalized to 'the total surface area concentration'. Accordingly, the unit on the y-axis in Fig. 2 has been changed to $dS/d\log D_p$, arb.

- During the preparation of the revised version of the manuscript, we have recognized that the concentration of Na^+ cations measured with HPLC was biased by Na^+ leaching from the sodium borosilicate glass bottle used for sample storage. Therefore we have excluded this data from the Fig. 3. The measurements of other the cations (K^+, Ca^{2+} and Mg^{2+}) were not affected since these elements are not present in the sodium borosilicate glass chemical formula.

- The polydisperse and size-selected data from the MRI-DCECC measurements in Fig. 6 are 'combined' for the overall data visibility.

- Two new sentences have been added in Acknowledgement.

  "D. Niedermeier acknowledges financial support from the Alexander von Humboldt-foundation, Germany."

  "N. Hiranuma also thanks the AIDA technical team, including R. Buschbacher, T. Chudy, O. Dombrowski, E. Kranz, G. Scheurig and S. Vogt, for their professional support for the chamber maintenance and operation."

Referee #2 (Prof. Gabor Vali)

Reviewer's comment: *This paper is the result of a large effort in organization and in execution. It represents a significant step in clarifying the power and the limitations of laboratory ice nucleation studies. It also adds considerable new information about the ice nucleating capacity of the mineral illite NX. The authors are congratulated on conceiving and carrying out this work. The main accomplishment of this investigation is to show that many different measurement methods can be used to arrive at a quantitative evaluation of the ice nucleating ability of illite NX. Using the same sample of the mineral and performing measurements with the instruments located at their home bases is a useful alternative approach to the inter-comparison workshops with co-located instruments. Discrepancies among the various measurements in this intercomparison were about the same magnitude as those found for simultaneous measurements with a dust sample in the 2007 workshop (DeMott et al. 2011). Here a larger number of instruments were involved, with a greater diversity of operating principles, so the comparable result represents a success and perhaps even some advantage. It is worth noting that the results represents a substantial improvement over the long term; the scatter was much worse in the results of the 1975 workshop (Vali, 1976).*

However, the results also demonstrate fairly serious limitations. Discrepancies of about two orders of magnitude in the derived measures of ice nucleating ability indicate that comparisons of data obtained in different experiments - past and future - will have to be compared with that sort of variability in mind. Furthermore, measurements of the abundance of INPs in the atmosphere or in other systems have to be accepted with similar possible error ranges. The approach of using a sample powder distributed to different locations has its own difficulties, principally that of ensuring sample stability. It could be expected that a mineral powder is fairly stable but that is not absolutely certain. The effects of oxidation, humidity changes, radiation, aging, vapor adsorption, etc., cannot be separated from differences that arise due to variations in measurement techniques. Tests conducted with the suspensions to diagnose changes in composition (last paragraph on page 22055) is a step in the right direction and shows the possible importance of such tests.

What do the results say about the success of this endeavor? First, the greater degree of agreement among the measurements with suspensions shows that those methods have greater control and fewer uncertainties than the tests with dry aerosols. The downside to the drop-freezing tests is that the background noise level is relatively high, restricting measurements to temperatures above -20 ºC or -25 ºC at best. Second, the scatter in the results for dry aerosol methods is due to diverse operating principles on which the measurements rely. These uncertainties are difficult to surmount. Third, the results support the notion that the frequency of nucleating sites per particle is proportional to the surface are of the particle for illite NX and similar materials.

Authors' response: The authors highly appreciate Prof. Gabor Vali for his comments above, giving a good overview and summary of our study along with previous achievements made by the ice nucleation research community. As mentioned above, there are indeed some important limitations, emerging from instrumental and analytical perspectives, which must be overcome in working towards a complete understanding of the deviation in ice-nucleating ability of examined (and future) techniques.

Here is our response to Prof. Vali's comments.

Reviewer's comment: *One could argue that the scatter of measurements are a combination of the instrumental variations and of incomplete fulfillment of the assumptions of the analysis.*

Authors' response: As mentioned in Page 22091 Lines 7-13, the individual uncertainties of each instrument cannot be greater than the discrepancy among the results from the different instruments (~8 ˚C

in terms of temperature and up to three orders of magnitude with respect to n_s), suggesting that all instruments may be reasonably precise but it is still difficult to find overall agreement between current IN measurement techniques, at least using illite NX as the standard and allowing partners to analyze it independently. For instance, it is still difficult to compare ice nucleation results because sample preparation techniques and measurement methods (e.g., particle dispersion and size distribution characterization) differ from group to group, which also can contribute to the scatter of data (i.e., n_s diversity). Hence, a continued investigation to obtain further insights into consistencies or diversity of IN measurement techniques, perhaps by assembling and comparing them using identically processed test dust samples over similar thermodynamic conditions as demonstrated in ICIS-2007, is important (i.e., Page 22092 Lines 5-13).

Reviewer's comment: *Can the authors state what they consider the proof of adequacy of the n_s analysis? The size-sorted results? Also, could they explain what is meant (22090/15) by "uniform distribution of active sites for available S_{total}"? Independence of site density from particle size? How well is that proven?*

Authors' response: *Hoose and Möhler* (2012) compiled ice nucleation efficiencies of atmospheric aerosol by evaluating aerosol-specific 'singular' freezing onsets when or after specific ambient conditions were met. Such time-independent and surface area-scaled n_s formulations, originally developed by *Connolly et al*. (2009) and *Niemand et al*. (2012) on the basis of earlier suggestions by *DeMott et al*. (1995), have been recently adapted to assess the nucleation in a wide range of atmospherically relevant *T*-RH_{ice} conditions (i.e., T > -78 °C; *Hiranuma et al*., 2014a).

In the present work, we examined two premises of the n_s analysis, namely time independence and size independence. For the former, strong temperature dependence and weak time dependence of immersion freezing using illite NX particles are presented in Sect. 4.3 of the current manuscript. For the latter, we previously demonstrated the size independence of the n_s value using two different sizes of submicron hematite particles (200 and 1000 nm volume equivalent diameter; *Hiranuma et al*., 2014a). This was based on the AIDA deposition mode nucleation experiments. We have evidence that this size independence of the n_s value remains true for submicron illite NX particles based on the AIDA and CSU-IS, in which the n_s values derived from polydisperse and quasi-monodisperse populations overlap (See Figs. 4b and 5b, Figs. 4g and 5g). We also present the magnified version of Fig. 5g below [Note temperature and n_s uncertainty for the AIDA immersion experiment is ± 0.3 ˚C and ± 35%, respectively (*Möhler et al*., 2003; *Steinke et al*., 2011)]. Additionally, a size independence of the freezing behavior for particles with different sizes was reported in *Wex et al*. (2014) and *Augustin-Bauditz et al*. (2014). Nevertheless, more experiments with size-selected particles, in particular those larger than 0.5 µm, are needed to further investigate the size dependence of n_s (*Wheeler et al*., 2014).

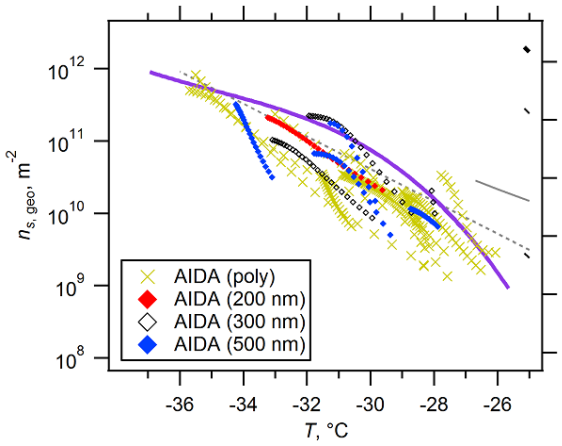

Extra Figure. Magnified section (*T* < -25 ºC and $n_s > 10^8$ m^{-2}) of Fig. 5G with three size subcategorizations. The number in brackets represents the DMA set point size in mobility diameter. This figure is not shown in the manuscript since the data used to generate this figure (i.e., *T*, n_s and DMA size setpoint) are summarized in publically accessible data base available at http://imk-aaf-s1.imk-aaf.kit.edu/inuit/ as already mentioned in Page 22059 Lines 6-9.

For clarity, we modified Page 22068 Lines 19-. The text now reads, "Ice-nucleating efficiencies of both polydisperse and quasi-monodisperse illite NX particles were investigated in this study. n_s of DMA size-selected illite NX particles (200, 300 and 500 nm mobility diameter) agreed well with that of the polydisperse population for immersion freezing experiments, within previously reported uncertainties (T ± 0.3 ˚C and n_s ± 35%; *Steinke et al*., 2011).".

We added the following sentence in Page 22068 Line 23.

Added text: "Previously, *Hiranuma et al* (2014a) demonstrated the size independence of the n_s value using two different sizes of submicron hematite particles (200 and 1000 nm volume equivalent diameter) based on AIDA deposition mode nucleation experiments. Such a similarity might remain true for the immersion mode freezing of mineral dust particles that are smaller than 1 µm diameter."

We also added the following sentences in Page 22071 Line 6.

Added text: "...were compared). Furthermore, a size independence of the immersion mode freezing was seen for Fluka-kaolinite particles with mobility diameters of 300 and 700 nm in *Wex et al*. (2014), and for illite NX particles when comparing particles with mobility diameters of 500 nm to bulk material (*Augustin-Bauditz et al*., 2014)."

In addition, Page 22053 Lines 13-15 now reads, "Results of freezing efficiencies at specific temperatures are presented using the ice nucleation active surface-site density (n_s) parameterization (e.g., *Connolly et al*., 2009; *Niemand et al*., 2012; *Hoose and Möhler*, 2012) developed on the basis of suggestions by *DeMott et al*. (1995).".

New Reference:

Augustin-Bauditz, S., Wex, H., Kanter, S., Ebert, M., Stolz, F., Prager, A., Niedermeier, D. and Stratmann, F.: The immersion mode ice nucleation behavior of mineral dusts: A comparison of different pure and surface modifed dusts, Geophys. Res. Lett., 41, doi:10.1002/2014GL061317, 2014.

DeMott, P. J.: Quantitative descriptions of ice formation mechanisms of silver iodide-type aerosols, Atmos. Res., 38, 63–99, doi:10.1016/0169-8095(94)00088-U, 1995.

Reviewer's comment: *The overview of the results in Fig. 6 is not as informative as should be. This graph is valuable in demonstrating the overall trend of the results. However, the author might consider also displaying the results in terms of the ratios of the individual measurements to the geometric mean of all the data across the temperature range covered. That type of display would provide a clearer depiction of the data for evaluating trends with respect to each measurement technique. Also, it would be useful to see results presented separately for the suspension measurements and for the dry aerosol measurements. The influence of sample size is neglected in the analysis. Weighting data points by error ranges resulting from sample sizes would have been useful.*

Authors' response: This is a good suggestion. We added new figures (Fig. S4-S8) in SI Lines 742-787. The authors would like to present these figures after introducing the *T*-binned figures (i.e., Fig. 8) because the ratios are in part calculated based on the *T*-binned interpolated data. Accordingly, we also add the following paragraph in the manuscript Page 22079 Line 2.

"In addition, *T*-binned $n_{s,BET}(T)$ and $n_{s,geo}(T)$ spectra averaged in the log space are presented in Fig. S3. Similarly, we also present *T*-binned ratios of the individual measurements to the log fit of the data [All (log), Sus (log) or Dry (log) from Table 3] across the temperature range covered for all the measurement techniques (-37 ˚C < T < -11 ˚C) in the Supplement Figs. S4-S8. These figures provide inter-comparisons of the n_s deviations across the various techniques employed in this study."

The text added in the updated version of SI Lines 742-754 reads, "Figures S4 depicts the n_s diversity in $\log(n_{s,ind.})/\log(n_{s,fit})$, which represents the ratio of the individual measurements ($n_{s,ind.}$) to the log fit line to either all data [All (log)], the suspension data [Sus (log)] or the dry-dispersed particle data [Dry (log)] as $n_{s,fit}$. The interpolated *T*-binned data (i.e., interpolated data points in Figs. 4 and 5) are used for $n_{s,ind.}$. The fit in the log space, which is derived from the parameters summarized in Table 3, is used as a denominator to avoid a bias of sudden jump of the reference value at certain temperatures where the number of available data changes. As shown in the figure, data deviation (i.e., scatter from the Avg. $\log(n_{s,ind.})/\log(n_{s,fit}) = 1$ line) can be seen in both suspension measurements and dry aerosol measurements. This deviation is observed with all the $n_{s,fit}$ cases [All (log), Sus (log) and Dry (log)]. Additionally, the scatter of individual non-*T*-binned data and the validity of interpolations are presented in Figs. S5-S8. In specific, these four figures (Figs. S5-S8) complement panels a.ii and a.iii, panels b.ii and b.iii, panels a.iv anda.v and panels b.iv and b.v. from Fig. S4, respectively, in greater detail."

As shown in these figures, data deviation (i.e., scatter from the Avg. $\log(n_{s,ind.})/\log(n_{s,fit}) = 1$ line) can be seen in both suspension measurements and dry aerosol measurements. This deviation is observed with all the $n_{s,fit}$ cases [All (log), Sus (log) and Dry (log)].

Page 22074 Lines 27-28 now reads, "Similarly, dry-dispersed particle measurements also exhibit scattered data for their measured temperature ranges.".

Page 22073 Lines 7-9 reads:

Original: "Overall, compared to suspension measurements, dry-dispersed particle measurements showed more pronounced diversity between measurements."
→
Modified: "Overall, compared to suspension measurements, dry-dispersed particle measurements showed higher n_s values."

Page 22073 Lines 14-15 deleted.

Deleted: "In-depth discussions of potential reasons for diversity specific to dry-dispersed particle measurements are given below (Sect. 4.)."

Reviewer's comment: *22059/Eq. (1) Since analysis of the data is being conducted with the time-independent singular approximation, it is somewhat misleading and needless to introduce Jimm in Eq. (1). This rate is not used in subsequent steps and there is no definition of what values of t are used for the different experimental methods. I recommend deleting the middle part of Eq. (1).*

Authors' response: The reviewer is correct in pointing out that we do not use J_{imm} in the rest of the manuscript. We simplified the equation as:

$$n_{s,\mathrm{geo}}(T) = -\ln\left(1 - \frac{N_{\mathrm{ice}}(T)}{N_{\mathrm{total}}}\right)\left(\frac{1}{S_{\mathrm{ve}}}\right), \qquad (1)$$

Reviewer's comment: *There seems to be another problem with Eq. (1) in that it is unclear whether the logarithms is taken over both bracketed terms or only the first one. Is the equation dimensionally correct?*

Authors' response: Eqn. 1 is dimensionally correct. Logarithm is taken over the first bracketed term. The units on both sides match.

Reviewer's comment: *The value of writing Eqs. (1) - (3) in terms of size bins isn't really useful for this paper, since no size-resolved data are presented and neither were the measurements performed in a size-resolved manner.*

Authors' response: Prof. Vali is correct. None of the measurement PI produced n_s as a function of size; therefore, size summation symbols ($\sum_{i=1}^{n}$) from Eqns. 1 to 3 are omitted.

Reviewer's comment: *Could the authors address what uncertainties arise due to shape assumption, conversion to BET and DLS surface area?*

Authors' response: Shape assumption: For SMPS and APS measurements, a dynamic shape factor of 1.49 (± 0.12) was accounted for and used to estimate the volume equivalent diameter as mentioned in Page 22057 Lines 1-5. As an OPC measures optical scattering intensities from the particles which are converted to actual particle sizes by the Mie theory assuming spherical particles of known refractive index, an OPC cannot accurately measure sizes of non-spherical or irregularly structured particles. This typically results in overestimations of their actual sizes compared to the optical particle sizes by a factor of about two for non-spherical particles as discussed in Page 22057 Lines 11-14. This correction was also included to estimate the volume equivalent diameter.

BET and DLS surface area: For BET surface area, our experimental uncertainty is 124.4 ± 1.5 $m^2 g^{-1}$. The manufacturer report for the reproducibility of the DLS measurement is <5% (1% for 100 nm Polystyrene). We note that, as discussed in Page 22061 Lines 17-20, the 'representativeness' of our DLS surface area highly depends on the degree of agglomeration, and it could vary up to a factor of 13 based on our size distribution comparisons (i.e., potential effect of agglomeration, Sect. 4.4). For instance, agglomeration can reduce the surface area exposed to air or available to water as well as the S_{total}/M_{total} value (mentioned in Page 22061 Lines 14-15). Since we do not have size distribution measurements and associated S_{total}/M_{total} for each suspension measurement, DLS-SSA is presumably used for the data evaluation for the measurements with polydsispersed suspended particles throughout this study. Nevertheless, the usage of DLS-SSA is reasonable since the presence of fewer agglomerates in suspended particles has been demonstrated with hematite particles as shown in Fig. 1 of *Hiranuma et al*. (2014b). We presume such a similarity might remain true for the illite NX particles. Furthermore, the use of DLS-SSA (= 6.54 $m^2 g^{-1}$) is reasonable because the conversion factor ranged for size-selected particle diameters from 200 nm to 1000 nm (as discussed in Page 22061 Lines 3-6) is similar to DLS-SSA (also similar to AIDA-SSA; i.e., Fig. 2b). We also note that the discussion of potential effect of agglomerates is separately given in Sect. 4.4.

For clarity, we modified Pages 22061-22062 Lines 10-3, and it now reads:

"...in which, $n_{m,sus}$ is the IN active mass for suspension measurements, α represents the ice activated fraction (= N_{ice}/N_{total}), which is the direct measurement of suspension experiments and some of the dry-dispersed particle methods. With an assumption of a uniform BET-SSA, the resulting $n_{s,BET}$ may be representative of measurements with suspended samples because minimal corrections (only α and θ) are involved when compared to that with dry-dispersed particles. Owing to internal surface area and surface roughness, BET-SSA may be greater than DLS-SSA (*O'Sullivan et al*., 2014).

Alternatively, we can also convert ice-nucleating mass derived from suspension measurements, $n_{m,sus}$, to $n_{s,geo}$ using DLS-SSA to provide a reasonable comparison to dry-dispersed particle measurements. However, this process requires one more step than when using $n_{s,BET}$ (with an additional assumption of constant size distribution for all suspensions) and two more steps than when using n_m. For our inter-comparison study, we used both $n_{s,BET}$ and $n_{s,geo}$. Because fewer conversion factors are involved, $n_{s,BET}$ may be best suited for suspension measurements, and $n_{s,geo}$ may be best suited for dry-dispersed particle measurements (Eqn. 3 to 4 or vice versa).

The usage of DLS-SSA for the calculation of S_{total}/M_{total} of suspension measurements appears to be reasonable, as this leads to $n_{s,geo}$ for suspension measurements nearly equivalent to $n_{s,geo}$ for dry-dispersed particles. When S_{total}/M_{total} is derived based on TSI-OPS measurements, a value of 0.49 m^2 g^{-1} is obtained, which is smaller by a factor of about thirteen compared to DLS-SSA. This difference may be mainly due to the fact that dry-dispersed particles are typically prone to agglomeration (discussed below, i.e., Sect. 3.1) compared to the measurements with suspended particles. The presence of fewer agglomerates in suspended particles is shown in Fig. 1 of *Hiranuma et al*. (2014b). Since the size distribution of a suspended sample for each experiment was not measured, DLS-SSA was used for the data evaluation for suspension measurements throughout this study."

Reviewer's comment: *22063/7-10 The authors state that the ". . . effects of impurities upon ice nucleation activity cannot be evaluated . . ." and that the impurities may be responsible for variations in ice nucleating efficiency at various temperatures. The underlying assumption here is that there is a specific temperature of activity associated with each component or impurity. If that is what the authors mean evidence need to be presented. Since that claim is made in the literature only for illite NX, the generalization here made is questionable.*

Authors' response: The authors agree that the generalization is not appropriate here. We modified the sentence in Page 22063 Lines 7-8:

Original: "Therefore, the possible effect of impurities upon the ice nucleation activity cannot be evaluated on the basis of its bulk analysis of the chemical composition."
→
Modified: "Therefore, the possible effect of these observed impurities in illite NX upon the ice nucleation activity cannot be evaluated on the basis of its bulk analysis of the chemical composition."

Reviewer's comment: *22063/13 It is unclear what special advantage illite NX has as a reference material over other minerals or other materials. The scatter in measured ice nucleating ability by different methods counters this statement.*

Authors' response: As stated in Page 22052 Line 27-, the objective of the INUIT project is to investigate the immersion freezing behavior of 'reference' particles. The INUIT group finds this commercially available illite NX is a quantitatively ideal reference of illite rich 'clay' material that can be shared among a large number of PIs. Moreover, illite NX samples contain relatively fewer impurities (e.g., quartz) when compared to other test dusts (e.g., IMt-1 illite contains 10 – 15% quartz based on manufacture report of clay mineral society; Arizona test dust contains ~17.1 % quartz as reported in Broadley et al. (2012)).

Besides illite NX, the INUIT group has comprehensively investigated the immersion freezing activities of Snomax (*Wex et al*., 2014b) and hematite (*Hiranuma et al*., 2014a and b) over the last three years. We will continue investigating the ice-nucleating ability of the other reference materials (e.g., K-feldspar) and more atmospherically relevant materials (e.g., soil dust, proteinaceous- and non-proteinaceous biological particles) in the next few years.

We now shorten and simplify the sentences for clarity:

Original: “Nonetheless, detection of non-illite mineral components implies the possibility of a wide range of ice nucleation efficiencies by the test sample at various temperatures. Hence, the illite NX sample may reflect the complexities of natural dust particles, which typically contain multiple sites with differing nucleation abilities, and can therefore be used as a reference material to mimic ice nucleation activity of physically and chemically complex natural dusts.”
→
Modified: “Nonetheless, detection of non-illite mineral components may reflect the complexities of natural dust particles, which typically contain multiple sites with differing nucleation abilities. Thus, illite rich clay mineral can be used as a reference material to mimic the ice nucleation activity of physically and chemically complex natural dusts (*Murray et al*., 2012).”

Reference:

Wex, H., Augustin-Bauditz, S., Boose, Y., Budke, C., Curtius, J., Diehl, K., Dreyer, A., Frank, F., Hartmann, S., Hiranuma, N., Jantsch, E., Kanji, Z. A., Kiselev, A., Koop, T., Möhler, O., Niedermeier, D., Nillius, B., Rösch, M., Rose, D., Schmidt, C., Steinke, I., and Stratmann, F.: Intercomparing different devices for the investigation of ice-nucleating particles using Snomax® as test substance, Atmos. Chem. Phys. Discuss., 14, 22321–22384, doi:10.5194/acpd-14-22321-2014, 2014b. (Accepted in Atmos. Chem. Phys. On Dec. 20, 2014).

Reviewer’s comment: *22066/8-10 What would it have meant if the results showed different $n_s(T)$ spectra for different mass concentrations? Dilution of samples with clean water is not normally expected to change the derived spectra. The statement here is a confirmation of that expectation not a new result.*

Authors’ response: Yes, this observation is indeed expected when the experiments work properly. Therefore such observation is an important consistency check for this type of experiment. We have added two sentences for explanation.

We modified Page 22066 Lines 8-10, and the text now reads,

“Immersion freezing efficiency of illite NX particles collapsed into a single $n_s(T)$ spectrum, i.e. IN efficiency does not depend on suspended particle mass for the concentration range studied here. This observation is a check for consistency and it implies that ice nucleation is indeed triggered by suspended illite NX particles, and neither by impurities contained in the water used for dilution nor at the glass surface supporting the droplets. If IN efficiency did depend on suspended particle mass, different $n_s(T)$ spectra would result from the various illite NX concentrations, which are shifted by the respective dilution factor.”

Reviewer’s comment: *22066/14-17 Do the values given represent a cut-off size or the center of a narrow band in sizes?*

Authors’ response: The latter is correct. The size is a narrow band of sizes centered at the mobility size selected by a DMA, as discussed in detail in the supplemental material (and as done by other PIs in this work).

Reviewer’s comment: *22067/5 Typo in $n_s(T)$*

Authors’ response: Corrected.

Reviewer’s comment: *22067 What is meant by ‘effective’ surface?*

Authors' response: The word 'effective' does not add any values in the text. For clarity, we removed "effective":

Original: "…, implying that the absence of an effective surface in contact with a substrate has a negligible effect on immersion freezing for our experimental conditions."
→
Modified: "…,implying that the surface making contact with the substrate has a negligible effect on immersion freezing for our experimental conditions."

Reviewer's comment: *22067/15 abbreviate pL and nL as in previous paragraphs*

Authors' response: Page 22068 Line 2 now reads, "~400 picoliter to 150 nanoliter".

Reviewer's comment: *22068/22 Size-independence is a significant finding and deserves more detailed description (limits if validity, degree of agreement . . .)*

Authors' response: Page 22068 Lines 19- now reads, "Ice-nucleating efficiencies of both polydisperse and quasi-monodisperse illite NX particles were investigated in this study. n_s of DMA size-selected illite NX particles (200, 300 and 500 nm mobility diameter) agreed well with that of the polydisperse population for immersion freezing experiments, within previously reported uncertainties ($T \pm 0.3$ ˚C and $n_s \pm 35\%$; *Steinke et al*., 2011).".

We now add the following sentence in Page 22068 Line 23.

Added text: "Previously, *Hiranuma et al* (2014a) demonstrated the size independence of the n_s value using two different sizes of submicron hematite particles (200 and 1000 nm volume equivalent diameter) based on AIDA deposition mode nucleation experiments. Such a similarity might remain true for the immersion mode freezing of mineral dust particles that are smaller than 1 µm diameter."

We also added the following sentences in Page 22071 Line 6.

Added text: "... were compared). Furthermore, a size independence of the immersion mode freezing was seen for Fluka-kaolinite particles with mobility diameters of 300 and 700 nm in *Wex et al*. (2014), and for illite NX particles when comparing particles with mobility diameters of 500 nm to bulk material (*Augustin-Bauditz et al*., 2014)."

Reviewer's comment: *In Fig. 4 what does "AIDA size selected" refer to?*

Authors' response: As discussed above, a DMA was used to generate quasi-monodisperse particles (200, 300 and 500 nm mobility diameter) in the AIDA study.

Reviewer's comment: *22069/21 What discrepancy is being referred to?*

Authors' response: For clarity, we replaced "the discrepancy" with "high n_s values when compared to the other measurements".

Reviewer's comment: *22073/16 The title of Section 3.3 is not a good reflection of what is actually described.*

Authors' response: We agree, and the title of the Sect. 3.3 now reads, "Inter-comparisons based on the slope parameter of $n_s(T)$ spectra".

Reviewer's comment: *22073/17 I would have found it useful to have Figure 6 ahead of the detailed presentation of the results from each instrument. Discussions refer to differences from the overall trend, etc. which are not readily perceived from Figs. 4 and 5.*

Authors' response: Considering the large number of instruments involved in this inter-comparison paper, we found (after internal discussion) that it is best to discuss the individual instrument results prior to the compiled results.

Reviewer's comment: *22073/21 Typo: inns*

Authors' response: Thank you. Corrected.

Reviewer's comment: *22073/22-27 It is unclear to me whether these statements refer to the overall trend or some group of data sets.*

Authors' response: Within this T range (i.e., -27 ˚C $\leq T \leq$ -18 ˚C), the immersion results from all suspension measurements and a majority of dry measurements coexist (see the investigated T range for each technique in Table 1). Exceptions include LACIS, EDB and IMCA-ZINC.

Accordingly, we rephrased the sentence as:

Original: "Diversity is especially pronounced (for several orders of magnitude inn_s) at -27 ˚C < T < -18 ˚C, where the results from suspension measurements and a majority of dry measurements coexist."
→
Modified: "Diversity is especially pronounced for several orders of magnitude in n_s at -27 ˚C $\leq T \leq$ -18 ˚C, where the results from suspension measurements and a majority of dry measurements coexist (see the investigated T range for each technique in Table 1)."

Reviewer's comment: *22074/5 Aren't the numerical values of the slopes negative?*

Authors' response: Prof. Vali is right. For consistency and clarity, we added the definition of the slope parameter in Page 22073 Line 24.

"…slope in the spectrum (i.e., the absolute value of $\Delta\log(n_s)/\Delta T$ in log m^{-2} ˚C^{-1}, hereafter denoted as $\Delta\log(n_s)/\Delta T$)…".

Reviewer's comment: *22074/10 Since the fraction of active sites is reflected by the absolute values of n_s, it is unclear what the authors want to express here.*

Authors' response: We have modified this part of sentence to read:

Original: "…, suggesting that a large fraction of active sites of our test dust may trigger immersion freezing at…"
→
Modified: "…,suggesting that a dominant fraction of INP contained in our test dust becomes ice active in immersion freezing at …"

Reviewer's comment: *22074/14-20 There appears to be some repetition here.*

Authors' response: The authors thank Prof. Vali for pointing out this error. We have rephrased Page 22074 Lines 13-21 as:

"Similar observations are made by most of the other suspension measurement techniques. In short, most suspension methods capture the … containing 1.0 wt% illite NX (see the Supplementary Methods)."

Reviewer's comment: *22074/27 A possibly significant point is being made here - the amount of scatter in suspension measurements versus dry aerosol measurements - but this is masked by the larger number of the latter type of data. The authors could examine this difference in a rather simple way and it would be very useful to have that analysis presented in the paper.*

Authors' response: Discussed above (i.e., Figs. S4-S8; SI Lines 742-787).

Reviewer's comment: *22076/11-14 A resounding conclusion is stated here only to be qualified in lines 14-17, with more analysis promised. This is confusing. The reference to uniform distribution is not supported by any specific result.*

Authors' response: We agree with you. We do not have evidence to support the premise that active sites are uniformly distributed. For this reason, we delete Page 22076 Lines 11-14.

Reviewer's comment: *22076/19 Grammar issue: the past tense in this sentence conflicts with the reference to the section to follow and the next sentence which uses the present tense.*

Authors' response: "was elucidated" → "is further discussed"

Reviewer's comment: *22077/2 Typo: space missing between in and* n_s.

Authors' response: Corrected.

Reviewer's comment: *22077/2 What does shifting of activation temperatures mean?*

Authors' response: Matching the n_s values by shifting *T*s horizontally rather than doing that for n_s vertically.

Page 22077 Lines 2-3 now reads:

"…whereas others may shift activation temperatures horizontally to match the n_s values from other instruments, perhaps biasing the overall accuracy and precision of instruments."

Reviewer's comment: *22077/5 So-called T-binned data presentation does hardly deserves to be used as section heading. It is a fairly standard procedure.*

Authors' response: Heading changed to "4.1 Dry vs. suspension $n_s(T)$ data".

Reviewer's comment: *22077/13 Typo: space between 'r' and 'for'*

Authors' response: Corrected.

Reviewer's comment: *22077/20 Grammar: past tene used here is out of sync with the rest of the writing*

Authors' response: Corrected.

Reviewer's comment: *22077/21 Don't the values of Hor(max − min) and Ver(max − min) depend on where those are taken? Are the values indicated in the graphs picked for particular reason? Are these the maxima within the gray bands for each value?*

Authors' response: Correct, $Hor_{Max-Min}$ and $Ver_{Max-Min}$ depend on temperature. The values shown on the Figure 7 are the "maximum" deviation we can find across all the measurements.

Fig. 7A Hor (-36.8 °C < T < -29.0 °C at n_s ~ 5.2e+09); Ver ($\log(n_{s,max}/n_{s,min})$ = 3.0 at -21 °C)
Fig. 7B Hor (-36.7 °C < T < -29.2 °C at n_s ~ 1.5e+11); Ver ($\log(n_{s,max}/n_{s,min})$ = 3.0 at -20 °C)

For clarity, we modified the Fig. 7 legend as:

"…The maximum deviation between maxima and minima in horizontal axis (in T ºC) and vertical axis [in $\log(n_{s,max}/n_{s,min})$] corresponds to $Hor_{Max-Min}$ and $Ver_{Max-Min}$, respectively."

We also modified Page 22077 Lines 20-22:

"It is observed that the largest deviation between the maxima and minima in the horizontal and vertical axes, corresponding to $Hor_{Max-Min}$ and $Ver_{Max-Min}$, respectively, shown in Fig. 7, is similar for both $n_{s,BET}$ (Fig. 7a) and $n_{s,geo}$ (Fig. 7b)."

Since $Ver_{Max-Min}$ and $Hor_{Max-Min}$ are similar for n_s BET and for n_s geo in this definition, we also modified Page 22077 Lines 22-26.

"Nevertheless, $n_{s,BET}$ is representative of measurements with suspended samples because fewer corrections are involved for its estimation when compared to that with dry-dispersed particles."

As discussed and shown above, we cannot say for certain that $n_{s,BET}$ is a better proxy for inter-comparison of the IN measurements. Therefore, Page 22091 Lines 13-15 now reads, "In addition, two different n_s metrics, $n_{s,geo}$ and $n_{s,BET}$, were compared, and we found that $n_{s,BET}$ is a better proxy for suspension-based IN measurements, while $n_{s,geo}$ is better for dry-dispersed particle measurements.".

Reviewer's comment: *22078/1-3 What is the reason for expecting the results here given?*

Authors' response: We mean the results are consistent with the results described in Sect. 3.3 (i.e., Inter-comparisons based on the slope parameter of $n_s(T)$ spectra). We modified:

Original: "As expected, the slope is comparable to A13 in the T_1 to T_3 segment (-11 to -27 ˚C), while the slope in the T_4 segment is similar to N12. The largest deviations in $Ver_{Max-Min}$, corresponding to two to three orders of magnitude of n_s, were…"
→
Modified: "The slopes are comparable to the slope of the A13 parameterization in the T_1 to T_3 segments (-11 to -27 ˚C), while the slope in the T_4 segment is similar to those of the N12 parameterizations. These results are consistent with the results described in Sect. 3.3. Further, $Ver_{Max-Min}$ for roughly three orders of magnitude with respect to n_s is …"

Reviewer's comment: *22078/3-7 The valuation of Ver(max − min) is too limited. Only the point of its highest value is commented on. It would be useful to provide more information about its numerical value across the entire temperature range. 22078/7-10 What meaning do the authors attach to Hor(max −*

min)? Clearly, the numerical value of Hor(max − min) is much larger than any temperature measurement error. Is the authors' interpretation related to variations in the activity of sites between one or other measurement method? If so, what reasons can be given for such changes? If Hor(max−min) is just a reflection of the spread along the abscissa, it does not merit the introduction of a new parameter.

Authors' response: The Ver $_{\text{Max-Min}}$ value provides the maximum deviation in $\log(n_{s,max}/n_{s,min})$, and we would like to keep it as is (discussed above). As now stated in Page 22078 Lines 3-4, $\text{Ver}_{\text{Max-Min}}$ values varied up to three orders of magnitude (or $\log(n_{s,max}/n_{s,min}) \sim 3.0$). The max Ver value was observed ~ -20 ºC (now reads, "…$\text{Ver}_{\text{Max-Min}}$ for roughly three orders of magnitude with respect to n_s is observed in a temperature region around ~ -20 ˚C for both $n_{s,BET}(T)$ and $n_{s,geo}(T)$ spectra.").

Likewise, the $\text{Hor}_{\text{Max-Min}}$ value provides the maximum deviation of the seventeen immersion freezing measurement techniques (about 8 ˚C in terms of temperature). We would also like to keep $\text{Hor}_{\text{Max-Min}}$ discussions. In the paper $\text{Hor}_{\text{Max-Min}}$ deviation is discussed, see Page 22078 lines 7-10 [now reads, "…our $\text{Hor}_{\text{Max-Min}}$ shows that the seventeen measurements are in reasonable agreement within 7.8 ˚C (-36.8 ˚C, -33.0 ˚C, -29.0 ˚C (*min, log fit, max*)) at $n_{s,BET}$ of 5.2 x 10^9 m^{-2} and 7.5 ˚C (-36.7 ˚C, -32.8 ˚C, -29.2 ˚C (*min, log fit, max*)) at $n_{s,geo}$ of 1.5 x 10^{11} m^{-2}"].

Accordingly, we also modified the following sentences in Abstract and Conclusion.

Abstract: Page 22048 Lines 1-3: "the seventeen immersion freezing measurement techniques deviate, within the range of about 8 ˚C in terms of temperature, by three orders of magnitude with respect to n_s.".

Conclusion: Page 22091 Lines 7-9: "the seventeen immersion freezing measurement techniques deviate, within a range of about 8 ˚C in terms of temperature, by three orders of magnitude with respect to n_s."

Reviewer's comment: *22078/17 Please clarify what you mean by pronounced freezing and differences. In fact, the intention behind this whole sentence is a bit vague.*

Authors' response: We modified the sentence to clarify this. We changed words: "pronounced freezing and differences" → "abrupt increase in $\Delta\log(n_s)/\Delta T$ and n_s deviations"

Reviewer's comment: *22078/19 This paragraph mixes past and present tense wording.*

Authors' response: We modified the sentence to clarify this. We changed words to, "…over a wide range is of great advantage…".

Reviewer's comment: *22078/23 The distinction drawn for experimental methods using dry aerosol inputs as 'working on a particle by particle basis' is vague. Doesn't the evaluation of suspension measurements also assume that each nucleating site is located on a different particle? The authors are hinting at a subtle point which is not explored in detail and is poorly expressed by what is said. The main difference, in my view, is that suspension methods run into background problems at cold temperatures and that dry aerosol methods lack sensitivity (sample volume) at warmer temperatures.*

Authors' response: We have changed the text according to the reviewer's suggestion.

Original: "In turn, dry-dispersed particle measurements were advantageous for their capacity to work on a particle by particle basis and can readily explore particle size dependencies. Further, these measurements…"
→

Modified: "suspension experiments with small picoliter or nanoliter droplets allow measurements right down to the homogeneous freezing limit (~ -37 ºC; *Koop et al*., 2000). In turn, suspension methods with microliter droplets may run into 'background problems' at temperatures below about -20 °C to -25 °C for samples that do not contain many IN active at these temperatures, because then impurities contained in the water may trigger freezing. Conversely, dry aerosol methods lack sensitivity for detecting rare IN at high temperatures because of their low sample volume. These dry particle measurements are in general good…"

We also add the text regarding background freezing in FRIDGE (SI Lines 304-307):

"Background freezing induced by impurities in the water was observed at T < -23 °C. This background freezing contributed to less than 15 % of the overall freezing in the range of -25 °C < T < -23 °C and was accounted for the n_s estimation."

Reviewer's comment: *22078/29 Freezing efficiency is not defined.*

Authors' response: Corrected. The authors meant n_s.

Reviewer's comment: *22079/4-11 While it is easy to agree with the general point being made here, the meaning of many parts of this paragraph is quite vague. What is meant by systematic uncertainty, absolute standard technique, . . .? I think that what is said in this paragraph would be better placed in the Introduction.*

Authors' response: We agree with Prof. Vali. This paragraph is not engaged with the IN discussion; therefore, the 1st paragraph discussion does not add any scientific merit to the manuscript. It is now removed.

Reviewer's comment: *22082/23 Was the SBM fit obtained using the LACIS data points or to the straight line shown in Fig. 9?*

Authors' response: A contact angle distribution was fitted to the frozen fractions measured with LACIS. When then SBM calculations are done and the resulting frozen fractions are converted to n_s, this results in the straight lines shown in Fig. 9.

The text in Page 22082 Lines 23-29 was modified.

"Specifically, a contact angle distribution was fitted to the LACIS measurements and was used, together with the soccer ball model (SBM; *Niedermeier et al*., 2011 and 2014), to simulate frozen fractions for different residence times varying over four orders of magnitude (i.e., 1, 10, 100 and 1000 s residence time). These frozen fractions were then used to calculate n_s, shown as lines in Fig. 9. More specifically, frozen fractions for 500 nm diameter illite NX particles were calculated based on SBM to obtain $n_s(T)$ spectra."

Reviewer's comment: *22085/5 Are particles removed from the filter with full efficiency in the washing process? If that is not sure, it should be mentioned as a potential explanation of the observed discrepancy.*

Authors' response: High efficiency particle removal has been demonstrated by the authors. SI Lines 286-288 now reads, "It is noteworthy that the application of the ultrasonic bath and its high efficiency in the washing process for particle removal were demonstrated with a similar experimental setup employed by *Ardon-Dryer and Levin* (2014).".

Reviewer's comment: *22085/7 Description of this method for FRIDGE is missing in the Supplementary Methods.*

Authors' response: We thank you for pointing out this error. We now add the texts for the FRIDGE immersion mode operation in SI lines 275-307.

Reviewer's comment: *22090/23 This paragraph is rather confusing, specially the first sentence.*

Authors' response: We rewrote the paragraph based on the modifications discussed earlier (i.e., Fig S4-S8; SI Lines 740-787):

"Furthermore, comparisons of the suspension subsets against the dry-dispersed particle techniques were performed. Dry samples alone showed higher n_s values compared to the pre-suspended samples above -27 ºC. A possible explanation for this deviation (i.e., n_s from dry-dispersed methods > n_s from suspension methods) may be the surface modification of the illite NX particles (e.g., due to ion dissolution effects in the aqueous suspension)."

Reviewer's comment: *22091/28 Could you clarify what is meant by 'temperature change is the major driver of immersion freezing"?*

Authors' response: We wanted to point out that our observations show that immersion freezing efficiency of illite NX particles is temperature-dependent and increases as the temperature decreases. We revised the text to clarify this point.

"…our observations show that temperature is the major variable influencing the immersion freezing of illite NX particles, as the n_s values in general increase while temperature decreases."

Reviewer's comment: *22092/1 What is the connection of this sentence to the previous one?*

Authors' response: There is no connection. For clarity, we modified the sentence. Page 22091/22092 Lines 28-4 now reads, "In addition, our results of n_s and absolute values of $\Delta\log(n_s)/\Delta T$ distributions across a wide range of temperatures imply that clay minerals may contain various freezing activation energies, and the immersion freezing nature of clay minerals (e.g., illite NX) in a wide range of temperatures cannot be fitted by simple exponential functions but are governed by a hybrid of multi-exponential functions (a combination of scaled A13 and N12 parameterizations).".

Additional revision: In addition to addressing the reviewers' comments, other editorial corrections (major ones) are made as seen in the last four pages (Pages 12-15) of our response to the reviewer #1.

In addition to addressing the reviewers‘ comments, all relevant changes made in the manuscript and SI are indicated by the highlighted sections in yellow below.

A comprehensive laboratory study on the immersion freezing behavior of illite NX particles: a comparison of seventeen ice nucleation measurement techniques

Naruki Hiranuma[1], Stefanie Augustin-Bauditz[2], Heinz Bingemer[3], Carsten Budke[4], Joachim Curtius[3], Anja Danielczok[3], Karoline Diehl[5], Katharina Dreischmeier[4], Martin Ebert[6], Fabian Frank[3], Nadine Hoffmann[1], Konrad Kandler[6], Alexei Kiselev[1], Thomas Koop[4], Thomas Leisner[1], Ottmar Möhler[1], Björn Nillius[3,*], Andreas Peckhaus[1], Diana Rose[3], Stephan Weinbruch[6], Heike Wex[2], Yvonne Boose[7], Paul J. DeMott[8], John D. Hader[9], Thomas C. J. Hill[8], Zamin A. Kanji[7], Gourihar Kulkarni[10], Ezra J. T. Levin[8], Christina S. McCluskey[8], Masataka Murakami[11], Benjamin J. Murray[12], Dennis Niedermeier[2,**], Markus D. Petters[9], Daniel O'Sullivan[9], Atsushi Saito[11], Gregory P. Schill[13], Takuya Tajiri[11], Margret A. Tolbert[13], André Welti[7], Thomas F. Whale[12], Timothy P. Wright[9], and Katsuya Yamashita[11,***]

[1]Institute for Meteorology and Climate Research – Atmospheric Aerosol Research, Karlsruhe Institute of Technology, Karlsruhe, Germany.
[2]Leibniz Institute for Tropospheric Research, Leipzig, Germany.
[3]Institute for Atmospheric Physics, University of Mainz, Mainz, Germany.
[4]Faculty of Chemistry, Bielefeld University, Bielefeld, Germany.
[5]Institute for Atmospheric and Environmental Science, Goethe University of Frankfurt, Frankfurt, Germany.
[6]Institute of Applied Geosciences, Technical University Darmstadt, Germany.
[7]Institute for Atmosphere and Climate Science, ETH, Zurich, Switzerland.
[8]Department of Atmospheric Science, Colorado State University, Fort Collins, CO, USA.
[9]Department of Marine Earth and Atmospheric Sciences, North Carolina State University, Raleigh, NC, USA.
[10]Atmospheric Science and Global Change Division, Pacific Northwest National Laboratory, Richland, WA, USA.
[11]Meteorological Research Institute (MRI), Tsukuba, Japan.
[12]Institute for Climate and Atmospheric Science, School of Earth and Environment, University of Leeds, Leeds, UK.
[13]Cooperative Institute for Research in Environmental Sciences and Department of Chemistry and Biochemistry, University of Colorado, Boulder, CO, USA.
Now at, *Max-Planck-Institut für Chemie, Mainz, Germany.
Now at, **Department of Physics, Michigan Technological University, Houghton, MI, USA.
Now at, ***Snow and Ice Research Center, Nagaoka, Japan.

Manuscript in preparation for *Atmospheric Chemistry and Physics*
ACP – Special Issue: Results from the ice nuclei research unit (INUIT)

December 21, 2014

Abstract

Immersion freezing is the most relevant heterogeneous ice nucleation mechanism through which ice crystals are formed in mixed-phase clouds. In recent years, an increasing number of laboratory experiments utilizing a variety of instruments have examined immersion freezing activity of atmospherically relevant ice-nucleating particles. However, an inter-comparison of these laboratory results is a difficult task because investigators have used different ice nucleation (IN) measurement methods to produce these results. A remaining challenge is to explore the sensitivity and accuracy of these techniques and to understand how the IN results are potentially influenced or biased by experimental parameters associated with these techniques.

Within the framework of INUIT (Ice Nuclei research UnIT), we distributed an illite rich sample (illite NX) as a representative surrogate for atmospheric mineral dust particles to investigators to perform immersion freezing experiments using different IN measurement methods and to obtain IN data as a function of particle concentration, temperature (T), cooling rate and nucleation time. Seventeen measurement methods were involved in the data inter-comparison. Experiments with seven instruments started with the test sample pre-suspended in water before cooling, while ten other instruments employed water vapor condensation onto dry-dispersed particles followed by immersion freezing. The resulting comprehensive immersion freezing dataset was evaluated using the ice nucleation active surface-site density, n_s, to develop a representative $n_s(T)$ spectrum that spans a wide temperature range (-37 ˚C < T < -11 ˚C) and covers nine orders of magnitude in n_s.

In general, the seventeen immersion freezing measurement techniques deviate, within a range of about 8 ˚C in terms of temperature, by three orders of magnitude with respect to n_s. In addition, we show evidence that the immersion freezing efficiency expressed in n_s of illite NX particles is relatively independent of droplet size, particle mass in suspension, particle size and cooling rate during freezing. A strong temperature dependence and weak time- and size dependence of the immersion freezing efficiency of illite rich clay mineral particles enabled the n_s parameterization solely as a function of temperature. We also characterized the $n_s(T)$ spectra and identified a section with a steep slope between -20 and -27 ˚C, where a large fraction of active sites of our test dust may trigger immersion freezing. This slope was followed by a region with a gentler slope at temperatures below -27 ˚C. While the agreement between different instruments was reasonable below ~ -27 ˚C, there seemed to be a different

trend in the temperature-dependent ice nucleation activity from the suspension and dry-dispersed particle measurements for this mineral dust, in particular at higher temperatures. For instance, the ice nucleation activity expressed in n_s was smaller for the average of the wet suspended samples and higher for the average of the dry-dispersed aerosol samples between about -27 and -18 ˚C. Only instruments making measurements with wet suspended samples were able to measure ice nucleation above -18 ˚C. A possible explanation for the deviation between -27 and -18 ˚C is discussed. Multiple exponential distribution fits in both linear and log space for both specific surface area and geometric surface area are provided. These new fits, constrained by using identical reference samples, will help to compare IN measurement methods that are not included in the present study and IN data from future IN instruments.

1. Introduction

1.1. Background

Primary ice formation by atmospheric ice-nucleating particles (INPs) markedly influences the formation and life cycle of mixed-phase clouds and very often also initiates precipitation formation. Therefore, ice-containing clouds play a significant role in the energy balance of the climate system and the hydrological cycle on Earth (Chapter 7 of IPCC 2013; *Boucher et al*., 2013). Currently, quantitative predictions for the impact of these clouds on the Earth's radiative budget and thereby the climate are highly uncertain. This uncertainty arises primarily from a lack of fundamental understanding of ice microphysical processes, the representation of these processes in cloud models and knowledge of the abundance of INPs (*Hoose and Möhler*, 2012; *Murray et al*., 2012). In particular, yearly emission rates of soil dust are 1000 to 4000 teragrams, accounting for a major proportion of both the dust component and the total particle loading in the atmosphere (*Boucher et al*., 2013). The resulting radiative forcing directly exerted by mineral dust is estimated to range from -0.3 to +0.1 W m^{-2}. Therefore, dust slightly contributes to the direct cooling effect of aerosols. However, our understanding of the influence of the dust burden upon overall climate forcing, including its secondary effect on cloud albedo, remains highly uncertain, in part due to the absence of accurate INP representations in atmospheric models. Thus, the effective radiative forcing effect of airborne dust on current climate predictions remains unresolved.

A small subset of all particles acts as INPs across a range of subzero temperatures, triggering ice formation in clouds via the process of heterogeneous ice nucleation. Previous laboratory experiments have taken diverse approaches in an attempt to mimic ice nucleation and freezing processes. These heterogeneous ice formation processes include deposition nucleation, immersion-, condensation- and contact freezing (*Vali*, 1985), inside-out contact freezing (i.e., freezing of an immersed INP in contact with the droplet surface from the inside; *Durant and Shaw*, 2005; *Fornea et al*., 2009) and surface condensation freezing (i.e., freezing of supercooled water or residual aqueous solution trapped on particle surfaces, e.g., by the inverse Kelvin effect; *Christenson*, 2013; *Hiranuma et al*., 2014a; *Marcolli*, 2014; *Welti et al*., 2014; *Wex et al*., 2014). Without INPs, pure cloud water droplets or solution within particles can be supercooled to below -37 ˚C before freezing (*Koop et al*., 2000; *Murray et al*., 2010; *Rosenfeld and Woodle*y, 2000).

Among the various modes of atmospheric ice nucleation, immersion freezing is one of the most important mechanisms for primary ice formation, accounting for 85% of ice formation in clouds that contain supercooled droplets (*Hoose et al*., 2010). Furthermore, many of the previous experimental studies have investigated heterogeneous ice nucleation at conditions where water is supercooled before freezing (e.g., *Murray et al*., 2012). However, the relative importance of the particles' physico-chemical properties [i.e., size, composition, solubility, hygroscopicity, cloud condensation nuclei activity, ice nucleation (IN) active sites, surface charge and/or crystallographic structure] for immersion freezing is not yet well known (e.g., *Hiranuma et al*., 2013; *Hiranuma et al*., 2014b; *Murray et al*., 2012). Hence, more in-depth investigations and understanding of heterogeneous ice nucleation processes in supercooled clouds (as well as mixed-phase clouds) is of particular importance.

1.2. State of the art of IN measurement techniques

The concept of condensation nuclei contributing to ice formation was first introduced by Alfred Wegener in 1911 (*Wegener*, 1911). Since then, various instruments and methods have been developed to investigate the composition of atmospherically relevant INPs as well as their abundance; for example, the rapid expansion cloud-simulation chamber (RECC) was first introduced as a detector of ionizing particles. Such instruments have been used in many ice nucleation studies since the 1940s (e.g., *Cwilong*, 1947; *Fournier d'Albe*, 1949; *Palmer*, 1949; *Bigg*, 1957; *Kline and Brier*, 1961). Supersaturated conditions with respect to water and ice, as a function of temperature, are created in the RECC vessel by a rapid pressure drop caused by mechanical expansion and concomitant cooling. Subsequently, water vapor in the supersaturated air can either deposit or condense on sample particles, leading to the formation of water droplets and/or ice.

A different type of instrument widely used to measure abundance and efficiency of INPs is the continuous flow diffusion chamber (CFDC). The need for portable instruments capable of obtaining continuous measurements for aircraft applications emerged in discussions during the 1970s and was a main driver of CFDC development. In CFDCs, particles are sampled into a region between two ice-coated concentric cylinders (or dual parallel plates) maintained at different temperatures, which generates a region of ice supersaturation between ice-coated walls. As the particles experience ice supersaturation conditions for a few seconds, INPs can be activated and diffusively grow to supermicron ice crystals. Typically, these large ice crystals can be detected and counted by an optical particle

counter (OPC) downstream of the instrument while the chamber temperature and humidity conditions are continuously recorded. Since its first appearance in the 1980s with horizontal parallel plates (*Hussain and Saunders*, 1984; *Tomlinson and Fukuta*, 1985), several new designs and operational principles have been introduced (e.g., vertically oriented cylinders; *Rogers et al*., 1988, horizontally oriented parallel plates; *Kanji and Abbatt*, 2009, vertically oriented parallel plates; *Stetzer et al*., 2008; *Chou et al*., 2011; *Friedman et al*., 2011). An alternative configuration is the continuous flow mixing chamber (e.g., Fast Ice Nucleus Chamber or FINCH; *Bundke et al*., 2008). The operation principle of this type of chamber does not involve water vapor diffusion from the ice walls, as in CFDC, but water vapor is available for ice growth from the humidified air within the chamber flow. This leads to an upper limit on INP concentrations that are observable with this methodology (*DeMott et al*., 2011). A flow tube (e.g., Leipzig Aerosol Cloud Interaction Simulator or LACIS, *Hartmann et al*., 2011) has also been developed in which a humidified stream containing aerosol particles is first cooled to activate droplets on the particles, which upon further cooling may then freeze.

In addition to chamber techniques, the mode-specific conditions for heterogeneous ice nucleation of a known INP placed on a substrate surface have been studied using optical microscope techniques. For example, by immersing ice nuclei in water droplets placed on a hydrophobic substrate surface and collecting a series of images at controlled cooling rates, the change in reflectivity and opacity following ice formation can be characterized, and the associated freezing conditions can be identified (e.g., *Knopf and Alpert*, 2013; *Murray et al*., 2011). More recently, other optical microscopy techniques coupled with a unique method of encapsulating particles into droplets followed by cooling (*Iannone et al., 2011*) or using the hydrophobic squalene/water emulsion (*Wright and Petters*, 2013) were introduced to the community. Using a similar approach, substrate-supported cooling studies have been applied to determine the freezing temperature in the contact mode (e.g., *Fornea et al*., 2009; *Niehaus et al*., 2014), or of deposition nucleation (e.g., *Kanji and Abbatt*, 2006; *Bingemer et al*., 2012; *Dymarska et al*., 2006). The microscopy-coupled substrate-supported freezing devices are advantageous to visualize the consequences of specific ice nucleation modes in controlled and simulated environments. In some studies, immersion freezing of microliter scale droplet volumes was analyzed at temperatures (*T*s) higher than -10 ˚C with a sensitivity of INP concentration as good as ~10^{-5} L^{-1} (*Ardon-Dreyer et al.*, 2011).

The freezing temperature of INPs either immersed in or in contact with levitated supercooled water droplets suspended in the air can also be determined by the change in light

scattering with a charge-coupled device (CCD) camera using an electrodynamic balance (EDB; *Hoffmann et al*., 2013), an acoustic levitator (*Diehl et al*., 2014) or in a vertical wind tunnel (*Szakáll et al*., 2009). The advantage of these methods is the ability to provide, via high-resolution images, substrate-free information for statistically representative ice nucleation processes on a single droplet basis. This advantage is shared with all of the above mentioned chamber and flow tube devices.

Undoubtedly, these enormous efforts to develop numerous IN measurement techniques have advanced our basic knowledge of atmospheric ice formation. As a consequence, the atmospheric science community will continue to pursue investigations of IN to unravel their associated effects on climate. Accordingly, exploring the sensitivities, uncertainties and biases of various experimental techniques (e.g., methods for particle generation, size segregation, size estimation, ice detection and any other notable experimental procedures) in nucleating ice on particles of known physico-chemical properties is crucial in order to compile comparative INP data of multiple and complex measurement techniques from various research institutions. The information obtained from one technique guides other measurement techniques (*DeMott et al*., 2011; *Riechers et al*., 2013). A better understanding of the sensitivity of multiple techniques and the role of associated experimental parameters upon INP measurements will also help in transferring the laboratory-based measurements of INPs of various atmospheric constituents to their reliable parameterizations in models of atmospheric processes.

Since the 1960s, four international workshops have been organized to compare the performance of IN measuring instruments that were emerging or available at the time (*DeMott et al*., 2011). In particular, effort was made during the fourth international ice nucleation workshop in 2007 (ICIS-2007) to assemble a total of nine laboratory and field IN instruments at the AIDA (Aerosol Interaction and Dynamics in the Atmosphere) facility and compare them using identical test dust samples (e.g., Arizona Test Dust, or ATD, and Saharan dust) over similar thermodynamic conditions. State-of-the-art knowledge was obtained from each workshop activity, and such measurement understanding was further incorporated to develop the next generation of IN instruments.

1.3. Objectives

The major aim of this study, and concurrent studies within the framework of the INUIT (Ice Nuclei research UnIT) project, is to investigate the immersion freezing behavior of reference particles (e.g., Snomax for bacterial IN processes and potassium rich feldspar, K-

feldspar, for mineral dust IN processes). In this work, we distributed illite NX samples from the same batch [with the exceptions of the samples used for Leeds-NIPI, ZINC and IMCA-ZINC (acronyms are defined in the Supplementary Information Sect. S4); *Broadley et al*., 2012; *Welti et al*., 2009] among the INUIT project and associated partners. With a total of seventeen different IN measuring instruments, we inter-compared IN data from each instrument in order to obtain a comprehensive dataset for evaluating immersion freezing properties of illite NX particles. The dataset captures the functional dependence of various experimental parameter variables, such as particle concentration, particle size, droplet size, temperature, cooling rate and nucleation time, on the immersion freezing properties of illite NX particles. Further, some instruments used test samples suspended in water prior to experiments, while others used dry-dispersed particles. The basic experimental methods and parameterization approaches used to interpret the overall results and perform the inter-comparison are discussed.

Results of freezing efficiencies at specific temperatures are presented using the ice nucleation active surface-site density (n_s) parameterization (e.g., *Connolly et al*., 2009; *Niemand et al*., 2012; *Hoose and Möhler*, 2012) developed on the basis of suggestions by *DeMott et al*. (1995). For instance, *Niemand et al*. (2012) showed that the singular parameterization approach of immersion freezing (i.e., freezing along water saturation conditions while cooling) of various desert dust particles derived from AIDA experiments converge upon one representative fit as a function of temperature, which is valid across a temperature range from -12 to -36 ˚C. The time-independent n_s parameterization has also been used in describing INP activation by several different constituents of clay minerals, e.g., microcline and kaolinite, using the cold stage droplet freezing technique (*Atkinson et al*., 2013; *Murray et al*., 2011; *Murray et al*., 2010). Hence, comparison of IN efficiencies can be readily performed for multiple types of instruments using n_s parameterizations. Moreover, such time-independent and surface-area-scaled n_s formulations can be further adapted to comprehensively assess ice nucleation in a wide range of atmospherically relevant temperatures and relative humidities with respect to ice (RH_{ice}), as was recently presented in *Hiranuma et al*. (2014a). The n_s parameterization for both immersion freezing and deposition nucleation can be directly implemented in cloud, weather and climate models to calculate the temperature-dependent abundance of INPs as a function of the aerosol surface area concentration.

2. Methods

2.1. Illite NX characterization

In this study, we have chosen illite NX (Arginotec, NX Nanopowder) as a surrogate for natural desert dusts. This choice of an illite rich material is based on a comparison of its mineralogical composition to that of desert dusts, which are also rich in illite but are also mixed with a range of other minerals (*Broadley et al*., 2012). The present work gives an overview of laboratory experiments for immersion freezing of particles of illite NX, used as a surrogate for atmospheric desert dust particles. Illite NX bulk powder was previously characterized for its physico-chemical properties, such as mineralogy and specific surface area (SSA or θ for brevity). It was observed that illite NX samples contained more than 74 weight percent (wt%) illite (*Broadley et al*., 2012; *Friedrich et al*., 2008) along with other components [kaolinite, quartz, calcite and feldspars (most likely orthoclase/sanidine), see Sect. 3.1 for more detail] which is similar to the X-ray diffraction (XRD) data specified by the manufacturer. These test particles typically have aggregates of many nanometer-sized grains, yielding an order of magnitude greater SSA (104.2 $m^2\ g^{-1}$; *Broadley et al*., 2012). The aspherical and elongated nature of illite NX particles (aspect ratio up to ~4.8; *Veghte and Freedman*, 2014) emphasizes the importance of considering its irregular shape. The manufacturer reports the particle density, after mechanical granulation, as 2.65 g cm^{-3}.

To determine the purity of our sample, and to compare this with previous observations, the dust mineralogy of a bulk illite NX sample was characterized using XRD (*Waseda et al*., 2011) prior to distribution. In addition, complementary energy dispersive X-ray (EDX) spectroscopy analysis was performed to characterize the elemental composition of individual particles. The illite NX particles were sampled directly from the AIDA chamber using a 47 mm Nuclepore® filter (Whatman, 0.2 μm pore-size, filter Cat. No. 111106) and used in the EDX analysis.

The N_2-adsorption-based SSA (or BET surface, *Brunauer, Emmett, and Teller*, 1938) of the illite NX sample was also measured. BET is a gas adsorption technique where the quantity of various gases required to form a monolayer over the entire available surface of dry particles, including internal surfaces, is measured (*Gregg and Sing*, 1982; *Bickmore et al*., 2002). From the knowledge of the size of a molecule on the surface, it is possible to determine the total surface area (S_{total}). In this work, BET surface areas were determined using

two different gas adsorbents: N_2 and H_2O (resulting in θ_{N_2} and θ_{H_2O}), with the latter being the surface area exposed to water. BET measurements with H_2O were limited to 28% relative humidity with respect to water (RH_w) to correctly account for a monolayer of H_2O (*Quantachrome Instruments*, 2013).

The effect of particle processing, such as removal of hydrophilic ions by water, in a water suspension was examined by ion chromatography (IC). The influence of dust washing and discharge of soluble materials on IN propensity has been previously proposed (*Welti et al*., 2014). More specifically, the authors postulated two different scenarios at different temperatures based on their observations. At temperatures below ~ -38 ºC, the washed dust component may have enhanced water condensation below water saturation, and a formed liquid layer presumably may have stabilized the subcritical ice embryo entrapped inside the liquid. The authors proposed this capillary condensation process as a part of condensation freezing or homogeneous nucleation based on the previous observation (*Christenson*, 2013) and the theoretical framework (*Marcolli*, 2013). Above ~ -38 ºC, on the other hand, heterogeneous nucleation might have been suppressed because the liquid layer derived from the deliquescence of soluble impurities from individual particles may have diminished accessibility of water vapor to active sites (e.g., localized surface features such as cracks and edges), originally proposed by *Koehler et al*. (2010), preventing the ice embryo formation. In this study, suspended samples were prepared by stirring illite NX powders (0.1 g in 10 mL of 18.2 MΩ cm nanopure water) over three weeks. IC (Dionex DX-500 IC System equipped with Dionex CD20 Conductivity Detector) was used to determine the concentrations of washed out cations (K^+, Ca^{2+} and Mg^{2+}) as a function of time. A weak solution of sulfuric acid [5mL H_2SO_4 (96 wt%) diluted in 2 L of Nanopure water] was used as the eluent. The measurements were conducted in three series: every 5 to 10 s (seconds) within the first 2 min (minutes) (ultra-short time series, USTS), then every 10 min within the first hour after immersion (short time series, STS) followed by a long time series (LTS) with cation concentration measurements conducted every 2 days thereafter for a three week period.

2.2. Particle size distribution

Size distributions and the S_{total} (in m^2 cm^{-3}) of both suspended and dry-dispersed illite NX particles were characterized using four size measurement techniques (i.e., aerosol size spectrometers and light scattering instruments). In particular, the dynamic light scattering

(DLS) size of suspended illite NX particles (0.05 to 1 mg bulk illite NX sample in 1 mL of triple-distilled water) was determined using the StabiSizer® (Microtrac Europe GmbH, PMX 200CS) over the range of 0.0008 to 6.5 μm hydrodynamic diameter. A more detailed description of this instrument and its application for studying the size of particles in suspension are addressed in *Hiranuma et al*. (2014b), and only a brief discussion is given here. The DLS measurements were carried out with negligible contribution of multiple scattering due to the utilized 180° backscattering mode. The hydrodynamic diameter, which was comparable to the volume equivalent diameter, is determined using a refractive index of 1.55 to 1.58 for illite and of 1.333 for water, and a viscosity of water of 1.002 and 0.797 mPa s at 20 and 30 °C, respectively. From this metric, the surface area was calculated assuming spherical particles.

Size distributions of dry polydisperse illite NX particles were measured at AIDA controlled expansion cloud-simulation chamber (CECC) and MRI dynamic CECC (DCECC) prior to the expansion experiments. For AIDA-CECC, de-agglomerated illite NX particles from a rotating brush disperser (PALAS, RGB 1000) were passed through a series of inertial cyclone impactor stages (D_{50} ~1 and 5 μm) and introduced to the 84 m^3 volume AIDA vessel. Subsequently, a scanning mobility particle sizer (SMPS, TSI Inc., Model 3081 differential mobility analyzer, DMA, and Model 3010 condensation particle counter, CPC) and an aerodynamic particle sizer (APS, TSI Inc., Model 3321) were used to measure particle size distributions over the range of 0.01 to 15.4 μm volume equivalent diameter. The assumption of particle sphericity, a dynamic shape factor (DSF or χ in equations) of 1.49 ± 0.12 (average of ten measurements ± standard deviation) and a particle density of 2.65 g cm^{-3} were used to obtain the geometric-based (volume equivalent) diameter from an APS (*Hiranuma et al*., 2014b). At MRI-DCECC, a combination of an SMPS (TSI Inc., Model 3936) and a welas optical particle counter (welas-OPC, PALAS, Sensor series 2500) was used to acquire a size distribution for the size range of 0.01 to 47.2 μm volume equivalent diameter directly from the 1.4 m^3 volume vessel. The same disperser type was used at both chambers for particle generation, and the upstream cyclone impactors (D_{50} ~1 and 2.5 μm) were similarly deployed to filter out any larger particles and safeguard against injecting these particles into the vessel. We note that a linear correction factor of ~2 was applied to convert the optical diameter measured by the welas-OPC to the APS-inferred volume equivalent diameter in several studies (*Wagner et al*., 2011; *Hiranuma et al*., 2014a).

The particle number size distribution of dry particles in the 0.3-10 μm diameter range was also measured by a TSI 3330 optical particle sizer (OPS, TSI Inc.; TSI-OPS hereafter).

For particle generation, the illite NX sample was dispersed using a magnetic stirrer in a 100 mL glass vessel that was purged with 200 mL min^{-1} of dry particle-free compressed laboratory air, and then diluted further in two stages by approximately 1:100 with dry air. Subsequently, the backward scattering intensity of scattered light from a particle illuminated by a laser (λ = 660 nm) was measured. The instrument estimated the particle size distribution, assuming spherical particles, using Mie theory. As a result, the reported size is a volume equivalent spherical diameter. Additionally, these dry-dispersed particles were used for the immersion mode experiments of FRIDGE as described in the Supplementary Methods.

2.3. Ice nucleation measurements

The ice nucleation measurement techniques contributing to this collaborative effort are listed in Table 1. Descriptions of each measurement technique and their acronyms are available in the Supplementary Information Sect. S4. Briefly, four CFDC-type instruments, one continuous flow mixing chamber, two cloud simulation chambers, one diffusion cell, two levitators, one vertical wind tunnel, one laminar flow tube and five cold stage-type systems were employed in the inter-comparison. As seen in Table 1, measurement techniques with the first seven instruments (i.e., ID 1 to 7) and the immersion mode measurements of FRIDGE (ID 12) examined droplets produced from bulk illite NX samples in suspension, while the rest used dry-dispersed illite NX powder, sometimes followed by size selection with a DMA. Methods working with suspensions and those using dry particles employed different ways to determine the particle surface area, and the influence of these differences on the determination of n_s was investigated. For instance, CSU-IS was used to investigate the freezing activity of both bulk suspension and size-segregated particles in suspension. Two cloud expansion chambers, AIDA-CECC and MRI-DCECC, examined both polydisperse and size-selected dry illite NX particles. LACIS and IMCA-ZINC measured immersion freezing of droplets, where each droplet contained a single particle, and examined differently sized dry particles. The role of IN modes upon the estimation of n_s was also examined across various temperature ranges. The EDB-based method was used to measure the contact and immersion mode efficiencies of size segregated dry illite NX particles around -30 ˚C. Immersion freezing results from IMCA-ZINC were compared to previously reported ZINC data (*Welti et al.*, 2009) at temperatures below -31 ˚C and to PINC data for temperatures below -26 ˚C. In the present study, we derived ZINC's n_s values from the results reported in *Welti et al.* (2009). Specifically, ice

formation above 105% RH_w up to the water drop survival line was used to calculate n_s based on given illite NX particle sizes. We note that the latent heat of condensation has minimal impact on droplet temperature, such that RH_w > 105% maintains a water supersaturating condition for droplet freezing.

FRIDGE investigated ice nucleation of both dry-dispersed particles on a substrate at fixed temperatures (-25 ˚C < T < -18 ˚C) with increasing humidity ('default' deposition mode nucleation) as well as immersed particles. In the case of immersion freezing experiments with suspended samples, the cell temperature was lowered by 1 °C min^{-1}.

The range of mass concentrations of the bulk illite NX sample in suspension varied from 3.1 x 10^{-6} wt% (CSU-IS) to 2.6 wt% (M-WT). For dry-dispersed particle measurements, particle concentrations varied from ~10 cm^{-3} (AIDA) up to ~9000 cm^{-3} (MRI-DCECC). Experiments with M-AL, M-WT, EDB, and IMCA-ZINC were performed on a single drop basis. The shortest residence time of roughly 1.6 s was used for the laminar flow tube, LACIS, and the slowest cooling rate of 0.3 ˚C min^{-1} (time-average cooling rate over an expansion, which translates to the equivalent updraft rate of ~0.5 m s^{-1}) was used in AIDA-CECC. Altogether, immersion freezing was examined across the temperature range from ~ -10 to ~ -38 ˚C, and over a varied range of cooling rates, nucleation times and particle concentrations (summarized in publically accessible data base available at http://imk-aaf-s1.imk-aaf.kit.edu/inuit/).

2.4. Ice nucleation parameterization

We now describe a method to parameterize surface area-scaled immersion freezing activities using the size equivalent ice nucleation active surface-site density based on geometric size ($n_{s,geo}$; *Connolly et al.*, 2009; *Niemand et al.*, 2012; *Hoose and Möhler*, 2012). In short, this surface-site density approach approximates ice crystal formation observed in an experiment as a function of temperature, thus not accounting for time dependence. Accordingly, $n_{s,geo}$ can be expressed by:

$$n_{s,\mathrm{geo}}(T) = -\ln\left(1 - \frac{N_{\mathrm{ice}}(T)}{N_{\mathrm{total}}}\right)\left(\frac{1}{S_{\mathrm{ve}}}\right), \quad (1)$$

in which, N_{ice} is the number concentration of formed ice crystals (cm^{-3}), N_{total} is the total number concentration of particles prior to any freezing event (cm^{-3}), and S_{ve} is the volume

equivalent surface area of an individual particle (m^2). As demonstrated in *Niemand et al.* (2012), if the activated ice fraction is small (<0.1), the Taylor series approximation can be applied to Eqn. 1. Assuming a uniform distribution of $n_{s,geo}$ over a given S_{total} and a size independency of $n_{s,geo}$, we can approximate $n_{s,geo}$ as:

$$n_{s,\mathrm{geo}}(T) \approx \frac{N_{\mathrm{ice}}(T)}{N_{\mathrm{total}} S_{\mathrm{ve}}} = \frac{N_{\mathrm{ice}}(T)}{S_{\mathrm{total}}}. \quad (2)$$

In addition, the IN efficiency can be related to the BET-SSA to estimate BET-inferred ice nucleation surface-site density, $n_{s,BET}$. A description of the procedures used to estimate both n_s metrics is given in *Hiranuma* et al. (2014b). The advantage of using $n_{s,geo}$ is its applicability to both measurements and modeling activities due to the assumption of particle sphericity. Conversely, $n_{s,geo}$ cannot be directly obtained through suspension experiments because the size distribution of a suspended sample for each experiment is not available; therefore, S_{total} is determined from BET and the sample mass suspended in water.

In order to convert $n_{s,geo}$ values of all dry-dispersed particle measurements into $n_{s,BET}$, the geometric size-based ice-nucleating mass, $n_{m,geo}$ (g^{-1}), is first calculated from the IN active surface using either the surface-to-mass conversion factor (in m^2 g^{-1}) of $6/D_{ve}\rho$ (size-selected case) or S_{total}/M_{total} (polydisperse case) by:

$$n_{m,\mathrm{geo}}(T) = \frac{N_{\mathrm{ice}}(T)}{N_{\mathrm{total}} M_{\mathrm{ve}}} = \frac{6}{D_{\mathrm{ve}}\rho} n_{s,\mathrm{geo}}(T) \approx \left(\frac{S_{\mathrm{total}}}{M_{\mathrm{total}}}\right) n_{\mathrm{s,geo}}(T) \quad (3)$$

where M_{ve} is the mass of a spherical particle of volume-equivalent diameter (g), D_{ve} is the volume equivalent midpoint diameter of particles (m), ρ is the particle density of illite NX (2.65×10^6 g m^{-3}), and M_{total} is the total particle mass concentration (g cm^{-3}). We note that the DLS size distribution-derived S_{total}/M_{total} (i.e., DLS-SSA) is 6.54 m^2 g^{-1} and use for the measurements with suspended particles. We also note that the conversion factor ranges from 11.3 to 2.26 m^2 g^{-1} for size-selected particle diameters from 200 nm to 1000 nm, respectively, where these sizes denote the range of particle diameters used in the size-selected cases in the present study. Therefore, ice-nucleating mass can be scaled to the BET-SSA (θ, 124.4 m^2 g^{-1}) to derive $n_{s,BET}$ as:

$$n_{s,\mathrm{BET}}(T) = \frac{n_{m,\mathrm{geo}}(T)}{\theta} \approx \frac{n_{m,\mathrm{sus}}(T)}{\theta} = \frac{\alpha}{M_{\mathrm{ve}}\theta}, \quad (4)$$

in which, $n_{m,sus}$ is the IN active mass for suspension measurements, α represents the ice activated fraction (= N_{ice}/N_{total}), which is the direct measurement of suspension experiments and some of the dry-dispersed particle methods. With an assumption of a uniform BET-SSA,

405 the resulting $n_{s,BET}$ may be representative of measurements with suspended samples because
406 minimal corrections (only α and θ) are involved when compared to that with dry-dispersed
407 particles. Owing to internal surface area and surface roughness, BET-SSA may be greater than
408 DLS-SSA (*O'Sullivan et al*., 2014).
409 Alternatively, we can also convert ice-nucleating mass derived from suspension
410 measurements, $n_{m,sus}$, to $n_{s,geo}$ using DLS-SSA to provide a reasonable comparison to dry-
411 dispersed particle measurements. However, this process requires one more step than when
412 using $n_{s,BET}$ (with an additional assumption of constant size distribution for all suspensions)
413 and two more steps than when using n_m. For our inter-comparison study, we used both $n_{s,BET}$
414 and $n_{s,geo}$. Because fewer conversion factors are involved, $n_{s,BET}$ may be best suited for
415 suspension measurements, and $n_{s,geo}$ may be best suited for dry-dispersed particle
416 measurements (Eqn. 3 to 4 or vice versa).
417 The usage of DLS-SSA for the calculation of S_{total}/M_{total} of suspension measurements
418 appears to be reasonable, as this leads to $n_{s,geo}$ for suspension measurements nearly equivalent
419 to $n_{s,geo}$ for dry-dispersed particles. When S_{total}/M_{total} is derived based on TSI-OPS
420 measurements, a value of 0.49 m^2 g^{-1} is obtained, which is smaller by a factor of about
421 thirteen compared to DLS-SSA. This difference may be mainly due to the fact that dry-
422 dispersed particles are typically prone to agglomeration (discussed below, i.e., Sect. 3.1)
423 compared to the measurements with suspended particles. The presence of fewer agglomerates
424 in suspended particles is shown in Fig. 1 of *Hiranuma et al*. (2014b). Since the size
425 distribution of a suspended sample for each experiment was not measured, DLS-SSA was
426 used for the data evaluation for suspension measurements throughout this study.

3. Results

3.1. Illite NX characterization

XRD results from the present and previous studies (*Friedrich et al.*, 2008; *Broadley et al.*, 2012) of the major minerals in bulk samples of illite NX are presented in Table 2. The results show that the bulk illite NX powder is composed of various minerals: illite, kaolinite, quartz, calcite and feldspar, but the relative mass of these minerals for this study differs from previous studies. For example, our measurement shows that the illite NX sample is composed of ~69 wt% illite mineral, whereas others report a larger amount of illite from 74 to 86 wt%. Similarly, we observed a somewhat different content of other minerals compared to previous studies as listed in Table 2 (see also the Supplement Fig. S1). We note that the fractional values in compositional fingerprints may deviate even within the same batch, as all three XRD measurements deviated from the manufacturer's data (Table 2). Furthermore, our XRD result indicates that the illite NX sample contains a smaller quartz fraction (3%) than IMt1-illite from the Clay Mineral Society (10 to 15% quartz according to the official XRF data and 20% based on our own measurements).

To complement bulk XRD analysis, the abundances of thirteen elements (Pt, K, C, Ca, O, Fe, Mg, Al, Si, P, S, Pb and Ti), which are commonly identified in illite rich samples, were measured by EDX spectroscopy on a single particle basis. Four representative EDX spectra are presented in Figure 1. The presence of Fe and Mg is typical and characteristic for illite NX particles. The observed large amounts of Si and Al are due to the presence of layered aluminosilicate structures (i.e., layer of SiO_2 and Al_2O_3). The observed dominant platinum (Pt) signals in all spectra originate from the sputter coating conducted prior to EDX analyses. Figure 1a shows the typical illite spectrum, which is similar to the one previously published in *Welton* (1984). Illite rich minerals, which included impurities of calcite, TiO_2 and Pb-P, were located by the brightness difference in the backscattered electron detector micrograph images. The results are shown in Fig. 1b, c and d (inclusion of calcite, TiO_2 and Pb-P, respectively). However, the EDX technique is not automated to detect these impurities present within the illite NX particles because of their very small weight fraction. Therefore, the possible effect of these observed impurities in illite NX upon the ice nucleation activity cannot be evaluated on the basis of its bulk analysis of the chemical composition. Nonetheless, detection of non-illite

mineral components may reflect the complexities of natural dust particles, which typically contain multiple sites with differing nucleation abilities. Thus, illite rich clay mineral can be used as a reference material to mimic the ice nucleation activity of physically and chemically complex natural dusts (*Murray et al*., 2012).

The measured BET-SSA are 124.4 and 123.7 $m^2\ g^{-1}$ with N_2 and H_2O vapor, respectively, as the adsorbing gas on illite NX particle surfaces. The similar BET surface areas for both N_2 and H_2O vapor gas adsorption suggest that the formation of a few monolayers of H_2O does not alter the surface morphology or the mineralogical phase of illite NX particles. For comparison, our measurements of θ_{N_2} for illite NX particles agreed with previously reported data within 20% (104.2 $m^2\ g^{-1}$; *Broadley et al*., 2012). Since illite NX particles have significant internal surface area, BET-derived surface areas can be expected to be larger than those derived from the laser diffraction technique. Supporting this notion, an SEM image of an illite NX particle from *Broadley et al*. (2012) shows how micron-sized particles are made up of many nanometer-sized grains.

Normalized surface area distributions to the total surface area concentration measured by four different techniques are shown in Fig. 2. According to the manufacturer, 95% (by mass) of the dry and mechanically de-agglomerated illite NX particles have a diameter smaller than 650 nm (i.e., D_{95}). This mass-based particle size is substantially smaller than that of another type of Arginotec illite (Arginotec, SE-illite, D_{95} = 5 μm). Interestingly, all mass size distributions measured in this study (not shown here) indicate a substantial mass fraction above 650 nm which is, in all cases, larger than 5% (18%, 24%, 77% and 99.9% for DLS, AIDA, MRI-DCECC and TSI-OPS for the FRIDGE immersion experiments, respectively), indicating the presence of agglomerates in the aerosol and suspension phases prepared for the IN experiments. The surface area distribution of the DLS hydrodynamic diameter-based measurement (Fig. 2a) agreed well with *in situ* measurements from the AIDA chamber (Fig. 2b), suggesting the size distributions of dry illite NX particles during AIDA experiments were similar to those of suspension measurements. This observation is consistent with results presented in *Hiranuma et al*. (2014b). Briefly, the authors found agreement between the DLS-based hydrodynamic diameter and the AIDA-derived volume equivalent diameter of hematite particles. As opposed to the AIDA observation, the wider distributions and the shift in the mode diameters in the MRI-DCECC measurements towards a larger size (0.62 μm, Fig. 2c) when compared to Fig. 2a and b may indicate a higher degree of particle agglomeration as a result of different degrees of pulverization during the particle generation processes or particle coagulation at the high aerosol number concentration used for these measurements. A more

pronounced agglomeration effect was observed by the TSI-OPS measurements (Fig. 2d), such that a surface area distribution of supermicron-sized particles was obtained. Thus, different types of dry particle dispersion methods can contribute to varying degrees of agglomeration and the observed differences in surface area distributions. Though all size segregating instruments used in the present study are well calibrated, we cannot rule out the effect of measurement techniques themselves on the observed differences in particle size distribution. In Sect. 4.4 we discuss whether agglomeration has an effect on the IN activity.

The cation release by illite NX in the aqueous suspension was measured with IC as a function of time. The suspension was kept mechanically agitated for three weeks. The following cations were identified in the samples: K^+, Ca^{2+} and Mg^{2+}. As seen in Fig. 3, IC data clearly demonstrates that roughly all cations were released into the aqueous environment by illite NX almost instantaneously. The concentration of the cations increased rapidly and reached equilibrium within the first 2 min after immersion of sample into water. Of all the cations measured, only Ca^{2+} exhibited a slow concentration raise on the longer time scales.

3.2. Immersion freezing measurements and inter-comparisons

All ice nucleation spectra with $n_{s,\mathrm{BET}}(T)$ and $n_{s,\mathrm{geo}}(T)$ are shown in Figs. 4 and 5, respectively. A similar figure with $n_m(T)$ is also shown in the Supplement Fig. S2. Furthermore, we compare the n_s data from seventeen instruments to four literature results. Specifically, IN spectra reference curves of previously reported illite NX particles (*Broadley et al*. 2012, hereafter B12), microcline particles (*Atkinson et al*., 2013, hereafter A13), ATD and desert dusts (*Niemand et al*., 2012, hereafter N12) are also expressed as both $n_{s,\mathrm{BET}}(T)$ and $n_{s,\mathrm{geo}}(T)$. The conversion between $n_{s,\mathrm{geo}}(T)$ and $n_{s,\mathrm{BET}}(T)$ was performed according to Eqns. 3 and 4. The $n_s(T)$ (m^{-2} as a function of ºC) fits from the reference literature are:

$$n_{s,\mathrm{BET}}^{\mathrm{A13}} = 10^4 \times \exp(-1.038(T - 273.150) + 275.260) \quad (5)$$

$$n_{s,\mathrm{BET}}^{\mathrm{B12}} = 10^4 \times \exp[(6.530 \times 10^4) + \left((-8.215 \times 10^2) \times (T - 273.150)\right) + (3.447 \times (T - 273.150)^2) + \left((-4.822 \times 10^{-3}) \times (T - 273.150)^3\right)] \quad (6)$$

$$n_{s,\mathrm{geo}}^{\mathrm{N12(ATD)}} = \exp(-0.380T + 13.918) \quad (7)$$

$$n_{s,\mathrm{geo}}^{\mathrm{N12(Dust)}} = \exp(-0.517T + 8.934). \quad (8)$$

For microcline (K-feldspar), the $n_{s,geo}$ to $n_{s,BET}$ conversion was performed using a laser diffraction-based surface-to-mass conversion factor of 0.89 m^2 $g^{-1}$and an N_2 BET-SSA of 3.2 m^2 g^{-1} (*Atkinson et al*., 2013). For ATD and natural dust, we used a surface-to-mass conversion factor of 3.6 m^2 g^{-1}, assuming a monodisperse particle size at the lognormal fit mode diameter of 0.64 μm (*Niemand et al*., 2012) and the measured N_2 BET-SSA of 34.4 m^2 g^{-1} (*this study*). We note that the ATD parameterization is valid only for -26.7 ˚C < T < -17.7 ˚C. In addition, we also present 14, 0.14 and 0.0014% scaled A13 n_s curves to see if K-feldspar (microcline) can be used as a scaling factor to determine the $n_s(T)$ of illite NX.

We do not attempt to completely discuss the immersion freezing activity of illite NX particles measured by each measurement technique. Instead, brief remarks regarding each method are summarized below. The detailed discussion of the methods inter-comparison follows in Sect. 3.3.

3.2.1. BINARY: This recently developed microliter droplet assay technique demonstrated its capability of measuring immersion freezing of clay minerals in the temperature range of -15 to -24 ˚C. Similar to most of the other suspension-based techniques, BINARY identified a steep $n_s(T)$ increase, which started just below -20 ˚C. The BINARY $n_s(T)$ spectrum was derived by compiling measurements with varied illite NX mass concentrations over two orders of magnitude (0.1 to 10 mg mL^{-1}, see the Supplementary Methods). Immersion freezing efficiency of illite NX particles collapsed into a single $n_s(T)$ spectrum, i.e. IN efficiency does not depend on suspended particle mass for the concentration range studied here. This observation is a check for consistency and it implies that ice nucleation is indeed triggered by suspended illite NX particles, and neither by impurities contained in the water used for dilution nor at the glass surface supporting the droplets. If IN efficiency did depend on suspended particle mass, different $n_s(T)$ spectra would result from the various illite NX concentrations, which are shifted by the respective dilution factor.

3.2.2. CSU-IS: This new immersion freezing device was used to investigate the freezing activity of both bulk suspension and size-segregated particles in suspension. A new approach was employed for size-selected measurements, wherein 500 nm mobility diameter size-selected particles were collected on a Nuclepore filter and then rinsed from it for the immersion freezing measurements. The results suggest size independence of n_s within the experimental uncertainties (a combination of binomial sampling error and the uncertainty of conversion of aerodynamic particle diameter to mass) for the range of examined size (500 nm vs. bulk) and mass concentrations of bulk illite NX powder in suspensions from 3.1 x 10^{-6} to

0.5 wt%, for non-size-segregated particles, and 2.2 x 10^{-5} to 4.4 x 10^{-4} wt% for size-segregated particles.

3.2.3. Leeds-NIPI: This suite of cold stage instruments has the capacity to operate using droplets with volumes in the microliter to picoliter range. This enables high resolution immersion freezing analysis for a wide range of temperatures from higher (-22 ˚C < T < -11 ˚C) to lower temperatures (-37 ˚C < T < -26 ˚C). The highest freezing temperatures are attained with the largest droplets, which contain the largest surface area of illite NX. Combined with the previous parameterization reported in *Broadley et al*. (2012), the Leeds-NIPI data follows the overall $n_s(T)$ spectrum defined by the bulk of the instruments. This suggests that immersion freezing efficiency, inferred by $n_s(T)$, of illite NX particles is dependent on neither droplet volume nor mass of illite NX particles in suspension (i.e., wt% 0.1 or 1%); instead the freezing efficiency only depends on the surface area per droplet. Together with CSU-IS, these two instruments provided data points for temperature as high as ~ -11 ˚C, estimating a similar lower-limit of $n_{s,BET}$ values of ~10 m^{-2}.

3.2.4. M-AL and M-WT: Both methods examine individual drops that are freely suspended without any contact with walls or substrates. In M-WT drops are floated at their terminal velocities in a laminar air stream, in which conditions of ventilation and heat transfer are similar to those of droplets falling through the atmosphere. Both M-AL and M-WT techniques analyzed the freezing efficiency of drops containing polydisperse illite NX particles in the temperature range between -14 and -26 °C. The n_s values agree reasonably well with substrate-supported suspension experiments (with the exception of FRIDGE experiments), implying that the surface making contact with the substrate has a negligible effect on immersion freezing for our experimental conditions.

3.2.5. NC State-CS: Extensive experimental conditions were realized by NC State-CS (*Wright and Petters*, 2013; *Hader et al.*, 2014). Unique aspects of this instrument are the sampling of drops within a squalene oil matrix that allows for experiments using cooling rates as slow as 0.01 K min^{-1} and an automated freeze detection algorithm that allows rapid processing of more than 1,000 drops per experiment to improve sample statistics. Drops containing ~0.0001 to 1.0 wt% of the illite NX test sample were studied at a cooling rate of 1 K min^{-1} to find the immersion freezing ability. A total of nine immersion mode freezing experiments, spanning a range of drop volumes from ~400 picoliter to 150 nanoliter, were performed. Using this instrument a wide range of temperatures was investigated (-34 ˚C < T < -14 ˚C) yielding $n_s(T)$ values ranging from 10^2 to 10^{10} m^{-2}. The data from the nine individual runs collapsed into a single $n_s(T)$ spectrum suggesting that the mass loading of dust in the

drop did not affect the measurements for the wt% values investigated. At the high T end (T > -20 °C), the data are in reasonable quantitative agreement with the CSU-IS measurements. At the low T end (T < -20 °C), the data are in agreement with the B12 reference spectrum.

3.2.6. CU-RMCS: The University of Colorado (CU)-RMCS examined the freezing abilities of droplets containing 1.0 wt% illite NX. CU-RMCS detected the warmest immersion freezing of illite NX particles at about -23 °C under the experimental conditions used in the present work (see the Supplementary Methods for further details). Results for -32 ˚C < T < -23 ˚C are from six different experiments using four different droplet size bins: 10-20 μm, 20-60 μm, 60-120 μm, and 120-200 μm (lateral diameter). These droplet sizes correspond to a variation in droplet volume from ~0.3 picoliter to 2.5 nanoliter.

3.2.7. AIDA: The AIDA cloud simulation chamber generates atmospherically relevant droplet sizes (several μm in diameter, varying with cooling rates), and therefore closely simulates mixed-phase cloud conditions. Ice-nucleating efficiencies of both polydisperse and quasi-monodisperse illite NX particles were investigated in this study. n_s of DMA size-selected illite NX particles (200, 300 and 500 nm mobility diameter) agreed well with that of the polydisperse population for immersion freezing experiments, within previously reported uncertainties (T ± 0.3 ˚C and n_s ± 35%; *Steinke et al*., 2011). Thus, a negligible size dependency of n_s for 'submicron' dry illite NX particles for temperatures below -27 ˚C was found. Previously, *Hiranuma et al* (2014a) demonstrated the size independence of the n_s value using two different sizes of submicron hematite particles (200 and 1000 nm volume equivalent diameter) based on AIDA deposition mode nucleation experiments. Such a similarity might remain true for the immersion mode freezing of mineral dust particles that are smaller than 1 μm diameter.

3.2.8. CSU-CFDC: This CFDC provided data for condensation/immersion freezing at around -21.2, -25.1 and -29.7 °C (a total of eight data points with two, two and four points at around each temperature, respectively), which extends to a warmer region than the AIDA measurements. As demonstrated in *DeMott et al*. (2014), higher RH_w values were required for full expression of immersion freezing in CSU-CFDC. The use of 105% RH_w in CSU- CFDC does not capture INP activity for many natural dusts, up to a factor of three INP activities. Comparably, the CSU-CFDC results agreed well with the AIDA measurements within a factor of three in $n_{s,geo}$ estimation (AIDA n_s > CSU-CFDC n_s; *DeMott et al*., 2014). All the CFDC measurements were conducted with 500 nm mobility diameter size-selected particles, as discussed in the Supplementary Methods.

3.2.9. EDB: With EDB, both the contact and immersion mode freezing efficiencies of illite NX particles were investigated. The contact nucleation mode n_s were clearly higher than the immersion mode n_s (by more than one order of magnitude in terms of $n_{s,geo}$, Fig. 5i). This was in part due to the fact that immersion freezing experiments were conducted only when illite NX particles were not frozen via contact nucleation but remained immersed in a supercooled droplet in the EDB cell (see the Supplementary Methods).

3.2.10. FINCH: The immersion freezing results from FINCH showed the highest n_s values in the -22 to -27 ˚C temperature range out of all of the other instrument results. All the FINCH measurements were conducted with 500 nm mobility diameter size-selected particles. Two possible reasons for high n_s values when compared to the other measurements are: 1) an overestimation of n_s due to excess N_{ice} and/or underestimated S_{total} or 2) a large temperature-uncertainty. It is noteworthy that the total INP concentration was kept below 140 L^{-1} in order to avoid saturation limitation due to a high number of growing ice crystals (*DeMott et al.*, 2011). A constant total concentration of particles continuously passing through the chamber was maintained at 1.07 ± 0.17 cm^{-3} (average ± standard deviation).

3.2.11. FRIDGE: FRIDGE data, which cover both measurements of dry and immersed particles with the same instrument but with different sample processing, lie within the upper edge of the bulk of other n_s data points. There are a few important implications from the FRIDGE results. First, on average, the measurements with dry particles in the 'default' setting showed more than an order of magnitude higher n_s in comparison to the immersed particles in FRIDGE experiments (both $n_{s,BET}$ and $n_{s,geo}$, Figs. 4 and 5) at -25 ˚C < T < -18 ˚C. For instance, FRIDGE experiments in the pure immersion mode showed much lower n_s than that with the default setting (i.e., combined deposition and immersion mode), but agreed with other immersion datasets. Second, a sudden increase in $n_s(T)$ was found for the measurements with immersed particles at ~ -20 ˚C, suggesting a dominant activation around -20 ˚C. This transition is a unique behavior only found with the FRIDGE's IN detecting sensitivity. A temperature shift (i.e., shifting the data ~7 ˚C lower) results in FRIDGE data overlapping with the bulk of other data and may offset discrepancies. However, other mechanistic interpretations (e.g., contribution of agglomeration) are also plausible causes of this discrepancy. More detailed discussions of the role of agglomerates upon n_s and sample processing are available in Sect. 4.4 and 4.5.

3.2.12. LACIS: With the shortest instrument residence time (~1.6 s), LACIS measured immersion mode freezing of illite NX particles for three different mobility diameters (300, 500 and 700 nm) from -31 ˚C down to the homogeneous freezing temperature. Similar to

AIDA results, a size independence of n_s of submicron illite NX particles was observed within defined experimental uncertainties (see the Supplementary Methods). Further, without any data corrections, the results of LACIS reasonably agreed with AIDA measurements. Furthermore, though there is no overlapping temperature range for LACIS and CSU-CFDC in the present study, consistency between data from LACIS and CSU-CFDC for other clay minerals (i.e., different kaolinite samples) has been described previously (*Wex et al*., 2014). The results from both instruments agreed well with each other from a data evaluation based on n_s, and this agreement was even improved when the different residence times in LACIS and the CSU-CFDC were accounted for (i.e., when nucleation rate coefficients were compared). Furthermore, a size independence of the immersion mode freezing was seen for Fluka-kaolinite particles with mobility diameters of 300 and 700 nm in *Wex et al*. (2014), and for illite NX particles when comparing particles with mobility diameters of 500 nm to bulk material (*Augustin-Bauditz et al*., 2014).

3.2.13. MRI-DCECC: Comparison between polydisperse and size-selected (300 nm mobility diameter) measurements in this cloud simulation chamber demonstrated the size independency of n_s for submicron illite NX particles for slightly higher temperatures (up to -21 ˚C) than AIDA results. Interestingly, MRI-DCECC data exhibited at least an order of magnitude higher n_s values than most other suspension measurements. We note that only negligible freezing events were detected above -21 ˚C even with a ~9000 cm^{-3} number concentration of polydisperse illite NX particles in part due to the detection limit of the welas optical counter of N_{ice} = 0.1 cm^{-3}.

3.2.14. PINC: PINC provided data for immersion freezing at around -25.4, -30.2 and -34.6 °C (a total of nine data points with one, four and four points at around each temperature, respectively). The estimated n_s values are in agreement with other measurements for the test range of -35 ˚C < T < -25 ˚C after applying a residence time correction of about a factor of three. The data are for ice nucleation onto 500 and 1000 nm mobility diameter illite NX particles; therefore, an OPC threshold size of 2 µm for ice detection is used. The impactor used for sampling particles into PINC was characterized for size-resolved particle losses and was found to have a cutoff (D_{50}) of 725 nm mobility diameter. As such, when determining $n_{s,geo}$ the particles losses (25 to 60%, see the Supplementary Methods for more details) were taken into account for calculating activated fractions. We note that $n_{s,geo}$ increased after adjusting the data, resulting in agreement between the data from PINC and data from LACIS, AIDA and UC-RMCS in the temperature range from -25 to -35 ˚C.

692 **3.2.15. PNNL-CIC:** The IN efficiency of illite NX particles in the immersion mode in
693 the temperature range of -35 ˚C < T < -27 ˚C was observed to increase at lower temperatures.
694 Estimated n_s values were somewhat higher in this temperature range when compared to those
695 from most of the other measurements. Data were obtained at conditions where PNNL-CIC
696 was operated at 105% RH_w at three different temperatures. Dust particles greater than ~1 μm
697 (50% cut size) were removed before they were size-selected and transported to the PNNL-
698 CIC. The OPC detection threshold was set ≥3 μm; see the Supplementary Methods for more
699 details.
700 **3.2.16. IMCA-ZINC:** Coupled with IMCA, ZINC showed reasonable agreement with
701 AIDA and PNNL-CIC. This reproducibility verified the performance of the IMCA-ZINC
702 combination, which was not tested during ICIS-2007 (*DeMott et al*., 2011), perhaps due to the
703 similarity in the experimental conditions (i.e., particle generation) to the other two methods.
704 We also note that the residence time in ZINC is about a factor of three longer than that in
705 PINC. The IMCA-ZINC measurements in comparison to the measurements with ZINC alone
706 (i.e., a combination of deposition nucleation, contact-, condensation-, surface condenstation-
707 and immersion freezing) is discussed in Sect. 4.5 in more detail.
708 Overall, as described above (Sects. 3.2.1 to 3.2.6), suspension experiments with cold
709 stage devices and levitation techniques provide IN measurements under more controlled (with
710 respect to droplet size, concentration and mass of particles) conditions and a wider
711 temperature range (up to -11 °C) than comparable dry-dispersed particle experiments. The
712 resulting n_s values from these suspension experiments are also independent of the total
713 number of droplets and suspended dust particle mass.
714 The estimated n_s values of dry test particles below -25.5 ºC are in reasonable
715 agreement with a previous study (*Broadley et al*., 2012) at temperatures below -25 ˚C.
716 Furthermore, the strong temperature dependence and size independence of n_s may suggest a
717 uniform distribution of freezing sites over the total surface of illite NX particles in the
718 immersion mode in this temperature range. Specifically, AIDA and MRI-DCECC have shown
719 size-independent n_s values for submicron dry-dispersed particles. Overall, compared to
720 suspension measurements, dry-dispersed particle measurements showed higher n_s values. For
721 example, FINCH is the only instrument which showed higher n_s values than the
722 parameterization by *Niemand et al*. (2012) for ATD. Likewise, AIDA results indicated
723 slightly higher n_s values than CSU-CFDC's results. The lower n_s of CSU-CFDC may be a
724 consequence of underestimation of N_{ice}, possibly due to its constrained RH_w (at 105%) and/or
725 the disturbance of aerosol lamina between two plates in a CFDC (*DeMott et al*., 2014).

3.3. Inter-comparisons based on the slope parameter of $n_s(T)$ spectra

A compilation of seventeen n_s spectra from seventeen instruments in a temperature range between -10.1 and -37.5 ˚C is presented in Fig. 6. For both the geometric area-based and the BET area-based n_s, the differences among measurements can be more than one order of magnitude at any given temperature. Diversity is especially pronounced for several orders of magnitude in n_s at -27 ˚C ≤ T ≤ -18 ˚C, where the results from suspension measurements and a majority of dry measurements coexist (see the investigated T range for each technique in Table 1). Another notable feature of this specific temperature range in Fig. 6 is the coincidence of the steepest slope in the spectrum (i.e., the absolute value of $\Delta\log(n_s)/\Delta T$ in log m^{-2} ˚C^{-1}, hereafter denoted as $\Delta\log(n_s)/\Delta T$) when compared to other temperature ranges. For instance, n_s increases sharply at temperatures colder than -18 ˚C to be nearly parallel to the A13 parameterization down to -27 ˚C, where it starts leveling off and is eventually overlapping with the N12 parameterization at the low temperature segment.

Correspondingly, the overall trend of the spectrum is traced by the measurements from NC State-CS alone (Fig. 4e). Moreover, the slopes of the spectrum for three sub-segments (-34 ˚C < T < -27 ˚C, -27 ˚C < T < -20 ˚C, and -20 ˚C < T < -14 ˚C) can be calculated from interpolated data and compared to N12 and A13 parameterizations. As expected, the steepest slope in the spectrum (= 0.66) of the NC State-CS data was found in the -27 ˚C < T < -20 ˚C range, which was similar to that of the A13 parameterization (0.45 for T > -25 ˚C). However, smaller slope values are found for the other two segments (0.18 for T < -27 ˚C and 0.29 for T > -20 ˚C), which are comparable to the temperature-independent N12 slopes (0.17 for ATD and 0.22 for Dust) and the B12 slope (0.25 for -35 ˚C < T < -27 ˚C), suggesting that a dominant fraction of INP contained in our test dust becomes ice active in immersion freezing at -27 ˚C < T < -20 ˚C. In addition, FRIDGE immersion mode measurements also show a sharp decrease in $\Delta\log(n_s)/\Delta T$ (from 0.59 to 0.25, Figs. 4k and 5k) for the measurements with immersed particles at ~ -20 ˚C. Similar observations are made by most of the other suspension measurement techniques. In short, most suspension methods capture the steepest segment of the $n_s(T)$ spectral slopes ($\Delta\log(n_s)/\Delta T$) at -27 ˚C < T < -20 ˚C, where the slope is nearly parallel to the A13 parameterization. One exception is CU-RMCS (Fig. 4f). The highest possible freezing temperature investigated by this experimental system was about -23 ˚C with ~2.5 nanoliter droplets containing 1.0 wt% illite NX (see the Supplementary Methods). Hence, CU-RMCS did not capture the transition in $\Delta\log(n_{s,BET})/\Delta T$ at around -20 ˚C, but the steep slope of the spectrum (= 0.36) validated the high density of IN active sites below -23 ˚C.

760 The error in temperature for this technique is always ± 0.5 ˚C, based on freezing experiments
761 without any foreign substances in supercooled drops (i.e., homogeneous freezing
762 experiments).
763 Similarly, dry-dispersed particle measurements also exhibit scattered data for their
764 measured temperature ranges. Both agreements and equally important disagreements were
765 observed. First, the agreements are summarized. AIDA data show that the values of
766 $\Delta\log(n_{s,geo})/\Delta T$ (= 0.22, Fig. 5g) are identical for both polydisperse and size-selected
767 measurements, perhaps suggesting a uniform distribution of active sites over the available
768 S_{total} of illite NX in this study. Similarly, IMCA-ZINC's $\Delta\log(n_{s,geo})/\Delta T$ (= 0.24, Fig. 5p)
769 derived from 200, 400 and 800 nm mobility diameters is virtually identical to the slope
770 estimated from AIDA measurements. PINC estimated $\Delta\log(n_{s,geo})/\Delta T$ (= 0.26, Fig. 5n) values
771 are in reasonable agreement with AIDA and IMCA-ZINC and N12 parameterizations at
772 temperatures below -25 ˚C. From the CSU-CFDC results, $\Delta\log(n_{s,geo})/\Delta T$ derived from
773 interpolated data is 0.40 (Fig. 5h). Considering the AIDA and CSU-CFDC data, the $n_s(T)$
774 spectrum depicts similar trends (i.e., n_s or temperature deviation around -27 ˚C) compared to
775 those seen in the NC State-CS results (Fig. 5e) and is also parallel to the A13 curve (slope =
776 0.45) down to temperatures around -27 ˚C and is parallel to the N12 Dust curve (slope = 0.22)
777 for the lower temperature segment. LACIS measurements show that $\Delta\log(n_{s,geo})/\Delta T$ (= 0.19,
778 Fig. 5l) is also in agreement with that from AIDA, verifying a deteriorated freezing ability of
779 illite NX particles in the investigated temperature range. EDB was used to examine both the
780 contact and immersion freezing modes. Nonetheless, the slopes of the spectra for both modes
781 (0.11 for immersion mode freezing and 0.16 for contact mode freezing, Fig. 5i) are similar to
782 the N12 ATD curve (slope = 0.17). From the fact that the value of $\Delta\log(n_{s,geo})/\Delta T$ of FINCH
783 (= 0.27, Fig. 5j) above -27 ˚C is similar to that of the N12 dust parameterization (whereas this
784 relationship would be expected below -27 ˚C), we suspect that a temperature uncertainty may
785 be the main cause of the observed deviation of its data from others. Lastly, at -35 ˚C < T < -27
786 ˚C, PNNL-CIC's $\Delta\log(n_{s,geo})/\Delta T$ (= 0.19, Fig. 5o) agreed well with that of the N12 dust
787 parameterization in the same temperature range.
788 Next, the disagreements between dry-dispersed particle and suspension measurements
789 are discussed. Specifically, the MRI-DCECC results show lower values of $\Delta\log(n_{s,geo})/\Delta T$ (=
790 0.29) up to -21 ˚C as compared to the suspension measurements. Additionally, in the
791 temperature range from -29 ˚C < T < -21 ˚C, the MRI-DCECC data show higher values of n_s
792 than those observed in suspension measurments. This relatively constant $\Delta\log(n_s)/\Delta T$ value
793 along with higher n_s values through the range contrasts with the observed sharp transition in

$\Delta\log(n_s)/\Delta T$ in suspension measurements. We note that MRI-DCECC experiments may have been carried out in the presence of a high degree of agglomeration (Fig. 2c and d). Hence, particle processing (i.e., drying and suspension) may not be the only factor causing this difference and other contributions cannot be ruled out (see Sect. 4).

To conclude, the results from suspension and dry measurements suggest evidence that the n_s of illite NX particles derived from immersion freezing is independent of or only weakly dependent on droplet size, mass percent of illite NX sample in suspension and droplets, particle size of the tested illite NX and cooling rate during freezing in the range of conditions probed; see the Supplementary Methods for more detailed information regarding experimental conditions for each instrument. Overall, the sample-processing (i.e., dry vs. suspension sample) may have an effect on the immersion freezing efficiency of illite clays. A more detailed discussion will follow in Sect. 4 below.

4. Discussion

For detailed comparison of methodologies, the immersion freezing properties of illite NX particles in a wide range of temperatures is further discussed by comparing $n_s(T)$ spectra from all seventeen instruments (Sect. 4.1). Specifically, we present T-binned average data (i.e., 1 ˚C bins for -37 ˚C < T < -11 ˚C). A moving average (where original data points are finer than 1 ˚C) or a Piecewise Cubic Hermite Interpolating Polynomial function (where original data points are coarser than 1 ˚C) was used for data interpolation. All data from the seventeen instruments, as shown in Figs. 4 and 5, were interpolated.

We also discuss potential reasons for the diversity observed from inter-comparisons of dry and suspension measurement techniques. Both systematic errors (Sect. 4.2) and mechanistic uncertainties (Sect. 4.3 to 4.6) are qualitatively evaluated to understand the measurement uncertainties of such techniques. Some factors may introduce diversity in n_s, whereas others may shift activation temperatures horizontally to match the n_s values from other instruments, perhaps biasing the overall accuracy and precision of instruments. Here we address the relative importance of those factors with respect to their effect on the estimation of n_s.

4.1. Dry vs. suspension $n_s(T)$ data

The multiple exponential distribution fits (also known as the Gumbel cumulative distribution function) for T-binned data are shown in Fig. 7. The fits for T-binned maxima and minima n_s from seventeen measurement techniques are presented as pink shaded areas. All fits presented in this figure are derived using parameters shown in Table 3. As can be inferred from the table, a higher correlation coefficient (r) was found when inter-comparing the suspension measurements as compared with inter-comparing the dry-dispersed methods, suggesting reasonable agreement and consistency for the results from immersion freezing studies with suspensions. Interestingly, a higher r for $n_{s,geo}$ than $n_{s,BET}$ was found for dry-dispersed particle measurements as compared to the suspension measurements. The use of more conversion factors to estimate $n_{s,BET}$ (i.e., from Eqn. 3 and 4) may introduce uncertainties and discrepancies between these measurement techniques. It is also noteworthy that the T-binned ensemble maximum and minimum values are largely influenced by dry-

dispersed particle and suspension results, respectively, implying the previously discussed discrepancy between these two techniques.

It is observed that the largest deviation between the maxima and minima in the horizontal and vertical axes, corresponding to $Hor_{Max\text{-}Min}$ and $Ver_{Max\text{-}Min}$, respectively, shown in Fig. 7, is similar for both $n_{s,BET}$ (Fig. 7a) and $n_{s,geo}$ (Fig. 7b). Nevertheless, $n_{s,BET}$ is representative of measurements with suspended samples because fewer corrections and assumptions are involved for its estimation when compared to that with dry-dispersed particles. Hence, $n_{s,BET}$ may be a good proxy for comparing IN efficiencies of dust particles from various instruments. We also report the absolute values of $\Delta\log(n_s)/\Delta T$ for four *T*-segregated segments based on *T*-binned Lin. Avg. (multiple exponential distribution fit to the *T*-binned average data in the linear space), *T*-binned Max. (fit to the *T*-binned maxima in the linear space) and *T*-binned Min. (fit to the *T*-binned minima in the linear space) in Fig. 7 (i.e., T_1 to T_4). The slopes are comparable to the slope of the A13 parameterization in the T_1 to T_3 segments (-11 to -27 ˚C), while the slope in the T_4 segment is similar to those of the N12 parameterizations. These results are consistent with the results described in Sect. 3.3. Further, $Ver_{Max\text{-}Min}$ for roughly three orders of magnitude with respect to n_s is observed in a temperature region around ~ -20 ˚C for both $n_{s,BET}(T)$ and $n_{s,geo}(T)$ spectra. Such high n_s variability was expected due to the contribution from MRI-DCECC, FINCH and FRIDGE measurements, which may have influenced the overall fit in that temperature range. Likewise, our $Hor_{Max\text{-}Min}$ shows that the seventeen measurements are in reasonable agreement within 7.8 ˚C (-36.8 ˚C, -33.0 ˚C, -29.0 ˚C (*min*, *log fit*, *max*)) at $n_{s,BET}$ of 5.2 x 10^9 m^{-2} and 7.5 ˚C (-36.7 ˚C, -32.8 ˚C, -29.2 ˚C (*min*, *log fit*, *max*)) at $n_{s,geo}$ of 1.5 x 10^{11} m^{-2}.

T-binned $n_{s,BET}(T)$ and $n_{s,geo}(T)$ spectra are presented in Fig. 8a and b, respectively. In this figure, panels i, ii and iii show *T*-binned data averaged in the linear space of all seventeen instruments, all suspension type measurements, and all measurements that involved dry particles, respectively, while panel iv shows a comparison between suspension and dry-particle measurements. We note that the data from 'EDB (contact)' and 'ZINC' (*Welti et al.*, 2009) were not used for generating *T*-binned data since our focus was on immersion mode freezing. We also note that the n_s results from nine IN measurement techniques provide n_s data at -23 ˚C and -24 ˚C, where we find an abrupt increase in $\Delta\log(n_s)/\Delta T$ and n_s deviations. Investigated *T* ranges for each instrument are listed in Table 1.

As described in Sect. 3.2, suspension measurements possess sensitivity at high temperatures (up to -11 ˚C), indicating that their ability to control the concentration or dilution of suspension over a wide range is of great advantage in detecting rare INPs. Moreover,

suspension experiments with small picoliter or nanoliter droplets allow measurements right down to the homogeneous freezing limit (~ -37 ºC; *Koop et al*., 2000). In turn, suspension methods with microliter droplets may run into 'background problems' at temperatures below about -20 °C to -25 °C for samples that do not contain many IN active at these temperatures, because then impurities contained in the water may trigger freezing. Conversely, dry aerosol methods lack sensitivity for detecting rare IN at high temperatures because of their low sample volume. These dry particle measurements are in general good for low temperature measurements, where the number of particles nucleating ice increases and instruments have higher ice detection efficiencies. For temperatures below -27 ˚C, our *T*-binned fits exhibit a reasonable agreement with the suspension experiments reported by *Broadley et al*. (2012). Furthermore, dry-dispersed particle measurements show higher n_s values when compared to suspension measurements above about -27 ºC (Fig. 8iv). We will discuss possible explanations for the observed diversity of data from different techniques in detail below.

In addition, *T*-binned $n_{s,\mathrm{BET}}(T)$ and $n_{s,\mathrm{geo}}(T)$ spectra averaged in the log space are presented in Fig. S3. Similarly, we also present *T*-binned ratios of the individual measurements to the log fit of the data [All (log), Sus (log) or Dry (log) from Table 3] across the temperature range covered for all the measurement techniques (-37 ˚C < T < -11 ˚C) in the Supplement Figs. S4-S8. These figures provide inter-comparisons of the n_s deviations across the various techniques employed in this study.

4.2. Limitations of instrument types

Groups participating in this study used different experimental setups to measure immersion freezing efficiencies of illite NX test samples. As a consequence, various experimental procedures, such as particle generation, particle size-segregation, S_{total} estimation, ice crystal detection or counting, ice crystal detection size limits for OPCs or CCDs, and particle loss at the inlet and/or in the chamber can potentially yield substantial systematic uncertainties in the estimation of n_s. Below we qualitatively discuss potential errors and limitations involved in each instrument-type (cold stage, levitator, CECC and CFDC).

Limitations of substrate-supported optical microscopy and cold stage experimental setups may come from inhomogeneous cooling of the substrate and the surrounding media, the effects of RH changes surrounding the drops for non-substrate-supported cold stage setups, potential contamination during sample preparation and measurements (e.g., particle

processing in a solvent) and/or uncontrollable heat transfer between the cold plate surface and the particle substrate (e.g., FRIDGE).

Levitator techniques require extensive pre-characterization of physico-chemical properties. Furthermore, since the overall system characterization is more complex and labor intensive, only specific subsets (i.e., suspended samples or reference particles) can be examined using this method.

The development of AIDA-CECC allows the simulation of atmospherically representative cloud parcel formation and evolution (*Möhler et al*., 2003). Therefore, it is an advantage of CECC that the parameterization derived from its experiments can be most readily extended to atmospheric conditions (*Niemand et al*., 2012). Development of large (up to 84 m^3, i.e., AIDA) and/or temperature-controlled dynamic cloud simulation chambers (e.g., MRI-DCECC; *Tajiri et al*., 2013, a design which follows from *DeMott and Rogers,* 1990) enabled the exploration of heterogeneous ice nucleation properties of typical particulate samples in a wide range of particle concentrations, temperatures (-100 ˚C < T < 0 ˚C), cooling rates and nucleation times. However, the utilization of such an instrument to correctly measure the totality of INPs with a reasonable detection sensitivity (<0.1 L^{-1}), both in the lab and field settings, has not yet been realized due to CECC's limitations. These limitations include ice losses by settling (e.g., *DeMott and Rogers,* 1990) over the relatively long expansion periods in the confined vessel and internal turbulence during the expansion leading to heterogeneously supersaturated water vapor and temperature fields. These artifacts can bias IN measurements.

CFDCs are the most widely used technique to measure INPs in the atmosphere, but their inability to quantify INPs at high temperatures is an issue that exists due to the physical principals of operation, the limited sample volume (typically 1 to 2 L min^{-1}) and background frost formation in the chamber over periods of operation. Based on the operational equations in *Rogers* (1988), the warmest operating temperature of a CFDC is approximately -6.5 °C, controlled by the fact that the warmest wall cannot exceed 0 °C. Low sample volumes necessitate integration over longer sample periods and result in a general lower detection limit of 0.2 L^{-1} of sampled air, absent any particle pre-concentration (*Prenni et al*., 2009). According to *Tobo et al*. (2013), the highest temperature that can be achieved in a CFDC is -9 ˚C. Above this threshold, temperature and ice saturation conditions cannot be maintained in the chamber. *Rogers et al.* (2001) and other papers since have identified measurement issues due to frost emanating from the walls of the chamber when the dew point temperature of the sample air is not effectively controlled, although this appears to be an operational issue that

can be mitigated if monitored properly, and will be most obtrusive for atmospheric sampling scenarios.

4.3. Stochastic nature of freezing and time dependence

The longstanding discussion of the stochastic theory (i.e., the freezing process is time-dependent) vs. the deterministic approximation (i.e., freezing occurs at specific temperature and humidity conditions) of heterogeneous freezing has introduced another complication towards complete understanding of heterogeneous ice nucleation in the atmosphere (*Vali*, 2014). Many studies have attempted to characterize ice nucleation based on the classical nucleation theory (CNT), which incorporates a nucleation rate (*Murray et al*., 2012; *Kashchiev*, 2000; *Mullin*, 2001). In this treatment, the ice nucleation process is always of a stochastic nature (i.e., time-dependent; *Bigg*, 1953; *Vali*, 1994; *Vali*, 2014). According to the nucleation rate approach, the heterogeneous ice nucleation rate is strongly sensitive to INP size and the kinetic activation energy of the ice embryo on the nucleating site/surface at a specific temperature (*Khvorostyanov and Curry*, 2000; *Fletcher*, 1962). A few variants of the CNT-based approaches have been developed over the past few decades. These approaches assume uniform surface characteristics and only one ice nucleation probability (i.e., a single contact angle), nominally categorized as the single component nucleation rate approach (e.g., *Bigg*, 1953). Several recent studies have applied a probability density function (PDF) of contact angles and active sites over the INP surface in CNT, or in other words described a distribution of nucleation efficiencies, bridging the gap between the stochastic theory and the deterministic treatment (*Marcolli et al*., 2007; *Lüönd et al*., 2010; *Kulkarni et al*., 2012; *Niedemeier et al*., 2011; *Wright and Petters*., 2013; *Broadley et al*., 2012).

The deterministic or time-independent singular approximation has been developed as an alternative option to quantitatively understand atmospheric ice nucleation. The concept was first developed by *Levine* (1950), while the term "active sites" per surface area was introduced by *Fletcher* (1969). More recently, *Connolly et al*. (2009) introduced the n_s density parameterization (see Sect. 2.4). This specific approach neglects the time dependence of freezing, and assumes that a characteristic condition (e.g., temperature) must be met to nucleate ice. The semi-deterministic forms of the singular approach have a cooling rate dependence incorporated (*Vali*, 2008; *Herbert et al*., 2014). Predicting ice nucleation from a singular perspective does not require a vast knowledge of particle-specific parameters (e.g., surface composition, structures, surface tension and solubility) that are particular to each ice

nucleus and, therefore, enables ice nucleation parameterization to be relatively simple and efficient compared to the CNT-based approaches (*Murray et al.*, 2011).

The assumption that the time dependence of the freezing of droplets is of secondary importance when compared to temperature dependence is supported by a recent modeling sensitivity study that shows that common INPs are substantially more sensitive to temperature than to time (*Ervens and Feingold*, 2013). Furthermore, while *Broadley et al.* (2012) shows that freezing by illite NX is time-dependent through isothermal experiments, the shift in freezing temperature on changing cooling rates by an order of magnitude is less than 0.6 ˚C, which is within the experimental uncertainty. A similar observation of weak time dependence of immersion freezing for various types of suspended samples, inferred by comparing the results with varied cooling rates from 0.01 ºC min^{-1} to 1 ºC min^{-1}, is reported by *Wright et al.* (2013).

In the context of dry-dispersed measurements, the sensitivity of the ice nucleation to a possible time dependence, and the respective influence on n_s, was examined to further discern its importance and uncertainty. Specifically, a contact angle distribution was fitted to the LACIS measurements and was used, together with the soccer ball model (SBM; *Niedermeier et al.*, 2011 and 2014), to simulate frozen fractions for different residence times varying over four orders of magnitude (i.e., 1, 10, 100 and 1000 s residence time). These frozen fractions were then used to calculate n_s, shown as lines in Fig. 9. More specifically, frozen fractions for 500 nm diameter illite NX particles were calculated based on SBM to obtain $n_s(T)$ spectra. To accomplish this, a contact angle distribution was used which was derived based on LACIS data for the illite NX particles as shown in this work, resulting in values of 1.90 rad for the mean and 0.27 rad for the width of the contact angle distribution. Frozen fractions were obtained for ice nucleation residence times of 1, 10, 100 and 1000 s. An increase in the residence time by a factor of 10 resulted in a shift of approximately 1 °C towards higher freezing temperatures. This is similar to the results found in a previous study by *Welti et al.* (2012) for measurements of kaolinite rich clay minerals. Indeed, $n_{s,geo}$ data obtained from AIDA agree within the measurement uncertainty with LACIS data without accounting for time dependence. These results suggest that time dependence of immersion freezing for illite NX particles can be neglected as a factor in the comparisons shown in Figs. 4, 5 and 6. They also imply that the immersion freezing nature of illite NX is only slightly dependent on cooling rate across a wider range of temperatures (as compared to a -26 ˚C to -37 ˚C range as shown in *Broadley et al.*, 2012), regardless of the sample preparation process.

4.4. Potential effect of agglomerates

As seen in the particle surface area distributions (Fig. 2) and agglomerated-fractions based on a relative comparison to D_{95}, aggregates are rather persistent and dominant for most of the dry-dispersed particle measurements. Since dry aggregates can have large 'supermicron' sizes, they may have different IN propensities and efficiencies (*Wheeler et al.*, 2014) as compared to the smaller sizes investigated in the present study (i.e., up to 1000 nm from PINC). Further, the degree of agglomeration may conceivably affect the surface area exposed to liquid water when suspended in supercooled droplets. Hence, an overall quantification of the effect of agglomerates is difficult. Moreover, the degree of agglomeration seems to vary from experiment to experiment, introducing diversity on the estimation of S_{total} of particles and n_s for dry-dispersed particle measurements. For instance, a combination of several methods for particle dispersion and subsequent particle size selection was employed for particle generation from illite NX samples. Further, most of the dry dispersion techniques used upstream impactors to filter out large agglomerated particles and avoid counting these large particles as INPs. The different types of dispersion methods, impactors and size segregating instruments used in the present work are listed in the Supplement Table S1. These different aerosol generation processes may have caused different degrees of agglomeration. This may in part explain why n_s measurements obtained using dry dispersion techniques deviated from those using suspension measurements. Further quantification of the influences of different methods for particle dispersion, size-segregation and particle impaction/filtration on the estimation of S_{total} and n_s is an important topic for future works.

In contrast, in suspension experiments, illite NX samples were directly suspended in water. Despite no pre-treatments (e.g., pre-impaction or size segregation), suspended particles appeared adequately de-agglomerated (Fig. 2a). Though the number of immersed particles can vary from droplet to droplet and the random placement of particles in the drop may have an effect on the n_s values, the n_s spectra from suspension measurements are in reasonable agreement with slight deviations even over a wide range of wt% of illite NX samples (the Supplement Figs. 6, 8, S4-S8). Thus, the influence of the random placement of particles in the drop and agglomeration on the n_s estimation for suspension measurements seems small. To support this, *Wright and Petters* (2013) and *Hader et al.* (2014) simulated the role of a statistical distribution in drops. The authors demonstrated that the random component due to drop placement seemed to be small relative to the statistical variation due to nucleation

probability. Hence, assuming the degree of agglomeration or flocculation is similar in all suspension samples, the degree of agglomeration and the random placement of particles in the drop may lead to less pronounced deviations in n_s when compared to dry-dispersed measurements.

4.5. Nucleation mode dependence

While all suspension methods only measured immersion mode freezing of the illite NX particles, a contribution of other nucleation or freezing modes cannot be ruled out for dry-dispersed particle measurements. Hence, we now discuss inferences in the present experiments regarding the mode dependency of the ice nucleation ability of illite NX particles. Figure 10a and b show the comparison of n_s derived from the two different operation types of FRIDGE measurements. For instance, 'default mode' considers deposition mode nucleation and immersion mode freezing of dry particles in which RH_w is scanned upwards and 'imm.mode' counts immersion freezing of suspended particles in which the particles are first washed into droplets and then placed on the substrate. With these two different operational modes, FRIDGE investigated the ice nucleation ability of both dry and droplet suspended particles deposited on a substrate (see the Supplementary Methods). FRIDGE scans RH_{ice} and RH_w (low to high) at a constant temperature. During such scans an abrupt increase in an activated ice fraction near water saturation as well as the highest N_{ice} is typically observed. We consider ice crystals formed at the highest RH_w (near 100% RH_w) as a measure of immersion N_{ice} from dry-dispersed particle measurements in this study. Some default runs of FRIDGE show much higher $n_{s,BET}$ values compared to the immersion mode runs. This difference may be a consequence of the different IN efficiencies of nucleation modes (deposition + immersion vs. immersion alone) in the examined temperature range (-25 °C < T < -18 °C), the different sample preparation processes (dry or suspended sample), effects of agglomeration or a combination of the three. We note that a major difference between the two measurement setups is the pressure within the instrument. For instance, default conditions involve processing at a few hPa of water vapor while the immersion measurements are conducted at atmospheric pressure. In addition, corrective post-analysis of droplet/ice separation was taken into account in this study, so that errors from counting large droplets as ice crystals were successfully removed. Interestingly, our comparison suggests that n_s values derived from the FRIDGE default mode seem similar to those from MRI-DCECC, in which experiments were carried out with a high degree of particle agglomeration (Fig. 2c).

Some other variations on applied methods suggest nucleation mode effects on the IN efficiency of illite NX particles at lower temperatures (Fig. 10c and d). For instance, the comparison between ZINC and IMCA-ZINC show about an order of magnitude diversity in $n_{s,BET}$ beyond experimental uncertainties at -33 ˚C, suggesting a mode-dependent IN efficiency of clay minerals at this temperature. This observation is consistent with a statement that the immersion freezing parameterization from CNT may not reliably predict the activated fraction observed at RH_w > 100% as observed from condensation freezing (*Welti et al*., 2014). However, this is in contrast to observations indicated by PNNL-CIC below -25 ˚C and to results presented in *Wex et al*. (2014), where $n_{s,geo}$ obtained from kaolinite measurements made with LACIS and the CSU-CFDC (at 104% > RH_w > 106% for the latter) agreed well. When a freezing point depression is taken into account, even data obtained with the CSU-CFDC for water-vapor-sub-saturated conditions is in agreement with data obtained from both LACIS and CSU-CFDC at water-vapor super-saturated conditions. Concerning data presented here, PNNL-CIC and IMCA-ZINC measure condensation/immersion and purely immersion mode freezing efficiency of particles, respectively, and are in reasonable agreement within experimental uncertainties (Fig. 10c and d). Thus, the observed inconsistencies between methods should be subject to further methodological improvements to provide accurate data as a basis for model parameterization. Similar heterogeneous ice nucleation mode-dependent observations were made by our EDB experiments. We observed that n_s values derived from contact freezing experiments were higher than those derived from immersion experiments (Fig. 10c and d). As described in the Supplementary Methods, immersion mode experiments were performed for the droplets, which were not activated via contact freezing.

4.6. Effect of mineralogical properties: which component of illite NX nucleates ice?

Atkinson et al. (2013) suggested that the mass fraction of K-feldspar in a sample can be used as a scaling factor to estimate the n_s values of other K-feldspar containing dust and soil samples. *O'Sullivan et al*. (2014) showed that this scaling rule could be used as an approximate predictor for the n_s of soil samples once the biological ice-nucleating particles were deactivated. However, inspection of Fig. 6 reveals that the line based on 14% feldspar (assuming all microcline) significantly over predicts the n_s values for illite NX. There are a number of reasons why this might be.

The K-feldspar sample used by *Atkinson et al*. (2013) was the British Chemical Standard Chemical Reference Material (BCS-CRM) number 376/1 and X-ray diffraction

analysis shows that the crystal structure is consistent with that of microcline. Microcline is one possible form of a K-feldspar and, as discussed above, other feldspars are sanidine and orthoclase, which have distinct crystal structures. The ice nucleation abilities of sanidine and orthoclase are not yet published, but given they have different crystal structures they may have different nucleating abilities. Unfortunately, the X-ray diffraction analysis of illite NX is unable to identify the K-feldspar(s) present in illite NX, although the minerological analysis conducted as part of this study concluded that there was no detectable microcline in illite NX. Hence, one explanation for the K-feldspar scaling rule not working for illite NX is that there is only a trace of the strongly ice active microcline present in illite NX. For suspension measurements, only the 0.0014% microcline parameterization reproduces the slope and magnitude of the illite NX data in Fig. 6, but this quantity of microcline is well below the detection limit of the X-ray diffraction technique. Perhaps, in the case of illite NX, it may not be the feldspar which triggers nucleation, but instead it could be another mineral present in this sample. For example, *Atkinson et al*. (2013) found that a quartz sample nucleated ice more efficiently than the clay minerals, but less efficiently than the feldspar samples they used. At about -28 ˚C, they reported an n_s of ~10^{10} m^{-2}. The X-ray analysis in this study revealed the presence of 3% quartz, hence we would predict an n_s of $3x10^{8}$ m^{-2}, which is consistent with the illite NX data. Finally, an alternative explanation is that the surfaces of K-feldspars are chemically altered in illite NX. The surfaces of feldspars are known to transform to an amorphous silicate which can then recrystallize as a clay if exposed to an acidic environment. *Wex et al*. (2014) suggested that it was the acid processing of K-feldspar which deactivated Fluka-kaolinite. It is feasible that the surfaces of feldspar grains in illite NX have at some point become deactivated. More quantitative investigations of the acid processing of both reference and atmospherically relevant materials and its influence on their immersion mode ice nucleation efficiencies are needed.

Recently, re-partitioning of soluble components of both swelling and non-swelling clay minerals and their effect on cloud condensation nucleation activity was reported (*Sullivan et al.*, 2010; *Kumar et al.*, 2011; *Garimella et al*., 2014). To address a potential importance of this effect on the ice-nucleating activity of illite NX in the wet dispersion experiments, we have measured the concentration of cations released by the illite NX sample placed into deionized water as a function of time, as described in Sect. 3.1 (i.e., Fig. 3).

It is instructive to compare the quantity of cations released by illite NX into an aqueous environment with the value of the Cation Exchange Capacity (CEC) for illite, which is known to be 25 to 40 cmol kg^{-1}(*Meunier and Velde*, 2004). CEC is defined as the amount of

cations retained by all the negative charges in 100g of clay immersed in water at *pH* 7 (e.g., see *Meunier*, 2005). Per this definition, CEC describes the total quantity of exchangeable cations, including interlayer cations which are in fact not accessible for substitution in non-swelling clays. The molar fraction of external cations, located on the basal planes of the crystals and on the crystal edges is roughly evaluated for illites as 20% of the total CEC, yielding 5 to 8 cmol kg^{-1}(*Wilson*, 2013). Remarkably, the total amount of all cations (K^+, Mg^{2+} and Ca^{2+}) released within the first hour by illite NX, if recalculated with account for cation valence and for the actual mass of illite in the aqueous suspension (0.1 g), gives the number 7.5 cmol kg^{-1}, which corresponds nicely with the upper bound of the external CEC (8 cmol kg^{-1}). Furthermore, *Grim* (1953) has shown that the CEC of illite increases with decreasing size of the clay particle size, with the upper bound (~40 cmol kg^{-1}) being characteristic for illite with a particle size below 100 nm. This is again consistent with the very small size of particles in illite NX.

These findings have two potential implications for the measurements of illite NX ice-nucleating efficiency obtained with different instruments. First, in the methods where dry illite NX particles are activated to droplets prior to cooling, the concentration of cations released into the water surrounding the particles is still far from the equilibrium and is a function of the residence time (e.g., ~2-3 s for LACIS, ~4 s for PINC, ~12 s for PNNL-CIC, and over the range of several tens of seconds to a few minutes for AIDA depending on initial chamber *T* and RH). At the same time, the amount of external cations retained on the surface of illite particles determines the charge properties, such as charge distribution landscape and zero charge point. A potential importance of the surface charge of hematite particles for their IN activity was suggested recently in *Hiranuma et al*. (2014b). These considerations, however speculative, might shed some light on the observed scattering of experimentally measured values of n_s. Second, for the freezing measurements where the illite rich sample was suspended in water prior to cooling, all accessible external cations were already released into the aqueous environment. In these cases the concentration of cations in the droplets is a function of mass concentration of illite in suspension. To access high freezing temperatures, high concentrations of illite are needed in the droplet assay techniques, resulting in the possibility that not all cations are released into solution due to the inhibition of the ion exchange process. Again, this would change the surface charge distribution and potentially affect the ice-nucleating efficiency of illite particles. If wet particle generation (dispersion of aqueous suspension by means of a pressurized air atomizer) is used, the redistribution of cations between suspended particles may be an issue, as suggested by *Garimella et al*. (2014)

for the case of CCN experiments. Further studies of samples without modification or ageing after dry dispersion or wet suspension are needed to get a better idea of the method inter-comparison.

5. Conclusion

The framework of the present work is designed to advance the existing state of knowledge regarding IN measurement techniques. After ICIS-2007, there has been an increase in new instrument development, especially off-line, substrate-supported cold stage techniques, and modifications of existing online techniques. Concepts to formulate area-scaled IN efficiency with n_s parameters have also since been introduced to the community. These improvements are comprehensively evaluated in this work.

The partners of the INUIT group and external partners have for the first time identified and shared a reference mineral dust sample (illite NX) in order to obtain a comprehensive dataset for evaluating immersion freezing properties of atmospherically relevant particles across a wide range of particle concentrations, temperatures, cooling rates and nucleation times. Illite NX samples were extensively characterized for their physico-chemical properties before they were distributed to INUIT partners and collaborators. Both bulk and single particle elemental composition analyses were conducted by XRD and EDX analyses, respectively.

A total of seventeen IN measurement techniques were inter-compared based on their immersion freezing measurements. Our inter-comparison exercise provided unique results that would not have been achieved by individual investigators in isolation. Both consistencies and discrepancies among the instruments have been identified. Our results suggest that the immersion freezing efficiency (i.e., n_s) of illite rich clay minerals is relatively independent of droplet size, mass percent of illite NX sample in droplets for the methods examining suspensions, physical size of illite NX particles for the methods examining dry-dispersed particles and cooling rate during freezing within typical experimental uncertainties, verifying the premise of the n_s concept (i.e., size independency for submicron illite NX particles, strong temperature dependency and weak time dependency of immersion freezing for illite rich clay mineral particles).

Furthermore, comparisons of the suspension subsets against the dry-dispersed particle techniques were performed. Dry samples alone showed higher n_s values compared to the pre-suspended samples above -27 ºC. A possible explanation for this deviation (i.e., n_s from dry-dispersed methods > n_s from suspension methods) may be the surface modification of the illite NX particles (e.g., due to ion dissolution effects in the aqueous suspension).

Comparisons of the absolute values of $\Delta\log(n_s)/\Delta T$ as an ice activation parameter suggest that the predominant freezing sites of illite NX particles exist in a temperature range between -20 ˚C and -27 ˚C for suspension experiments. In comparison to previous measurements, our synergetic work, which covers a wide temperature range, shows a similar result to the Broadley parameterization (B12), and our overall fit for the low temperature region below -27 ˚C also agrees with the Niemand parameterization (N12).

Overall accuracy and precision of the IN measurement techniques was examined by evaluating T-binned (i.e., 1 ˚C bins) $n_s(T)$ data derived from all seventeen instruments for the temperature range from -11 ˚C to -37 ˚C. Our analysis revealed that discrepancies among measurements were within about 8 ˚C in terms of temperature and up to three orders of magnitude with respect to n_s. This diversity is much larger than the individual uncertainties of each instrument, suggesting that all instruments may be reasonably precise but it is still difficult to find overall accuracy of current IN measurement techniques, at least while using illite NX as the standard and allowing partners to investigate it independently. In addition, two different n_s metrics, $n_{s,geo}$ and $n_{s,BET}$, were compared, and we found that $n_{s,BET}$ is a better proxy for suspension-based IN measurements, while $n_{s,geo}$ is better for dry-dispersed particle measurements.

Other than the inter-comparison aspects described above, several important implications were inferred from our study and enhanced our basic knowledge of immersion freezing. First, the existence of only a comparably small contribution of time dependence to the inter-comparison was reconciled by the SBM simulation. Specifically, a change of the residence time, from 1 to 10 s, shifts n_s values towards higher temperatures by only about 1 ˚C. Second, several nucleation modes and their contribution to nucleation efficiency were also evaluated. A comparison among EDB, ZINC and IMCA-ZINC below -25 ˚C implied some mode dependencies. Likewise, a mode dependency was also pronounced based on FRIDGE results at temperatures above -25 ˚C. Third, immersion freezing experiments were performed with both polydisperse and size-selected illite NX particles for the AIDA-CECC, MRI-DCECC and CSU-IS measurements, and size independence of n_s for immersion freezing of submicron illite NX particles (DMA size-selected 200, 300 and 500 nm diameter) was also demonstrated. Finally, our observations show that temperature is the major variable influencing the immersion freezing of illite NX particles, as the n_s values in general increase while temperature decreases. In addition, our results of n_s and absolute values of $\Delta\log(n_s)/\Delta T$ distributions across a wide range of temperatures imply that clay minerals may contain various freezing activation energies, and the immersion freezing nature of clay minerals (e.g.,

illite NX) in a wide range of temperatures cannot be fitted by simple exponential functions but are governed by a hybrid of multi-exponential functions (a combination of scaled A13 and N12 parameterizations).

Though we shared identical test samples with each other, it is still difficult to compare n_s results because sample preparation techniques and measurement methods (e.g., particle dispersion and size distribution characterization) differ from group to group, which can result in different degrees of agglomeration or different nucleation modes. Therefore, a continued investigation to obtain further insights into consistencies or diversity of IN measurement techniques from an experimental perspective is important to explore freezing conditions for specific compositions and more atmospherically relevant particles (e.g., soil dusts and long range transported weathered dusts). In parallel, an empirically constrained model including parameterizations of immersion freezing that correctly and efficiently represent particle-specific experimental data is also in high demand for overall predictions of current and future climate. We demonstrated that the n_s formulation offers a simplified expression for quantitatively parameterizing immersion freezing. Further developments of more simplified (efficient but accurate) descriptions, constrained by more accurate IN counting techniques, of governing atmospheric IN processes are needed.

Acknowledgements

Part of this work is funded by Deutsche Forschungsgemeinschaft (DFG) under contracts BU 1432/4-1, DI 1539/1-1, KO2944/2-1, MO668/4-1 and WE 4722/1-1 within Research Unit FOR 1525 (INUIT). The authors acknowledge partial financial support by Deutsche Forschungsgemeinschaft and Open Access Publishing Fund of Karlsruhe Institute of Technology. The authors gratefully acknowledge skillful and continuous support from their technical teams. G. Kulkarni acknowledges support from the Department of Energy (DOE) Atmospheric System Research Program and thanks J. Fast for useful discussion. Battelle Memorial Institute operates the Pacific Northwest National Laboratory for DOE under contract DE-AC05-76RLO 1830. Z. A. Kanji acknowledges funding from Swiss National Funds. P. J. DeMott and T. Hill were funded by NSF grant award number AGS-1358495. M. A. Tolbert and G. P. Schill were funded by NSF Grant AGS 1048536. The MRI-DCECC work was partly funded by JSPS KAKENHI Grant Numbers 23244095. T. P. Wright, J. D. Hader, and M. D. Petters were funded by NSF Grant AGS 1010851. B. J. Murray, D. O'Sullivan and T. F. Whale acknowledge the Natural Environment Research Council (NE/K004417/1; NE/I020059/1; NE/I013466/1; NE/I019057/1) and The European Research Council (240449 – ICE) for funding. D. Niedermeier acknowledges financial support from the Alexander von Humboldt-foundation, Germany.

T. C. J. Hill would like to thank E. Levin and C. McCluskey for generation of size-selected particles. K. Diehl would like to thank S. K. Mitra for technical support on M-AL and M-WT and fruitful discussions. A. Kiselev and A. Peckhaus acknowledge O. Dombrowski for her support in IC measurements. N. Hiranuma thanks C. Anquetil-Deck for useful discussion. N. Hiranuma and G. Kulkarni thank T. Kisely and R. Ahmad for the N_2 BET and H_2O BET measurements, respectively. M. Ebert acknowledges R. Petschik for the additional high precision XRD measurements. N. Hiranuma and O. Möhler gratefully acknowledge technical support from M. Koyro and F. Schwartz for setting up the database for storing and updating the INUIT laboratory results. N. Hiranuma also thanks the AIDA technical team, including R. Buschbacher, T. Chudy, O. Dombrowski, E. Kranz, G. Scheurig and S. Vogt, for their professional support for the chamber maintenance and operation.

Author contributions

J. Curtius and O. Möhler proposed the framework of this collaborative multi-institutional laboratory work. The overall manuscript, coordinated and led by N. Hiranuma, was a collaborative effort of the partners of the INUIT group and external partners. C. Budke and T. Koop designed and conducted the BINARY experiments, analyzed the data, and contributed the BINARY text. T. C. J. Hill carried out the CSU-IS measurements, analyzed the data, and contributed to the CSU-IS text. B. J. Murray, D. O'Sullivan and T. F. Whale performed the Leeds-NIPI experiments, analyzed the data, and contributed to the Leeds-NIPI text. K. Diehl performed the experiments and data analysis of M-AL and W-WT, and K. Diehl also contributed to their method summary text. J. D. Hader performed the NC State-CS experiments and analyzed the data, T. P. Wright contributed the analysis software, M. D. Petters designed the experiments, and J. D. Hader and M. D. Petters contributed to the NC State-CS text. G. P. Schill and M. A. Tolbert conducted the CU-RMCS experiments, analyzed the data, and contributed to the CU-RMCS text. N. Hiranuma and O. Möhler conceived the AIDA experiments, analyzed and discussed the results and contributed to the AIDA text. P. J. DeMott, E. J. T. Levin and C. S. McCluskey performed CSU-CFDC experiments, analyzed the data, and contributed to the CSU-CFDC text. N. Hoffmann and A. Kiselev carried out the EDB measurements with input on experimental techniques from T. Leisner and SEM measurements and contributed to the associated data analysis and text. Björn Nillius and Fabian Frank performed the FINCH experiments and analyzed the data, and D. Rose contributed to the FINCH uncertainty analysis and method summary text. A. Danielczok and H. Bingemer conducted the FRIDGE experiments, analyzed the data, and contributed to the FRIDGE text. S. Augustin-Bauditz did the LACIS experiments, D. Niedermeier derived contact angle distributions with SBM, and H.Wex performed SBM calculations and contributed to the LACIS text. M. Murakami, K. Yamashita, T. Tajiri and A. Saito designed and performed the MRI-DCECC experiments with assistance and contributions from N. Hiranuma and O. Möhler, K. Yamashita and N. Hiranuma analyzed the MRI-DCECC data, and K. Yamashita contributed to the method summary text. Z.A. Kanji conducted the PINC experiments, Y. Boose analyzed the data, Y. Boose and Z.A. Kanji interpreted and discussed the PINC data, and contributed to the PINC text. G. Kulkarni carried out the PNNL-CIC measurements, analyzed the data, and contributed to the PNNL-CIC text. A. Welti performed the IMCA-ZINC experiments, analyzed the data, and A. Welti and Z. A. Kanji contributed to

the supplementary text. XRD measurements and analysis of illite NX were conducted by M. Ebert, K. Kandler and S. Weinbruch, and M. Ebert contributed the XRD text. IC measurements and analysis were carried out by A. Peckhaus and A. Kiselev, and A. Kiselev contributed to the IC text. DLS measurements and analysis were performed by K. Dreischmeier, and K. Dreischmeier also contributed to the DLS text. N. Hiranuma interpreted and analyzed the compiled data and wrote the paper. A. Kiselev and B. J. Murray co-wrote Sect. 4.6 with N. Hiranuma. All authors discussed the results and contributed to the final version of the manuscript.

References

Ardon-Dryer, K., Levin, Z., and Lawson, R. P.: Characteristics of immersion freezing nuclei at the South Pole station in Antarctica, Atmos. Chem. Phys., 11, 4015–4024, doi:10.5194/acp-11-4015-2011, 2011.

Atkinson, J. D., Murray, B. J., Woodhouse, M. T., Carslaw, K., Whale, T. F., Baustian, K., Dobbie, S., O'Sullivan, D., and Malkin, T. L.: Nature, 498, 355–358, doi:10.1038/nature12278, 2013.

Augustin-Bauditz, S., Wex, H., Kanter, S., Ebert, M., Stolz, F., Prager, A., Niedermeier, D. and Stratmann, F.: The immersion mode ice nucleation behavior of mineral dusts: A comparison of different pure and surface modifed dusts, Geophys. Res. Lett., 41, 7375–7382, doi:10.1002/2014GL061317, 2014.

Bickmore, B. R., Nagy, K. L., Sandlin, P. and Crater, T. S.: Quantifying surface areas of clays by atomic force microscopy, American Mineralogist, 87, 780–783, 2002.

Bigg, E. K.: The supercooling of water, Proc. Phys. Soc. B, 66, 688–694, doi:10.1088/0370-1301/66/8/309, 1953.

Bigg, E. K., A new technique for counting ice-forming nuclei in aerosols. Tellus, 9: 394–400. doi:10.1111/j.2153-3490.1957.tb01895.x, 1957.

Bingemer, H., Klein, H., Ebert, M., Haunold, W., Bundke, U., Herrmann, T., Kandler, K., Müller-Ebert, D., Weinbruch, S., Judt, A., Wéber, A., Nillius, B., Ardon-Dryer, K., Levin, Z., and Curtius, J.: Atmospheric ice nuclei in the Eyjafjallajökull volcanic ash plume, Atmos. Chem. Phys., 12, 857–867, doi:10.5194/acp-12-857-2012, 2012.

Boucher, O., Randall, D., Artaxo, P., Bretherton, C., Feingold, G., Forster, P., Kerminen, V.-M., Kondo, Y., Liao, H., Lohmann, U., Rasch, P., Satheesh, S. K., Sherwood, S., Stevens, B., and Zhang, X. Y.: Clouds and Aerosols. In: Climate Change 2013: The Physical Science Basis. Contribution of Working Group I to the Fifth Assessment Report of the Intergovernmental Panel on Climate Change [Stocker, T. F., D. Qin, G.-K. Plattner, M. Tignor, S. K. Allen, J. Boschung, A. Nauels, Y. Xia, V. Bex and P. M. Midgley (eds.)]. Cambridge University Press, Cambridge, United Kingdom and New York, NY, USA, 571–657, 2013.

Broadley, S. L., Murray, B. J., Herbert, R. J., Atkinson, J. D., Dobbie, S., Malkin, T. L., Condliffe, E., and Neve, L.: Immersion mode heterogeneous ice nucleation by an illite rich powder representative of atmospheric mineral dust, Atmos. Chem. Phys., 12, 287–307, doi:10.5194/acp-12-287-2012, 2012.

Brunauer, S., Emmett, P. H., and Teller, E.: Adsorption of gases in multimolecular layers, J. Am. Chem. Soc., 60, 309–319, doi:10.1021/ja01269a023, 1938.

Budke, C. and Koop, T.: BINARY: an optical freezing array for assessing temperature and time dependence of heterogeneous ice nucleation, Atmos. Meas. Tech. Discuss., 7, 9137–9172, doi:10.5194/amtd-7-9137-2014, 2014.

Bundke, U., Nillius, B., Jaenicke, R., Wetter, T., Klein, H., and Bingemer, H.: The fast ice nucleus chamber FINCH, Atmos. Res., 90, 180–186, doi:10.1016/j.atmosres.2008.02.008, 2008.

Chou, C., Stetzer, O.,Weingartner, E., Jurányi, Z., Kanji, Z. A., and Lohmann, U.: Ice nuclei properties within a Saharan dust event at the Jungfraujoch in the Swiss Alps, Atmos. Chem. Phys., 11, 4725–4738, doi:10.5194/acp-11-4725-2011, 2011.

Christenson, H.: Two-step crystal nucleation via capillary condensation, Cryst. Eng. Comm., 15, 2030–2039, doi:10.1039/C3CE26887J, 2013.

Connolly, P. J., Möhler, O., Field, P. R., Saathoff, H., Burgess, R., Choularton, T., and Gallagher, M.: Studies of heterogeneous freezing by three different desert dust samples, Atmos. Chem. Phys., 9, 2805–2824, doi:10.5194/acp-9-2805-2009, 2009.

Cwilong, B. M.: Sublimation centers in a Wilson chamber, Proc. Roy. Soc. A, 190, 137–143, doi:10.1098/rspa.1947.0066, 1947.

DeMott, P. J. and Rogers, D. C.: Freezing nucleation rates of dilute solution droplets measured between -30˚ and -40 ˚C in laboratory simulations of natural clouds. J. Atmos. Sci., 47, 1056–1064, doi:http://dx.doi.org/10.1175/1520-0469(1990)047<1056:FNRODS>2.0.CO;2, 1990.

DeMott, P. J.: Quantitative descriptions of ice formation mechanisms of silver iodide-type aerosols, Atmos. Res., 38, 63–99, doi:10.1016/0169-8095(94)00088-U, 1995.

DeMott, P. J. and Coauthors: Resurgence in ice nuclei measurement research, B. Am. Meteorol. Soc., 92, 1623–1635, doi:http://dx.doi.org/10.1175/2011BAMS3119.1, 2011.

DeMott, P. J., Prenni, A. J., McMeeking, G. R., Sullivan, R. C., Petters, M. D., Tobo, Y., Niemand, M., Möhler, O., Snider, J. R., Wang, Z., and Kreidenweis, S. M.: Integrating laboratory and field data to quantify the immersion freezing ice nucleation activity of mineral dust particles, Atmos. Chem. Phys. Discuss., 14, 17359–17400, doi:10.5194/acpd-14-17359-2014, 2014.

Diehl, K., Mitra, S. K., Szakáll, M., Blohn, N. v., Borrmann, S., and Pruppacher, H.R.: Chapter 2. Wind Tunnels: Aerodynamics, Models, and Experiments. In: The Mainz Vertical Wind Tunnel Facility: A Review of 25 Years of Laboratory Experiments on Cloud Physics and Chemistry [Pereira, J. D. (eds.)], Nova Science Publishers, Inc., Hauppauge, NY, USA, 2011.

Diehl, K., Debertshäuser, M., Eppers, O., Schmithüsen, H., Mitra, S.K., and Borrmann, S.: Particle-area dependence of mineral dust in the immersion mode: investigations with freely suspended drops in an acoustic levitator. Atmos. Chem. Phys., 14, 12343–12355, doi:10.5194/acp-14-12343-2014, 2014.

Durant, A.J. and Shaw, R. A.: Evaporation freezing by contact nucleation inside-out, Geophys. Res. Lett., 32, L20814, doi:10.1029/2005GL024175, 2005.

Dymarska, M., Murray, B. J., Sun, L. M., Eastwood, M. L., Knopf, D. A., and Bertram, A. K.: Deposition ice nucleation on soot at temperatures relevant for the lower troposphere, J. Geophys. Res., 111, D04204, doi:10.1029/2005JD006627, 2006.

Ervens, B. and Feingold, G.: Sensitivities of immersion freezing: Reconciling classical nucleation theory and deterministic expressions, Geophys. Res. Lett., 40, 3320–3324, doi:10.1002/grl.50580, 2013.

Fletcher, N. H.: Physics of Rain Clouds, Cambridge Univ. Press, New York, NY, USA, 386 pp, 1962.

Fletcher, N. H.: Active sites and ice crystal nucleation, J. Atmos. Sci., 26, 6, 1266–1271, doi:http://dx.doi.org/10.1175/1520-0469(1969)026<1266:ASAICN>2.0.CO;2, 1969.

Fornea, A.P., Brooks, S. D., Dooley, J. B., and Saha, A. Heterogeneous freezing of ice on atmospheric aerosols containing ash, soot, and soil, J. Geophys. Res., 114, D13201, doi:10.1029/2009JD011958, 2009.

Fournier D'albe, E. M.: Some experiments on the condensation of water vapour at temperatures below 0°C, Q. J. R. Meteorol. Soc., 75, 1–16, doi:10.1002/qj.49707532302, 1949.

Friedman, B., Kulkarni, G., Beránek, J., Zelenyuk, A., Thornton, J. A., and Cziczo, D. J.: Ice nucleation and droplet formation by bare and coated soot particles, J. Geophys. Res., 116, D17203, doi:10.1029/2011JD015999, 2011.

Friedrich, F., Steudel, A., and Weidler, P. G.: Change of the refractive index of illite particles by reduction of the Fe content of the octahedral sheet, Clays Clay Miner., 56, 505–510, doi:10.1346/CCMN.2008.0560503, 2008.

Garimella, S., Huang, Y.-W., Seewald, J. S., and Cziczo, D. J.: Cloud condensation nucleus activity comparison of dry- and wet-generated mineral dust aerosol: the significance of soluble material, Atmos. Chem. Phys., 14, 6003–6019, doi:10.5194/acp-14-6003-2014, 2014.

Gregg, S. L. and Sing, K. S. W.: Adsorption, Surface Area and Porosity, Academic Press, London, UK, 303 pp, 1982.

Grim, R. E.: Clay mineralogy, McGraw-Hill, New York, USA, 384 pp, 1953.
Hader, J. D., Wright, T. P., and Petters, M. D.: Contribution of pollen to atmospheric ice nuclei concentrations, Atmos. Chem. Phys., 14, 5433–5449, doi:10.5194/acp-14-5433-2014, 2014.

Hartmann, S., Niedermeier, D., Voigtländer, J., Clauss, T., Shaw, R. A., Wex, H., Kiselev, A., and Stratmann, F.: Homogeneous and heterogeneous ice nucleation at LACIS: operating principle and theoretical studies, Atmos. Chem. Phys., 11, 1753–1767, doi:10.5194/acp-11-1753-2011, 2011.

Herbert, R. J., Murray, B. J., Whale, T. F., Dobbie, S. J., and Atkinson, J. D.: Representing time-dependent freezing behaviour in immersion mode ice nucleation, Atmos. Chem. Phys., 14, 8501–8520, doi:10.5194/acp-14-8501-2014, 2014.

Hill, T. C. J., Moffett, B. F., DeMott, P. J., Georgakopoulos, D. G., Stump, W. L., Franc, G. D.: Measurement of Ice Nucleation-Active Bacteria on Plants and in Precipitation by Quantitative PCR, Appl. Environ. Microbiol., 80, 1256–1267, doi:10.1128/AEM.02967-13, 2014.

Hiranuma, N., Brooks, S. D., Moffet, R., Glen, A., Laskin, A., Gilles, M. K., Liu, P., MacDonald, M. A., Strapp, W., and McFarquhar, G. M.: Chemical characterization of individual particles and residuals of cloud droplets and ice crystals collected on board research aircraft in the ISDAC 2008 study, J. Geophys. Res., 118, 6564–6579, doi:10.1002/jgrd.50484, 2013.

Hiranuma, N., Paukert, M., Steinke, I., Zhang, K., Kulkarni, G., Hoose, C., Schnaiter, M., Saathoff, H., and Möhler, O.: A comprehensive parameterization of heterogeneous ice nucleation of dust surrogate: laboratory study with hematite particles and its application to atmospheric models, Atmos. Chem. Phys., 14, 13145–13158, doi:10.5194/acp-14-13145-2014, 2014a.

Hiranuma, N., Hoffmann, N., Kiselev, A., Dreyer, A., Zhang, K., Kulkarni, G., Koop, T., and Möhler, O.: Influence of surface morphology on the immersion mode ice nucleation efficiency of hematite particles, Atmos. Chem. Phys., 14, 2315–2324, doi:10.5194/acp-14-2315-2014, 2014b.

Hoffmann, N., Kiselev, A., Rzesanke, D., Duft, D., and Leisner, T.: Experimental quantification of contact freezing in an electrodynamic balance, Atmos. Meas. Tech., 6, 2373–2382, doi:10.5194/amt-6-2373-2013, 2013.

Hoose, C., Kristjansson, J. E., Chen, J.-P., and Hazra, A.: A classical-theory-based parameterization of heterogeneous ice nucleation by mineral dust, soot, and biological particles in a global climate model, J. Atmos. Sci., 67, 2483–2503, doi:http://dx.doi.org/10.1175/2010JAS3425.1, 2010.

Hoose, C. and Möhler, O.: Heterogeneous ice nucleation on atmospheric aerosols: a review of results from laboratory experiments, Atmos. Chem. Phys., 12, 9817–9854, doi:10.5194/acp-12-9817-2012, 2012.

Hussain, K. and Saunders, C. P. R.: Ice nucleus measurement with a continuous flow chamber. Q.J.R. Meteorol. Soc., 110: 75–84. doi:10.1002/qj.49711046307, 1984.

Iannone, R., Chernoff, D. I., Pringle, A., Martin, S. T., and Bertram, A. K.: The ice nucleation ability of one of the most abundant types of fungal spores found in the atmosphere, Atmos. Chem. Phys., 11, 1191–1201, doi:10.5194/acp-11-1191-2011, 2011.

Kanji, Z. A. and Abbatt, J. P. D.: Laboratory studies of ice formation via deposition mode nucleation onto mineral dust and n-hexane soot samples, J. Geophys. Res., 111, D16204, doi:10.1029/2005JD006766, 2006.

Kanji, Z. A. and Abbatt, J. P. D.: The University of Toronto Continuous Flow Diffusion Chamber (UT-CFDC): A simple design for ice nucleation studies, Aerosol Sci. Technol., 43, 730–738. doi:10.1080/02786820902889861, 2009.

Kanji, Z. A., Welti, A., Chou, C., Stetzer, O., and Lohmann, U.: Laboratory studies of immersion and deposition mode ice nucleation of ozone aged mineral dust particles, Atmos. Chem. Phys., 13, 9097–9118, doi:10.5194/acp-13-9097-2013, 2013.

Kashchiev, D.: Nucleation: Basic Theory with Applications, Butterworth-Heinemann, Oxford, UK, 544 pp, 2000.

Khvorostyanov, V. I. and Curry, J. A.: A new theory of heterogeneous nucleation for application in cloud and climate models, Geophys. Res. Lett., 27, 4081–4084, doi:10.1029/1999GL011211, 2000.

Kline, D. B. and Brier, G. W.: Some experiments on the measurement of natural ice nuclei, Mon. Wea. Rev., 89, 263–272, doi:http://dx.doi.org/10.1175/1520-0493(1961)089<0263:SEOTMO>2.0.CO;2, 1961.

Knopf, D. A. and Alpert, P. A.: A water activity based model of heterogeneous ice nucleation kinetics for freezing of water and aqueous solution droplets, Faraday Discuss., 165, 513–534, doi:10.1039/C3FD00035D, 2013.

Koehler, K. A., Kreidenweis, S. M., DeMott, P. J., Petters, M. D., Prenni, A. J., and Möhler, O.: Laboratory investigations of the impact of mineral dust aerosol on cold cloud formation, Atmos. Chem. Phys., 10, 11955–11968, doi:10.5194/acp-10-11955-2010, 2010.

Koop, T., Luo, B., Tsias, A., and Peter, T.: Water activity as the determinant for homogeneous ice nucleation in aqueous solutions, Nature, 406, 611–614, doi:10.1038/35020537, 2000.

Kulkarni, G., Fan, J., Comstock, J. M., Liu, X., and Ovchinnikov, M.: Laboratory measurements and model sensitivity studies of dust deposition ice nucleation, Atmos. Chem. Phys., 12, 7295–7308, doi:10.5194/acp-12-7295-2012, 2012.

Kumar, P., Sokolik, I. N., and Nenes, A.: Cloud condensation nuclei activity and droplet activation kinetics of wet processed regional dust samples and minerals, Atmos. Chem. Phys., 11, 8661–8676, doi:10.5194/acp-11-8661-2011, 2011.

Levine, J.: Statistical Explanation of Spontaneous Freezing of Water Droplets, NACA Tech. Notes, no. 2234, 1950.

Lüönd, F., Stetzer, O., Welti, A., and Lohmann, U.: Experimental study on the ice nucleation ability of size-selected kaolinite particles in the immersion mode, J. Geophys. Res., 115, D14201, doi:10.1029/2009JD012959, 2010.

Marcolli, C., Gedamke, S., Peter, T., and Zobrist, B.: Efficiency of immersion mode ice nucleation on surrogates of mineral dust, Atmos. Chem. Phys., 7, 5081–5091, doi:10.5194/acp-7-5081-2007, 2007.

Marcolli, C.: Deposition nucleation viewed as homogeneous or immersion freezing in pores and cavities, Atmos. Chem. Phys., 14, 2071–2104, doi:10.5194/acp-14-2071-2014, 2014.

Meunier, A.: Clays, Springer, 472pp, 2005.

Meunier, A., and Velde.: Illite: Origins, Evolution and Metamorphism, Springer, 286pp, 2004.

Möhler, O., Stetzer, O., Schaefers, S., Linke, C., Schnaiter, M., Tiede, R., Saathoff, H., Krämer, M., Mangold, A., Budz, P., Zink, P., Schreiner, J., Mauersberger, K., Haag, W., Kärcher, B., and Schurath, U.: Experimental investigation of homogeneous freezing of sulphuric acid particles in the aerosol chamber AIDA, Atmos. Chem. Phys., 3, 211–223, doi:10.5194/acp-3-211-2003, 2003.

Mullin, J. W.: Crystallization, Elsevier Butterworth-Heinemann, Oxford, UK, Forth edn., 600 pp, 2001.

Murray, B. J., Broadley, S. L., Wilson, T. W., Bull, S. J., Wills, R. H., Christenson, H. K., and Murray, E. J.: Kinetics of the homogeneous freezing of water, Phys. Chem. Chem. Phys., 12, 10380–10387, doi:10.1039/c003297b, 2010.

Murray, B. J., Broadley, S. L., Wilson, T. W., Atkinson, J. D., and Wills, R. H.: Heterogeneous freezing of water droplets containing kaolinite particles, Atmos. Chem. Phys., 11, 4191–4207, doi:10.5194/acp-11-4191-2011, 2011.

Murray, B. J., O'Sullivan, D., Atkinson, J. D., and Webb, M. E.: Ice nucleation by particles immersed in supercooled cloud droplets, Chem. Soc. Rev., 41, 6519–6554, doi:10.1039/c2cs35200a, 2012.

Niedermeier, D., Shaw, R. A., Hartmann, S., Wex, H., Clauss, T., Voigtländer, J., and Stratmann, F.: Heterogeneous ice nucleation: exploring the transition from stochastic to singular freezing behavior, Atmos. Chem. Phys., 11, 8767–8775, doi:10.5194/acp-11-8767-2011, 2011.

Niedermeier, D., Ervens, B., Clauss, T., Voigtländer, J., Wex, H., Hartmann, S., and Stratmann, F.: A computationally efficient description of heterogeneous freezing: A simplified version of the soccer ball model, Geophys. Res. Lett., 41, 736–741, doi:10.1002/2013GL058684, 2014.

Niehaus, J, Bunker, K. W., China, S., Kostinski, A., Mazzoleni, C., Cantrell, W.: A technique to measure ice nuclei in the contact mode, J. Atmos. Oceanic Technol., 31, 913–922, doi:http://dx.doi.org/10.1175/JTECH-D-13-00156.1, 2014.

Niemand, M., Möhler, O., Vogel, B., Vogel, H., Hoose, C., Connolly, P., Klein, H., Bingemer, H., DeMott, P., and Skrotzki, J.: A particle-surface-area-based parameterization of immersion freezing on desert dust particles, J. Atmos. Sci., 69, 3077–3092, doi:10.1175/Jas-D-11-0249.1, 2012.

O'Sullivan, D., Murray, B. J., Malkin, T. L., Whale, T. F., Umo, N. S., Atkinson, J. D., Price, H. C., Baustian, K. J., Browse, J., and Webb, M. E.: Ice nucleation by fertile soil dusts: relative importance of mineral and biogenic components, Atmos. Chem. Phys., 14, 1853–1867, doi:10.5194/acp-14-1853-2014, 2014.

Palmer, H. P., Natural ice-particle nuclei, Q. J. R. Meteorol. Soc., 75, 17–22, doi:10.1002/qj.49707532303, 1949.

Prenni, A. J., DeMott, P. J., Rogers, D. C., Kreidenweis, S. M., McFarquhar, G. M., Zhang, G., and Poellot, M. R.: Ice nuclei characteristics from M-PACE and their relation to ice formation in clouds, Tellus, 61B, 436–448, doi:10.1111/j.1600-0889.2009.00415.x, 2009.

Quantachrome Instruments.: autosorb iQ/ASiQwin Operating Manual, Sect. J. Theory and Discussion, 359–360 pp, 2013.

Riechers, B., Wittbracht, F., Hütten, A., and Koop, T.: The homogeneous ice nucleation rate of water droplets produced in a microfluidic device and the role of temperature uncertainty, Phys. Chem. Chem. Phys., 15, 5873–5887, doi:10.1039/c3cp42437e, 2013.

Rogers, D. C.: Development of a continuous flow thermal gradient diffusion chamber for ice nucleation studies, Atmos. Res., 22, 149–181, doi:10.1016/0169-8095(88)90005-1, 1988.

Rogers, D. C., DeMott, P. J., Kreidenweis, S. M., and Chen, Y.: A continuous-flow diffusion chamber for airborne measurements of ice nuclei, J. Atmos. Oceanic Technol., 18, 725–741, doi:http://dx.doi.org/10.1175/1520-0426(2001)018<0725:ACFDCF>2.0.CO;2, 2001.

Rosenfeld, D. and Woodley, W. L.: Deep convective clouds with sustained supercooled liquid water down to -37.5 °C, Nature, 405, 440–442, doi:10.1038/35013030, 2000.

Schill, G. P. and Tolbert, M. A.: Heterogeneous ice nucleation on phase-separated organic-sulfate particles: effect of liquid vs. glassy coatings, Atmos. Chem. Phys., 13, 4681–4695, doi:10.5194/acp-13-4681-2013, 2013.

Steinke, I., Möhler, O., Kiselev, A., Niemand, M., Saathoff, H., Schnaiter, M., Skrotzki, J., Hoose, C., and Leisner, T.: Ice nucleation properties of fine ash particles from the Eyjafjallajökull eruption in April 2010, Atmos. Chem. Phys., 11, 12945–12958, doi:10.5194/acp-11-12945-2011, 2011.

Stetzer, O., Baschek, B., Luond, F., and Lohmann, U.: The Zurich Ice Nucleation Chamber (ZINC) – A new instrument to investigate atmospheric ice formation, Aerosol Sci. Technol., 42, 64–74, doi:10.1080/02786820701787944, 2008.

Sullivan, R. C., Moore, M. J. K., Petters, M. D., Kreidenweis, S. M., Qafoku, O., Laskin, A., Roberts, G. C., and Prather, K. A.: Impact of particle generation method on the apparent hygroscopicity of insoluble mineral particles, Aerosol Sci. Tech., 44, 830–846, doi: 10.1080/02786826.2010.497514, 2010.

Szakáll, M., Diehl, K., Mitra, S. K., and Borrmann, S.: A wind tunnel study on the shape, oscillation, and internal circulation of large raindrops with sizes between 2.5 and 7.5 mm, J. Atmos. Sci., 66, 755–765, doi:http://dx.doi.org/10.1175/2008JAS2777.1, 2009.

Tajiri, T., Yamashita, K., Murakami, M., Orikasa, N., Saito, A., Kusunoki, K., and Lilie, L.: A novel adiabatic-expansion-type cloud simulation chamber. J. Meteor. Soc. Japan, 91, 5, 687–704, doi:http://dx.doi.org/10.2151/jmsj.2013-509, 2013.

Tobo, Y., Prenni, A. J., DeMott, P. J., Huffman, J. A., McCluskey, C. S. , Tian,G., Pöhlker,C., Pöschl, U., and Kreidenweis, S. M.: Biological aerosol particles as a key determinant of ice nuclei populations in a forest ecosystem, J. Geophys. Res. Atmos., 118, 10,100–10,110, doi:10.1002/jgrd.50801, 2013.

Tomlinson, E. M. and Fukuta, N.: A new horizontal gradient, continuous flow, ice thermal diffusion chamber. J. Atmos. Oceanic Technol., 2, 448–467, doi:10.1175/1520-0426(1985)002<0448:ANHGCF>2.0.CO;2., 1985.

Vali, G.: Nucleation terminology, J. Aerosol Sci., 16, 575–576, doi:10.1016/0021-8502(85)90009-6, 1985.

Vali, G.: Freezing rate due to heterogeneous nucleation, J. Atmos. Sci., 51, 1843–1856, doi:http://dx.doi.org/10.1175/1520-0469(1994)051<1843:FRDTHN>2.0.CO;2, 1994.

Vali, G.: Repeatability and randomness in heterogeneous freezing nucleation, Atmos. Chem. Phys., 8, 5017–5031, doi:10.5194/acp-8-5017-2008, 2008.

Vali, G.: Interpretation of freezing nucleation experiments: singular and stochastic; sites and surfaces, Atmos. Chem. Phys., 14, 5271–5294, doi:10.5194/acp-14-5271-2014, 2014.

Veghte, D. P. and Freedman, M. A.: Facile method for determining the aspect ratios of mineral dust aerosol by electron microscopy, Aerosol Sci. Technol., 48, 715–724, doi:10.1080/02786826.2014.920484, 2014.

Wagner, R., Möhler, O., Saathoff, H., Schnaiter, M., and Leisner, T.: New cloud chamber experiments on the heterogeneous ice nucleation ability of oxalic acid in the immersion mode, Atmos. Chem. Phys., 11, 2083–2110, doi:10.5194/acp-11-2083-2011, 2011.

Waseda, Y., Matsubara, E., and Shinoda, K.: X-Ray Diffraction Crystallography: Introduction, Examples and Solved Problems, Springer, 310 pp, 2011.

Wegener, A.: Thermodynamik der Atmosphäre. J. A. Barth Verlag, 311 pp, 1911.

Welti, A., Lüönd, F., Stetzer, O., and Lohmann, U.: Influence of particle size on the ice nucleating ability of mineral dusts, Atmos. Chem. Phys., 9, 6705–6715, doi:10.5194/acp-9-6705-2009, 2009.

Welti, A., Lüönd, F., Kanji, Z. A., Stetzer, O., and Lohmann, U.: Time dependence of immersion freezing: an experimental study on size selected kaolinite particles, Atmos. Chem. Phys., 12, 9893–9907, doi:10.5194/acp-12-9893-2012, 2012.

Welti, A., Kanji, Z. A., Lüönd, F., Stetzer, O., and Lohmann, U.: Exploring the mechanisms of ice nucleation on kaolinite: from deposition nucleation to condensation freezing, J. Atmos. Sci., 71, 16–36, doi:10.1175/JAS-D-12-0252.1, 2014.

Welton, J. E.: SEM Petrology Atlas, The American Association of Petroleum Geologists, Tulsa, OK, USA, 240 pp, 1984.

Wex, H., DeMott, P. J., Tobo, Y., Hartmann, S., Rösch, M., Clauss, T., Tomsche, L., Niedermeier, D., and Stratmann, F.: Kaolinite particles as ice nuclei: learning from the use of

different kaolinite samples and different coatings, Atmos. Chem. Phys., 14, 5529–5546, doi:10.5194/acp-14-5529-2014, 2014.

Wheeler, M. J., Mason, R. H., Steunenberg, K., Wagstaff, M., Chou, C. and Bertram, A. K.: Immersion freezing of supermicron mineral dust particles: freezing results, testing different schemes for describing ice nucleation, and ice nucleation active site densities, J. Phys. Chem. A, Article ASAP, doi: 10.1021/jp507875q, 2014.

Wilson, M. J.: Sheet Silicates: Clay Minerals In: Rock-Forming Minerals, Volume 3C, [Deer, W. A., R. A. Howie and J. Zussman (eds.)]. The Geological Society, 736 pp, 2013.

Wright, T. P. and Petters, M. D.: The role of time in heterogeneous freezing nucleation, J. Geophys. Res. Atmos., 118, 3731–3743, doi:10.1002/jgrd.50365, 2013.

Wright, T. P., Petters, M. D., Hader, J. D., Morton, T., and Holder, A. L.: Minimal cooling rate dependence of ice nuclei activity in the immersion mode, J. Geophys. Res.-Atmos., 118, 1–9, doi:10.1002/jgrd.50810, 2013.

Tables and figures of "A comprehensive laboratory study on the immersion freezing behavior of illite NX particles: a comparison of seventeen ice nucleation measurement techniques"

Corresponding Author

Naruki Hiranuma[a,*]: seong.moon@kit.edu

INUIT project partners (alphabetical order)

Stefanie Augustin-Bauditz[b]: augustin@tropos.de
Heinz Bingemer[c]: Bingemer@iau.uni-frankfurt.de
Carsten Budke[d]: carsten.budke@uni-bielefeld.de
Joachim Curtius[c]: curtius@iau.uni-frankfurt.de
Anja Danielczok[c]: Danielczok@iau.uni-frankfurt.de
Karoline Diehl[e]: kdiehl@uni-mainz.de
Katharina Dreischmeier[d]: katharina.dreischmeier@uni-bielefeld.de
Martin Ebert[f]: mebert@geo.tu-darmstadt.de
Fabian Frank[c]: frank@iau.uni-frankfurt.de
Nadine Hoffmann[a]: nadine.hoffmann@kit.edu
Konrad Kandler[f]: kandler@geo.tu-darmstadt.de
Alexei Kiselev[a]: alexei.kiselev@kit.edu
Thomas Koop[d]: thomas.koop@uni-bielefeld.de
Thomas Leisner[a]: thomas.leisner@kit.edu
Ottmar Möhler[a]: ottmar.moehler@kit.edu
Björn Nillius[c,n]: b.nillius@mpic.de
Andreas Peckhaus[a]: andreas.peckhaus@kit.edu
Diana Rose[c]: rose@iau.uni-frankfurt.de
Stephan Weinbruch[f]: weinbruch@geo.tu-darmstadt.de
Heike Wex[b]: wex@tropos.de

Associated partners (alphabetical order)

Yvonne Boose[g]: yvonne.boose@env.ethz.ch
Paul J. DeMott[h]: pdemott@lamar.colostate.edu
John D. Hader[i]: jdhader@ncsu.edu
Thomas C. J. Hill[h]: Thomas.Hill@ColoState.EDU
Zamin A. Kanji[g]: zamin.kanji@env.ethz.ch
Gourihar Kulkarni[j]: Gourihar.Kulkarni@pnnl.gov
Ezra J. T. Levin[h]: elevin@atmos.colostate.edu
Christina S. McCluskey[h]: mccluscs@atmos.colostate.edu
Masataka Murakami[k]: mamuraka@mri-jma.go.jp
Benjamin J. Murray[l]: B.J.Murray@leeds.ac.uk
Dennis Niedermeier[b,o]: niederm@tropos.de
Markus D. Petters[i]: markus_petters@ncsu.edu
Daniel O'Sullivan[l]: D.OSullivan@leeds.ac.uk
Atsushi Saito[k]: asaito@mri-jma.go.jp
Gregory P. Schill[m]: gregory.schill@colorado.edu
Takuya Tajiri[k]: ttajiri@mri-jma.go.jp
Margret A. Tolbert[m]: tolbert@colorado.edu
André Welti[g]: andre.welti@env.ethz.ch
Thomas F. Whale[l]: eetfw@leeds.ac.uk
Timothy P. Wright[i]: timothy.wright@gmail.com
Katsuya Yamashita[k,p]: yamashita@bosai.go.jp

- [a]Institute for Meteorology and Climate Research – Atmospheric Aerosol Research, Karlsruhe Institute of Technology, Karlsruhe, Germany.
- [b]Leibniz Institute for Tropospheric Research, Leipzig, Germany.
- [e]Institute for Atmospheric Physics, University of Mainz, Mainz, Germany.
- [d]Faculty of Chemistry, Bielefeld University, Bielefeld, Germany.
- [c]Institute for Atmospheric and Environmental Science, Goethe University of Frankfurt, Frankfurt, Germany.
- [f]Institute of Applied Geosciences, Technical University Darmstadt, Germany.
- [g]Institute for Atmosphere and Climate Science, ETH, Zurich, Switzerland.
- [h]Department of Atmospheric Science, Colorado State University, Fort Collins, CO, USA.
- [i]Department of Marine Earth and Atmospheric Sciences, North Carolina State University, Raleigh, NC, USA.
- [j]Atmospheric Science and Global Change Division, Pacific Northwest National Laboratory, Richland, WA, USA.
- [k]Meteorological Research Institute (MRI), Tsukuba, Japan.
- [l]Institute for Climate and Atmospheric Science, School of Earth and Environment, University of Leeds, Leeds, UK.
- [m]Cooperative Institute for Research in Environmental Sciences and Department of Chemistry and Biochemistry, University of Colorado, Boulder, CO, USA.
- Now at, [n]Max-Planck-Institut für Chemie, Mainz, Germany.
- Now at, [o]Department of Physics, Michigan Technological University, Houghton, MI, USA.
- Now at, [p]Snow and Ice Research Center, Nagaoka, Japan.

Citation:
N. Hiranuma, et al. **A comprehensive laboratory study on the immersion freezing behavior of illite NX particles: a comparison of seventeen ice nucleation measurement techniques**, for *Atmospheric Chemistry and Physics* – **Special Issue: Results from the ice nuclei research unit (INUIT).**

Table 1. Summary of INUIT measurement techniques and instruments. All acronyms are available in the Supplementary Information Sect. S4. Note 'poly' and 'mono' denote polydisperse and quasi-monodisperse size-selected particle distributions, respectively.

ID	Instrument	Description	Portable ?	Reference	Investigable *T* range	Ice detected *T* range for this study
1	BINARY*	Cold stage-supported droplet assay	No	*Budke and Koop*., 2014	-25 ˚C < *T* < ~0 ˚C	-24 ˚C < *T* < -15 ˚C
2	CSU-IS	Immersion mode ice spectrometer	Yes	*Hill et al*., 2014	-30 ˚C < *T* < ~0 ˚C	poly: -25 ˚C < *T* < -11 ˚C mono: -26 ˚C < *T* < -20 ˚C
3	Leeds-NIPI	Nucleation by immersed particles instrument	No	*O'Sullivan et al*., 2014	-36 ˚C < *T* < ~0 ˚C	-21 ˚C < *T* < -11 ˚C
4	M-AL*	Acoustic droplet levitator	No	*Diehl et al*., 2014	-30 ˚C < *T* < ~0 ˚C	-25 ˚C < *T* < -15 ˚C
5	M-WT*	Vertical wind tunnel	No	*Szakáll et al*., 2009; *Diehl et al*., 2011	-30 ˚C < *T* < ~0 ˚C	-21 ˚C < *T* < -19 ˚C
6	NC State-CS	Cold stage-supported droplet assay	No	*Wright and Petters*, 2013	-40 ˚C < *T* < ~0 ˚C	-34 ˚C < *T* < -14 ˚C
7	CU-RMCS	Cold stage-supported droplet assay	No	*Schill and Tolbert*, 2013	-40 ˚C < *T* < -20 ˚C	-32 ˚C < *T* < -23 ˚C
8	AIDA*	CECC	No	*Möhler et al*., 2003 *Hiranuma et al*., 2014a,b	-100 ˚C < *T* < -5 ˚C	poly: -35 ˚C < *T* < -27 ˚C mono: -34 ˚C < *T* < -28 ˚C
9	CSU-CFDC	Cylindrical plates CFDC	Yes	*Tobo et al*., 2013	-34 ˚C < *T* < -9 ˚C	-29 ˚C < *T* < -22 ˚C
10	EDB*	Electrodynamic balance levitator	No	*Hoffmann et al*., 2013	-40 ˚C < *T* < -1 ˚C	[a]imm.: -31 ˚C < *T* < -28 ˚C [b]contact: -34 ˚C < *T* < -27 ˚C
11	FINCH*	Continuous flow mixing chamber	Yes	*Bundke et al*., 2008	-60 ˚C < *T* < -2 ˚C	-27 ˚C < *T* < -22 ˚C
12	FRIDGE*	Substrate-supported diffusion and condensation/immersion cell	Yes	*Bingemer et al*., 2012	-25 ˚C < *T* < -8 ˚C	[c]default: -25 ˚C < *T* < -18 ˚C [d]imm.: -25 ˚C < *T* < -18 ˚C
13	LACIS*	Laminar flow tube	No	*Hartmann et al*., 2011; *Wex et al*., 2014	-40 ˚C < *T* < -5 ˚C	-37 ˚C < *T* < -31 ˚C
14	MRI-DCECC	Dynamic CECC	No	*Tajiri et al*., 2013	-100 ˚C < *T* < ~0 ˚C	poly: -26 ˚C < *T* < -21 ˚C mono: -29 ˚C < *T* < -21 ˚C
15	PINC	Parallel plates CFDC	Yes	*Chou et al*., 2011; *Kanji et al*., 2013	-40 ˚C < *T* < -9 ˚C	-35 ˚C < *T* < -26 ˚C
16	PNNL-CIC	Parallel plates CFDC	Yes	*Friedman et al*., 2011	-55 ˚C < *T* < -15 ˚C	-35 ˚C < *T* < -27 ˚C
17	IMCA-ZINC	Parallel plates CFDC	No	*Lüönd et al*., 2010 *Stetzer et al*., 2008; *Welti et al*., 2009	-65 ˚C < *T* < -5 ˚C	[e]imm.: -36 ˚C < *T* < -31 ˚C [f]ZINC: -33 ˚C < *T* < -32 ˚C

*Instruments of INUIT project partners, a. immersion freezing, b. contact freezing, c. default deposition nucleation, d. immersion freezing with suspended particles, e. immersion freezing with IMCA, f. ZINC alone.

Table 2. X-ray diffraction analyses of the bulk composition of illite NX powder.

Mineral	Weight Percentage (wt%)			
	This study	Manufacturer Data	Broadley et al., 2012	Friedrich et al., 2008[†]
Illite	69	86	74	76
Kaolinite	10	10	7	5
Quartz	3	4	7	<1
Calcite/Carbonate	3	N/A	2	2
Feldspar (Orthoclase/Sanidine)	14	N/A	10	4

[†]*Friedrich et al*. (2008) noted 11 wt% additional impurities, including phlogopite (7.8 wt%), anhydrite (1.4 wt%), plagioclase (1.1 wt%), and apatite (0.7 wt%).

Table 3. List of the Gumbel cumulative distribution fit parameters to the $n_{s,BET}$ and $n_{s,geo}$ for *T*-binned ensemble dataset fitted in the linear space [All (lin)], ensemble dataset fitted in the log space [All (log)], ensemble maximum values (All_{max}), ensemble minimum values (All_{min}), suspension subset fitted in the linear space [Sus (lin)], suspension subset fitted in the log space [Sus (log)], dry-dispersed particle subset fitted in the linear space [Dry (lin)] and dry-dispersed particle subset fitted in the log space [Dry (log)]. Note that All_{max} and All_{min} are fitted in the linear space. The correlation coefficient, *r*, for each fit is also shown. *T* is in ˚C.

Fitted dataset	Fitted *T* range	Fit Parameters [$n_{s,BET}(T) = \exp(a \cdot \exp(-\exp(b \cdot (T + c))) + d)$]				
		a	*b*	*c*	*d*	*r*
†All (lin)	-37 ˚C < *T* < -11 ˚C	23.82	0.16	17.49	1.39	0.60
†All (log)	-37 ˚C < *T* < -11 ˚C	22.00	0.16	20.07	3.00	0.80
†All_{max}	-37 ˚C < *T* < -11 ˚C	24.72	0.15	17.27	1.56	0.63
†All_{min}	-37 ˚C < *T* < -11 ˚C	21.86	0.16	22.73	2.70	0.94
Sus (lin)	-34 ˚C < *T* < -11 ˚C	24.38	0.14	19.61	1.89	0.99
Sus (log)	-34 ˚C < *T* < -11 ˚C	24.28	0.14	21.19	2.70	0.99
†Dry (lin)	-37 ˚C < *T* < -18 ˚C	27.35	0.07	16.48	3.19	0.59
†Dry (log)	-37 ˚C < *T* < -18 ˚C	26.22	0.07	16.27	3.31	0.72

Fitted dataset	Fitted *T* range	Fit Parameters [$n_{s,geo}(T) = \exp(a \cdot \exp(-\exp(b \cdot (T + c))) + d)$]				
		a	*b*	*c*	*d*	*r*
†All (lin)	-37 ˚C < *T* < -11 ˚C	25.75	0.13	17.17	3.34	0.73
†All (log)	-37 ˚C < *T* < -11 ˚C	22.93	0.16	20.31	5.72	0.80
†All_{max}	-37 ˚C < *T* < -11 ˚C	25.72	0.15	16.39	3.52	0.75
†All_{min}	-37 ˚C < *T* < -11 ˚C	22.16	0.16	22.13	5.64	0.98
Sus (lin)	-34 ˚C < *T* < -11 ˚C	22.72	0.16	19.52	5.50	1.00
Sus (log)	-34 ˚C < *T* < -11 ˚C	22.64	0.16	20.93	5.92	0.98
†Dry (lin)	-37 ˚C < *T* < -18 ˚C	29.38	0.05	16.49	7.19	0.64
†Dry (log)	-37 ˚C < *T* < -18 ˚C	27.92	0.05	13.25	6.32	0.83

†To derive the fits that are representative for immersion mode freezing, we excluded EDB (contact) and ZINC data.

Figure 1. EDX spectra of representative illite NX particles. (a) typical illite, (b) calcite rich mineral, (c) titanium oxide rich mineral, and (d) lead rich mineral. Scanning electron microscopy images of characterized particles are shown in subpanels. A schematic representation of the illite's crystal structure (silicon in yellow, aluminum in black, oxygen in red and potassium in purple) is also shown.

Figure 2. Surface area distributions of (a) suspended and (b-d) dry illite NX particles. Hydrodynamic size-based surface area distributions are measured in suspension using DLS. The average (± standard error) of five measurements with different concentrations of suspended illite NX powder (0.05, 0.1, 0.25, 0.5 and 1 mg mL^{-1}) is presented in (a). Volume equivalent diameter-based dry-dispersed particle surface area distributions measured in the AIDA chamber (mean of ten measurements ± standard error) and MRI-DCECC (two individual measurements) are shown in (b) and (c), respectively. Panel (d) shows optical diameter-based particle surface area distributions measured by a TSI-OPS used for the FRIDGE immersion mode experiments. Dotted lines represent log-normal fits, and corresponding mode diameters are (a) 0.32 μm, (b) 0.36 μm, (c) 0.62 μm and (d) 4.75 μm. The width-parameters of log-normal fittings are (a) 0.55, (b) 0.65, (c) 0.95 and (d) 1.10.

Figure 3. Evolution of the cation concentration in aqueous suspension of 0.1g illite in 10ml deionized water with time. The scaling of the time-axis is different for three different subsections of the time series (USTS, STS and LTS).

Figure 4. Inter-comparison of seventeen instruments using $n_{s,BET}$. Black or red cross markers are interpolated $n_s(T)$ used for T-binned averaging. Note that M-AL and M-WT results are presented in (d). In (k), FRIDGE results of default (solid square) and imm.mode (open diamond) measurements are presented. Both ZINC (solid square) and IMCA-ZINC (open diamond) data are shown in (p). Reference immersion freezing $n_s(T)$ spectra for illite NX (B12; *Broadley et al*., 2012), K-feldspar (A13; *Atkinson et al*., 2013), ATD and desert dusts (Dust) (N12; *Niemand et al*., 2012) are also shown (See Sect. 3.2).

Figure 5. Geometric size-based ice nucleation active surface-site density, $n_{s,geo}$, of seventeen measurement techniques. Black or red cross markers are interpolated $n_s(T)$ used for T-binned averaging. Note that M-AL and M-WT results are presented in (d). In (k), FRIDGE results of default (solid square) and imm.mode (open diamond) are presented. Both ZINC (solid square) and IMCA-ZINC (open diamond) data are shown in (p). Reference immersion freezing $n_s(T)$ spectra are provided as in Fig. 4.

Figure 6. Immersion freezing $n_s(T)$ spectra of illite NX particles from seventeen instruments calculated as a function of the BET (a) and geometric (b) surface areas. Reference immersion freezing $n_s(T)$ spectra are provided as in Figs. 4 and 5. Dry-dispersed particle (red markers) and suspension (blue markers) results for $n_{s,BET}$ and $n_{s,geo}$ are shown in (c) and (d), respectively, to highlight the difference between dry particle and suspension subsets.

Figure 7. The n_s parameterization, based on the BET (a) and geometric (b) surface areas, as a function of temperature (T). The multiple exponential distribution fit in the linear space (T-binned Lin. Avg.) is expressed as $n_{s,BET}(T) = \exp(23.82 \times \exp(-\exp(0.16 \times (T + 17.49))) + 1.39)$ or $n_{s,geo}(T) = \exp(25.75 \times \exp(-\exp(0.13 \times (T + 17.17))) + 3.34)$. The same fit in the log space (T-binned Log. Avg.) is expressed as $n_{s,BET}(T) = \exp(22.00 \times \exp(-\exp(0.16 \times (T +$

20.07))) + 3.00) or $n_{s,geo}(T)$ = exp(22.93 × exp(-exp(0.16 × (T + 20.31))) + 5.72). Note that n_s and T are in m^{-2} and ˚C, respectively. The maximum deviation between maxima and minima in horizontal axis (in T ºC) and vertical axis [in log($n_{s,max}/n_{s,min}$)] corresponds to $Hor_{Max-Min}$ and $Ver_{Max-Min}$, respectively. All fit parameters are shown in Table 3.

Figure 8. T-binned $n_{s,geo}$ (a) and $n_{s,BET}$ (b). T-binned data (i.e., average in the linear space with 1 ˚C bins for -37 ˚C < T < -11 ˚C) of $n_s(T)$ spectra are presented for (i) All interpolated dataset (All), (ii) Suspension measurements (Sus), (iii) Dry-dispersed particle measurements (Dry), and (iv) comparison between Sus and Dry. Red sticks represent maxima (positive direction) and minima (negative direction) and black sticks represent ± standard error. Literature results (B12, A13, and N12) are also shown.

Figure 9. Soccer ball model analysis for time dependency of immersion freezing of illite NX particles. Comparison to LACIS measurements in $n_{s,geo}$ space is also shown. Error bars represent experimental uncertainties (T ± 0.3 ˚C and n_s ± 28%). The subpanel shows a magnified section of T (-31 to -38 °C) and $n_{s,geo}$ (1.2×10^{10} to 5.1×10^{11} m^{-2}) space without error bars. A shift in the residence time from 1s to 10 s shifts n_s (as well as n_m, not shown) towards higher temperatures by about 1 ˚C.

Figure 10. Examination of mode dependency of heterogeneous ice nucleation of illite NX particles. A comparison of FRIDGE (default) and FRIDGE (imm.mode) in $n_{s,BET}$ and $n_{s,geo}$ are shown in (a) and (b), respectively. (c) and (d) show a comparison between EDB (contact), EDB (imm.), ZINC, IMCA-ZINC, and PNNL-CIC data in $n_{s,BET}$ and $n_{s,geo}$, respectively.

Supplementary Information to "A comprehensive laboratory study on the immersion freezing behavior of illite NX particles: a comparison of seventeen ice nucleation measurement techniques"

Corresponding Author

Naruki Hiranuma[a,*]: seong.moon@kit.edu

INUIT project partners (alphabetical order)

Stefanie Augustin-Bauditz[b]: augustin@tropos.de
Heinz Bingemer[c]: Bingemer@iau.uni-frankfurt.de
Carsten Budke[d]: carsten.budke@uni-bielefeld.de
Joachim Curtius[c]: curtius@iau.uni-frankfurt.de
Anja Danielczok[c]: Danielczok@iau.uni-frankfurt.de
Karoline Diehl[e]: kdiehl@uni-mainz.de
Katharina Dreischmeier[d]: katharina.dreischmeier@uni-bielefeld.de
Martin Ebert[f]: mebert@geo.tu-darmstadt.de
Fabian Frank[c]: frank@iau.uni-frankfurt.de
Nadine Hoffmann[a]: nadine.hoffmann@kit.edu
Konrad Kandler[f]: kandler@geo.tu-darmstadt.de
Alexei Kiselev[a]: alexei.kiselev@kit.edu
Thomas Koop[d]: thomas.koop@uni-bielefeld.de
Thomas Leisner[a]: thomas.leisner@kit.edu
Ottmar Möhler[a]: ottmar.moehler@kit.edu
Björn Nillius[c,n]: b.nillius@mpic.de
Andreas Peckhaus[a]: andreas.peckhaus@kit.edu
Diana Rose[c]: rose@iau.uni-frankfurt.de
Stephan Weinbruch[f]: weinbruch@geo.tu-darmstadt.de
Heike Wex[b]: wex@tropos.de

Associated partners (alphabetical order)

Yvonne Boose[g]: yvonne.boose@env.ethz.ch
Paul J. DeMott[h]: pdemott@lamar.colostate.edu
John D. Hader[i]: jdhader@ncsu.edu
Thomas C. J. Hill[h]: Thomas.Hill@ColoState.EDU
Zamin A. Kanji[g]: zamin.kanji@env.ethz.ch
Gourihar Kulkarni[j]: Gourihar.Kulkarni@pnnl.gov
Ezra J. T. Levin[h]: elevin@atmos.colostate.edu
Christina S. McCluskey[h]: mccluscs@atmos.colostate.edu
Masataka Murakami[k]: mamuraka@mri-jma.go.jp
Benjamin J. Murray[l]: B.J.Murray@leeds.ac.uk
Dennis Niedermeier[b,o]: niederm@tropos.de
Markus D. Petters[i]: markus_petters@ncsu.edu
Daniel O'Sullivan[l]: D.OSullivan@leeds.ac.uk
Atsushi Saito[k]: asaito@mri-jma.go.jp
Gregory P. Schill[m]: gregory.schill@colorado.edu
Takuya Tajiri[k]: ttajiri@mri-jma.go.jp
Margret A. Tolbert[m]: tolbert@colorado.edu
André Welti[g]: andre.welti@env.ethz.ch
Thomas F. Whale[l]: eetfw@leeds.ac.uk
Timothy P. Wright[i]: timothy.wright@gmail.com
Katsuya Yamashita[k,p]: yamashita@bosai.go.jp

- [a]Institute for Meteorology and Climate Research – Atmospheric Aerosol Research, Karlsruhe Institute of Technology, Karlsruhe, Germany.
- [b]Leibniz Institute for Tropospheric Research, Leipzig, Germany.
- [e]Institute for Atmospheric Physics, University of Mainz, Mainz, Germany.
- [d]Faculty of Chemistry, Bielefeld University, Bielefeld, Germany.
- [c]Institute for Atmospheric and Environmental Science, Goethe University of Frankfurt, Frankfurt, Germany.
- [f]Institute of Applied Geosciences, Technical University Darmstadt, Germany.
- [g]Institute for Atmosphere and Climate Science, ETH, Zurich, Switzerland.
- [h]Department of Atmospheric Science, Colorado State University, Fort Collins, CO, USA.
- [i]Department of Marine Earth and Atmospheric Sciences, North Carolina State University, Raleigh, NC, USA.
- [j]Atmospheric Science and Global Change Division, Pacific Northwest National Laboratory, Richland, WA, USA.
- [k]Meteorological Research Institute (MRI), Tsukuba, Japan.
- [l]Institute for Climate and Atmospheric Science, School of Earth and Environment, University of Leeds, Leeds, UK.
- [m]Cooperative Institute for Research in Environmental Sciences and Department of Chemistry and Biochemistry, University of Colorado, Boulder, CO, USA.
- Now at, [n]Max-Planck-Institut für Chemie, Mainz, Germany.
- Now at, [o]Department of Physics, Michigan Technological University, Houghton, MI, USA.
- Now at, [p]Snow and Ice Research Center, Nagaoka, Japan.

Citation:
N. Hiranuma, et al. **A comprehensive laboratory study on the immersion freezing behavior of illite NX particles: a comparison of seventeen ice nucleation measurement techniques**, for *Atmospheric Chemistry and Physics* – **Special Issue: Results from the ice nuclei research unit (INUIT).**

S1. Supplementary Methods

This supplementary information provides additional details for the measurement techniques of immersion freezing of illite NX particles with S1.1. suspension techniques and S1.2. dry-dispersed particle measurement techniques (both in alphabetical order as in Table 1). The discussions of measurement uncertainties of temperature and n_s for each measurement technique are also provided. We note that the uncertainty in frozen fraction (α) used in calculating n_s may not be adequate, since the sensitivity of $\Delta\alpha$ (an increase or a decrease in frozen fraction) is much higher at high temperatures which unexceptionally coincide with a low fraction of frozen illite NX.

S1.1. Suspension techniques

Bielefeld Ice Nucleation ARraY (BINARY)

The BINARY setup is an optical freezing apparatus that makes use of the change in droplet brightness during freezing for the automated and simultaneous detection of ice nucleation in 36 microliter-sized droplets. The droplets are positioned on a hydrophobic glass slide that rests on top of a Peltier cooling stage (Linkam LTS 120). The 36 droplets are separated from each other by a polydimethylsiloxane (PDMS) spacer in order to prevent a Wegener-Bergeron-Findeisen process. For a particular illite NX concentration (0.1, 0.5, 2, 5 and 10 mg mL^{-1} based on the amount of suspended mass of illite NX sample per H_2O volume) at least 3 experiments with 36 drops each were conducted, resulting in a minimum of at least 108 freezing events at each concentration. The droplet temperature was calibrated based on phase transition temperatures of several compounds over the range from 0 to -40 °C and for rates between 0.1 and 10 °C min^{-1}. Details of the setup and its temperature calibration are presented elsewhere (*Budke and Koop*, 2014). In addition to this temperature calibration no further corrections were made to the dataset of observed individual droplet freezing temperatures. However, if any droplet freezing temperatures of a particular concentration were below -25 °C, this concentration was excluded from the analysis. At these temperatures, the derived n_s for different illite NX mass concentrations deviate from each other, indicating

that ice nucleation in these droplets was not induced by illite NX particles, but rather by ice-nucleating impurities contained in the water. This lower temperature limit is also in agreement with the observed 25th percentile freezing temperature value of about -26 °C for pure water samples. Additionally, if at a specific temperature less than 1% of the freezing events in a concentration series occur, the corresponding data point was also excluded.

Experimental uncertainties: The spread of experimentally found transition temperatures in the calibration indicates a quartiles-based error of ± 0.3 °C. Assuming 10% errors in the mass concentration, the droplet volume, and the frozen fraction an error of about 20% is associated to the active site density per mass based on Gaussian error calculation. The maximal error is 35%. For the active site density per surface area an additional error has to be included due to the uncertainty in the specific surface area.

Colorado State University Ice Spectrometer (CSU-IS)

An immersion-freezing method was used to obtain INP temperature spectra for NX-illite clay, both when in bulk suspension and for size-selected particles.

For the bulk clay, a 0.5 wt% suspension was made in 10 mM sodium phosphate buffer (at *pH* 8.7 to match the *pH* of the sample and to prevent flocculation, and filtered through a 0.02 µm Anotop syringe filter (Whatman)) and mixed by tumbling end-over-end at 1 cycle s^{-1} for 30 min (Cole-Palmer, Roto-Torque). Measures of INP were made on this suspension and on a series of 20-fold dilutions to 3.1 x 10^{-6} wt% in the same buffer.

Polydisperse NX-illite particles were generated for size selection using the simple flask generator as described in *Tobo et al*. (2014). For collection of size-selected particles, several grams of dust were placed in a 250 mL conical flask, and dust released by blowing nitrogen in at the base base (~2 L min^{-1}) while agitating the flask in an ultrasonic bath. The particle stream was passed through a dilution tank (N_2 flow rate into the tank ~5 L min^{-1}) and then through a ^{210}Po neutralizer before size selection of particles with a mobility diameter of 500 nm in a DMA (TSI Inc., Model 3081; sheath flow: 4.5 L min^{-1}, sample flow: 1.8 L min^{-1}). This stream was then divided, with 0.3 L min^{-1} passed to a condensation particle counter (CPC, TSI Inc., Model 3010) and 1.50 L min^{-1} drawn through a 47 mm diameter in-line aluminum filter holder (Pall) fitted with a 0.2 µm-diameter-pore Nuclepore track-etched polycarbonate membrane (Whatman). Concentration of 500 nm particles was maintained at around 1,500 cc^{-1} and flow was continued until 127 million particles were collected. Filters and dissembled filter holders had been pre-cleaned, separately, by soaking in 10% H_2O_2 for

10 and 60 min, respectively, followed by three rinses in deionized water (18 MΩ cm and 0.2 µm-diameter-pore filtered). Filters were dried on foil in a particle-free, laminar flow cabinet, as were filter holder components after excess water was removed with a gas duster.

After particle collection, the filter was transferred to a sterile, 50 mL Falcon polypropylene tube (Corning Life Sciences), 5.0 mL of 0.2 µm-pore-diameter-filtered deionized water added (which contained 1-3 INP mL^{-1} at -23 °C), and particles re-suspended by tumbling for 30 min on the rotator. Measures of INP were made on this suspension and on a 20-fold dilution.

To obtain INP temperature spectra, suspensions were first aliquoted into sterile, 96-well polypropylene polymerase chain reaction (PCR) trays (Life Science Products Inc.) in a laminar flow cabinet. For each dilution, 32 aliquots of 60 µL were dispensed. Trays were capped with polystyrene lids (Nunc microwell plates, Thermo Fisher Scientific Inc.) and transferred to CSU-IS.

The IS was constructed using two 96-well aluminum incubation blocks for PCR plates (VWR) placed end-to-end and encased on their sides and base by cold plates (Lytron). A ULT-80 low temperature bath (Thermo Neslab) circulating SYLTHERM XLT heat transfer fluid (Dow Corning Corporation) was used for cooling. PCR plates were placed in the blocks, the device covered with a plexiglass window and the headspace purged with 1.2 L min^{-1} of filtered (HEPA-CAP, Whatman) nitrogen. Temperature was then lowered at 0.33 °C min^{-1}, measured using a thermistor verification probe (Bio-Rad, Hercules, CA, VPT-0300) inserted into a side well. The number of frozen wells were counted at 0.5 or 1 °C degree intervals, and cumulative numbers of INP mL^{-1} suspension estimated using the formula $\ln(f)/V$, where f is the proportion of droplets not frozen and V is the volume of each aliquot (*Vali*, 1971). This was converted to INP g^{-1} illite and thence to INP m^{-2} illite assuming a surface area of 124 m^2 g^{-1} dust. For size-selected particles, mass was calculated assuming particles were spherical and had a density of 2.65 g cm^{-3}.

Experimental uncertainties: The temperature uncertainty in the CSU-IS technique is ± 0.2 °C (a combination of the uncertainty in the probe and the temperature variation across the blocks due to gradients in cooling). Binomial sampling confidence intervals (95%) were derived using as recommended by *Agresti and Coull* (formula number 2, 1998). Their ranges varied according to the proportion of wells frozen. For a single well frozen out of 32 aliquots, the 95% confidence interval ranged from 18% to 540% of the estimated n_s value, while for 31/32 wells frozen it was 53-149% of the n_s value.

Leeds Nucleation by Immersed Particles Instrument (Leeds-NIPI)

Picoliter (pL)-NIPI: the experimental approach employed to study freezing by illite NX particles in droplets 10's µm in diameter has been described in detail by *Broadley et al*. (2012). This instrument has been used in a number of studies of hetereogeneus ice nucleation (*Atkinson et al*., 2013; *Murray et al*., 2011; *O'Sullivan et al*., 2014). Briefly, droplets of dust suspension are generated using a nebuliser and allowed to settle onto a hydrophobic coated glass slide. The droplets are sealed in oil and then transferred to a microscope cold stage where they are cooled at a controlled rate. The droplet freezing temperatures are recorded using a camera coupled to the microscope.

Microliter (µL)-NIPI: This more recently developed technique makes use of larger droplets (~1 mm) which thereforecontain a greater surface area of dust for a constant dust concentration. The µL-NIPI is sensitive to smaller values of n_s than the pL-NIPI. This instrument is described by *Atkinson et al*. (2013), *O'Sullivan et al*. (2014) and also used by *Herbert et al*. (2014) for heterogeneous ice nucleation studies. It has not previously been used for illite NX particles. Briefly, experiments involve pippetting 1 µL volume droplets of suspension onto a hydrophobic glass slide positioned on a cold stage. The cold stage is cooled by a stirling engine (Grant-Asymptote EF600) and droplet freezing is recorded using a digital camera.Values of n_s have been extended to much higher temperatures using the µL-NIPI.

The recorded images of droplets freezing for both NIPI experiments are analysed in order to determine the freezing temperature of each droplet. For the pL-NIPI the size of each droplet is also recorded. In the µL-NIPI experiments droplets are of a uniform size since they were pipetted onto the surface.

Experimental uncertainties: To calculate error in n_s the Leeds-NIPI measurement, errors from the BET surface area, the weights used to make up suspensions, dust density and estimated pipetting error to calculate an error in the amount of IN surface area per droplet were propagated. The resulting error for 0.1wt% and 1wt% suspension was ± 18.9% and ± 10.8% in n_s, respectively. The temperature error was calculated by taking the random error of the thermocouple used to measure temperature in a cold stage and propagated this with the melting point range observed for water. This resulted in a maximum error of less than ± 0.4 °C.

Mainz Acoustic Levitator (M-AL)

Inside the acoustic levitator (type APOS BA 10 from TEC59) a standing ultrasonic wave is produced by interference where drops can be levitated at the nodes. It is installed inside a walk-in cold chamber where the setup includes the acoustic levitator, a platinum-resistor thermometer Pt100 to measure the ambient temperature, a digital video camera to determine the drop sizes, and an infra-red thermometer to directly and contact-free measure the temperature of the freezing drops. These measurements require a circular spot of approximately 1 mm in diameter and, therefore, the investigated drops had sizes of 2 ± 0.2 mm in diameter. Because of their rather large volume and missing ventilated heat transfer the levitated drops cool down rather slowly while exchanging heat with the ambient air in the cold chamber. This results in a non-linear cooling rate. During the experiments with illite-NX, the temperature of pure water drops developed as follows (*Diehl et al.*, 2014):

$$T_{\mathrm{drop}}(T) = -27.050\ ^{\circ}\mathrm{C} + 27.082\ ^{\circ}\mathrm{C}\ \exp\left(-\frac{t}{16.374}\right) \qquad \text{(Eqn. S1)}$$

where $T_{\mathrm{drop}}(t)$ *is* the drop surface temperature, t the time. Individual drops containing polydisperse illite NX particles were levitated one after another and cooled down according to Eqn. S1. The transition from the liquid to the ice phase was clearly defined by a sudden increase of the drop temperature (because of the release of latent heat) recorded from the infra-red thermometer (*Diehl et al.*, 2014). For each particle concentration, approximately 100 drops were observed until they froze and the freezing temperatures, i.e. the lowest drop temperatures were recorded with a measuring error of ± 0.7 K. Afterwards, for temperature steps of 1 K the fractions of frozen drops were counted.

Experimental uncertainties: The uncertainties for T and n_s are ± 0.7 ˚C and ± 30%, respectively. The n_s uncertainty includes errors of the frozen fractions of drops, the specific particle surface area, the particle masses per drop, and the drop sizes.

Mainz vertical Wind Tunnel (M-WT)

In the Mainz vertical wind tunnel drops are freely floated at their terminal velocities in an air stream. Thus, ventilation and heat transfer are similar to the situation as in the real atmosphere. The wind speed is uniformly distributed around the entire cross section area up to

the boundary layer at the tunnel walls. This ensures that drops float in a stable fashion in the observation section of the tunnel (*Szakáll et al.,* 2009; *Diehl et al*., 2011). The drop size was determined from the recorded wind speed in the tunnel as it must be equal to the terminal velocity of the drop to keep the drop floating in the observation section. The drop temperature was calculated afterwards from the ambient temperature in the wind tunnel and the dew point with an estimated error of ± 1 K. Drop sizes of 680 ± 60 µm in diameter were selected because the onset of freezing was determined by direct observation (*Diehl et al.,* 2014). The experiments were performed at constant ambient temperatures, i.e., the wind tunnel was pre-cooled to certain temperatures in steps of 1 K. The adaption time of the drops, i.e., the time after which the drop temperature was equal to the ambient temperature was 4 to 5 s (*Diehl et al.*, 2014). Individual drops containing polydisperse illite NX particles were observed for approximately 30 to 40 s. 50 drops were investigated per temperature interval and particle concentration. Afterwards, the fractions of frozen drops were counted for a total observation time of 30 s.

Experimental uncertainties: The uncertainties for T and n_s are ± 1 ˚C and ± 35%, respectively. Similar to M-AL, the n_s uncertainty of M-WT includes errors of the frozen fractions of drops, the specific particle surface area, the particle masses per drop, and the drop sizes.

North Carolina State cold stage (NC State-CS)

The design of the NC State cold stage-supported droplet freezing assay (NC State-CS for brevity) and data reduction technique is described in detail in *Wright and Petters* (2013) and *Hader et al*. (2014). For the experiments reported here, aqueous suspensions ranging from 0.0001 to 1.0 wt% of dry illite NX powder and (18.2 MΩ cm resistivity) were prepared. Droplet populations of two distinct size ranges were investigated. Picodrops were generated by mixing a 15 µL aliquot of bulk suspension with squalene and emulsifying the hydrocarbon-water mixture using a vortex mixer. The emulsion was poured into an aluminum dish holding a hydrophobic glass slide. This resulted in between ~400 and 800 usable droplets per experiment with a typical diameter D ~ 85 µm. Nanodrops were generated by manually placing drops with a syringe needle tip on a squalene covered glass slide and letting the drops settle to the squalene-glass interface. This resulted in ~80 droplets per experiment with a typical diameter D ~ 660 µm. For all experiments the aluminum dish was cooled at a constant rate of 1 ºC min^{-1} and the fraction of unfrozen drops was recorded using a microscope in

increments of ΔT = 0.17 ºC resolution. To account for slightly higher temperatures of the squalene relative to the glass slide, a temperature calibration was applied to the nanodrop data (*Hader et al*., 2014). The resulting fraction of droplets frozen versus temperature data were inverted to find the concentration of INPs using the method of *Vali* (1971):

$$c_{\mathrm{IN}}(T) = -\frac{\ln(f_{\mathrm{unfrozen}})}{V_{\mathrm{drop}}} \qquad \text{(Eqn. S2)}$$

where $c_{\mathrm{IN}}(T)$ is the concentration of INPs per unit volume of water (m^{-3} water), f_{unfrozen} is the fraction of unfrozen drops at each particular temperature, and V_{drop} is the median drop volume of the population. To minimize sample heterogeneity, only droplets with 78 μm < D < 102 μm were included in the calculation of $c_{\mathrm{IN}}(T)$ for picodrops. No restriction was applied to the nanodrops. Furthermore, the warmest two percent of data was removed after the calculation of $c_{\mathrm{IN}}(T)$ before plotting due to large uncertainty stemming from poor counting statistics (*Hader et al*., 2014). The nuclei content of the ultrapure water was measured in the above manner, resulting in $c_{\mathrm{impurities}}(T)$. A best fit line was determined between -20 ºC and -35 ºC (approximately a homogeneous freezing point for the size of drops used). No impurities were detected at T > -20 ºC. The effective INP content was determined by subtracting the nuclei content in the water, $c_{\mathrm{impurities}}(T)$, from the measured $c_{\mathrm{IN}}(T)$ in the illite NX suspensions. For most conditions $c_{\mathrm{impurities}}(T)$ was negligible relative to $c_{\mathrm{IN}}(T)$. The ice nucleation surface active site density was then calculated via

$$n_{\mathrm{s,BET}}(T) = -\frac{c_{\mathrm{IN}}(T) - c_{\mathrm{impurities}}(T)}{\rho_{\mathrm{w}} w \theta_{\mathrm{N_2}}} \qquad \text{(Eqn. S3)}$$

where ρ_{w} is the density of water (997.1 kg H_2O m^{-3} H_2O), w is the mass ratio of dust and water (g dust g^{-1} water), θ_{N2} is the N_2-based SSA obtained by BET analysis (124.4 m^2 g^{-1} dust) and $n_{\mathrm{s,BET}}$ is the BET-normalized IN active surface-site density (m^{-2} dust).

Experimental uncertainties: The thermistor embedded in the lower aluminum block was capable of operating in the -40 < T < 0 °C range with a stated tolerance of ± 1 °C (Model TR141-170, Oven Industries). Repeatability of the temperature where 50% of pure water picodrops froze via homogeneous nucleation was -35.7 ± 0.1 °C (n = 5, average diameter of drops ~86 μm). In comparison, *Langham and Mason* (1958) report a median freezing temperature of drops ~ -34.4 °C for this size range. The spread in $n_s(T)$ reported as $\square n_s(T)$ =

232 [$n_{s,max}(T)$ - $n_{s,min}(T)/n_{s,average}(T)$] was □$n_s$(-30 °C) = 0.6 (n=4), □$n_s$(-25 °C) = 1.75 (n=4), □$n_s$(-
233 23 °C) = 1.28 (n=3) and □n_s(-20 °C) = 0.59 (n=2).
234
235 **University of Colorado Raman microscope cold stage (CU-RMCS)**
236
237 CU-RMCS has been described previously in detail (*Baustian et al*., 2010; *Schill and*
238 *Tolbert*, 2013). Briefly, a Nicolet Almega XR Raman spectrometer has been coupled to a
239 research grade Olympus BX-51 microscope with 10x, 20x, 50x, and 100x magnification
240 objectives. This Raman microscope has been outfitted with a Linkam THMS600
241 environmental cell. Temperature of a cold stage inside the cell is controlled by a Linkam
242 TMS94 automated temperature controller with an accuracy of 0.1 K. Water partial pressure
243 inside the cell is controlled by mixing dry and humidified flows of N_2 and measured by a
244 Buck Research CR-A1 dew point hygrometer in line with the cell. In the present experiments,
245 however, droplets are isolated from the cell humidity by a layer of silicon oil.
246 To generate droplets for an immersion freezing experiment, a known wt% solution of
247 illite NX sample was aspirated into a Meinhard TR-30 glass concentric nebulizer. The
248 concentration of clay in suspensions was determined gravimetrically. Illite NX powder was
249 used as provided without any previous size selection or modification. Clay solutions were
250 mixed for at least 12 hours with a magnetic stir bar prior to use in ice nucleation experiments.
251 To mitigate gravimetric settling prior to nebulization, humidified nitrogen was vigorously
252 bubbled through the clay solutions immediately before aspiration. Humidified N_2 was used as
253 the carrier gas to prevent excess evaporation at the nebulizer nozzle. The nebulized spray was
254 directed at a hydrophobically treated fused-silica disc, and the nebulized droplets were
255 allowed to coagulate into supermicron droplets. After nebulization, a drop of silicon oil was
256 placed over the supermicron droplets, and the entire disk was transferred to the environmental
257 cell. Despite low relative humidities inside the cell, droplets inside the drop of silicon oil did
258 not visibly grow or shrink, even after sitting for 12 hours. Prior to each experiment, droplets
259 were examined under 50x magnification to ensure that suspended material was visually
260 evenly distributed between droplets. Thus, the concentration of clay in the droplets was
261 assumed to be the same as the concentration of clay in the bulk solution. Experiments were
262 video recorded under 10x or 20x magnification at 30 frames per second and freezing events
263 were identified by the sudden appearance of structure within droplets. Ice nucleation frozen
264 fractions were calculated as a function of temperature. Depending on the size of the droplets,
265 frozen fraction curves were separated into four different size bins: 10-20 µm, 20-60 µm, 60-

120 µm, and 120-200 µm (lateral diameter). These size bins span droplet volumes from ~0.3 picoliter to 2.5 nanoliter. In the present experiment, the droplets were cooled from approximately 5 to -40 °C at a rate of 10 K min^{-1}. Errors in n_s values are based on the range of surface areas available in each experiment. The temperature error for all droplets, 0.5 K, were determined by repeated homogeneous freezing experiments on ultra-pure water.

Experimental uncertainties: For CU-RMCS, the errors (%) in log-scaled $n_{s,\mathrm{BET}}$ $\left(= 100 \times \frac{\log\left(n_{s,\mathrm{BET}}^{\mathrm{measred}}\right) - \log\left(n_{s,\mathrm{BET}}^{\mathrm{error}}\right)}{\log\left(n_{s,\mathrm{BET}}^{\mathrm{measred}}\right)}\right)$ derived from surface area deviations were estimated as 4.3%.

FRankfurt Ice Deposition freezinG Experiment (FRIDGE) diffusion cell

FRIDGE is an isothermal static vacuum vapor diffusion chamber that freezes droplets with immersed particles on a cold stage (S1.1; immersion mode operation) or nucleates ice on dry particles deposited on a substrate (S1.2; default mode operation).

Measurements of immersed particles: Aerosol was generated by dry dispersion of illite NX particles in air and diluted further with purified air. The particle number size distribution of this aerosol in the 0.3-10 µm diameter range was measured by a TSI 3330-OPS. Illite NX particles were collected by filtration of the aerosol using cellulose nitrate membrane filters (Millipore, HABP04700). After sampling the filters were placed in vials with 10 mL of deionized water. Particles were extracted from the filters by agitating for 10 min in an ultrasonic bath. It is noteworthy that the application of the ultrasonic bath and its high efficiency in the washing process for particle removal were demonstrated with a similar experimental setup employed by *Ardon-Dryer and Levin* (2014). About 80 droplets of 0.5 µL volume each were taken from the washing solution with an Eppendorff-pipette and were placed randomly on a silicon wafer on the cold stage. The temperature of the cold stage was lowered by 1 °C min^{-1} and the number of drops that froze at each temperature was recorded by the CCD camera and counted. This process was repeated several times with fresh droplets. The actual number concentration of INP derived from this measurement builds on the drop freezing concept of *Vali* (1971) as modified by *Ardon-Dryer and Levin* (2014), and is given by

$$K'(T) = \frac{1}{V} \times [\ln(N_0) - \ln(N(T))] \times \frac{x}{y} \quad \text{(Eqn. S4)}$$

where $K'(T)$ is the cumulative INP concentration at a temperature T. The droplet volume is given by V, N_0 is the total number of droplets, $N(T)$ is the number of frozen droplets at temperature, T. The variable x is the volume of water used to wash the particles from the filter and y the volume of air sampled through the filter.

Experimental uncertainties: FRIDGE measurement uncertainties are T ± 0.2 °C and n_s ± 40% at -20 °C. The n_s error may become lower with decreasing temperature. Background freezing induced by impurities in the water was observed at T < -23 °C. This background freezing contributed to less than 15 % of the overall freezing in the range of -25 °C < T < -23 °C and was accounted for the n_s estimation.

S1.2. Dry-dispersed particle measurement techniques

Aerosol Interaction and Dynamics in the Atmosphere (AIDA) cloud simulation chamber

Immersion freezing activity of dry illite NX particles pulverized by a rotating brush generator (PALAS, RBG1000) was investigated using AIDA-CECC. A series of expansion experiments with elevated temperature was performed in the temperature range between -27 and -35 ˚C. The results of a total of eighteen expansion experiments with ten polydisperse and eight size-selected illite NX particles (200, 300 and 500 nm mobility diameter segregated by a DMA) are reported in the present study.

AIDA-CECC consists of an 84 m^3 aluminum cylindrical vessel housed in a thermally insulated room. A mechanical pumping system is mounted directly under the AIDA vessel and used for expansion cooling, which actuates cooling during steady pressure drop from 1000 to 800 mb (*Möhler et al*., 2003). During the expansion cooling experiment controlled by a mechanical pump, the cooling rates of gas temperature in the vessel typically decrease from ~5 to <0.1 ˚C min^{-1}. The conditions in the vessel, such as temperature and relative humidity, can be continuously homogenized by a mixing ventilator installed on the base of the vessel. The chamber conditions are also monitored by temperature sensors (*Möhler et al*., 2003) and tunable diode laser (TDL) water vapor absorption measurement (*Fahey et al*., 2014) prior to and while running each experiment. The use of AIDA for both immersion mode and deposition mode freezing experiment is described in detail in previous reports (e.g., *Hiranuma et al.*, 2014a and 2014b, respectively) so only a brief description is provided here.

For the immersion mode experiment, spontaneous formation of water droplet occurs at water saturation while continuously cooling. Thereafter, water supersaturation condition in the vessel is maintained by controlled mechanical expansion. At droplet activation, most of clay mineral particles are presumably immersed in water drops leading to droplet-freezing at a characteristic temperature (*Hiranuma et al*., 2014b). Thus, within our definition of singular freezing, immersion ice nucleation activity of clay minerals solely depends on temperature.

Temporal evolution of size distribution and associated particle phase is measured using the welas optical spectrometers (PALAS, Sensor series 2300 and 2500; *Benz et al*., 2005) and a light scattering instrument, *Streulicht-intensitätsmessungen zum optischen Nachweis von Eispartikeln*, (SIMONE in *German*; *Schnaiter et al*., 2012) that are directly

mounted to the wall of the AIDA vessel. Two independent sensors of a welas deployed on the bottom vessel of AIDA in side by side position are used together to measure ice crystal size distributions over the size range of 0.5 to 150 μm optical diameter every 5 s. Assuming spherical shape of particles, the optical diameter is equivalent to a volume equivalent geometric diameter. The droplet-ice threshold diameter, D_{thresh}, is determined by SIMONE depolarization measurements (*Schnaiter et al*., 2012). The total ice number was calculated by summing ice numbers above the observed D_{thresh}, typically ~30 μm diameter. For the immersion experiments, we typically observe a full activation of droplets (i.e. number of droplets, $N_{droplet}$ > number of aerosols, N_{ae}), but in case of incomplete droplet activation (i.e. $N_{droplet} < N_{ae}$), the total geometric surface is normalized to a droplet number measured by a welas-OPC.

Experimental uncertainties: Temperature and humidity uncertainty is ± 0.3 ˚C and ± 5%, respectively (*Möhler et al*., 2003; *Fahey* et al. ,2014). The uncertainty involved in the n_s estimation for immersion freezing in AIDA-CECC was previously estimated as 35% (*Steinke et al*., 2011).

CSU Continuous Flow Diffusion Chamber (CSU-CFDC)

CSU-CFDC operating principles are described in the earlier works of *Rogers* (1988), *Rogers et al.* (2001) and *Eidhammer et al.* (2010). The current versions of CSU-CFDC used in ground based (CFDC-1F) and aircraft studies (CFDC-1H) are geometrically identical and composed of cylindrical walls that are coated with ice via flooding and expelling water from the chamber when the walls are set at a controlled temperature of ~ -27 °C before each experimental period. The plate separation is 1.12 cm prior to ice application, which has a typical thickness of 0.015 cm. The chamber is divided into two sections vertically, separated by a Delrin collar. A temperature gradient between the colder (inner) and warmer (outer) ice walls in the upper 50 cm section creates an ice supersaturated field into which an aerosol lamina is directed. The Delrin inlet manifold has a stainless steel knife edge ring threaded into it, so that aerosol flow is directed centrally between two sheath flows of clean and dry air. The ratio of aerosol and sheath flows can be varied, but typically the aerosol lamina represents 15% of the 10 L min^{-1} total flow. Ice crystals forming on ice nuclei in the growth region of the chamber enter the lower 30 cm “evaporation” section of the chamber where the two walls are held equivalently to the original low (inner) wall temperature. When the temperature gradient

in the growth section is adjusted to create water supersaturated conditions that activate cloud droplets, these will evaporate to haze sizes in the evaporation section, at least up to some RH_w where they survive, referred to by many as the droplet breakthrough RH_w. Until that high RH_w, only ice crystals and haze particles will exit the CFDC. Upstream of the CFDC, aerosol particle concentrations are measured by a CPC, sometimes after size selection with a DMA. Small numbers of large aerosol particles are removed just in advance of the CFDC inlet manifold using dual single-jet impactors typically set to cutpoint sizes between 1.5 and 2.4 μm depending on the nature of the experiment. Ice crystals and aerosols exiting the CFDC at sizes above approximately 500 nm are counted with an OPC, where the two populations are readily distinguished in different size modes. For the data collected in this work, we counted all particles in size bins above 3 μm as ice particles.

Present CFDC-1F measurements were focused into 5-10 min periods of sampling alternating with periods in which the aerosol sample was filtered in order to determine background frost influences on ice particle counts in the OPC, as described in a number of prior publications. Background counts were quite low, and so were subtracted as a simple average of filter periods before and after sampling.

Polydisperse illite NX particles were generated for size selection using the simple flask generator as described in *Tobo et al*. (2014). For collection of size-selected particles, several grams of dust were placed in a 250 mL conical flask, and dust released by blowing nitrogen in at the base (~2 L min^{-1}) while agitating the flask in an ultrasonic bath. The particle stream was passed through a dilution tank (N_2 flow rate into the tank ~5 L min^{-1}) and then through a ^{210}Po neutralizer before size selection of particles with a mobility diameter of 500 nm in a DMA (TSI Inc., Model 3081; sheath flow: 4.5 L min^{-1}, sample flow: 1.8 L min^{-1}). This stream was then divided, with 0.3 L min^{-1} passed to a CPC (TSI Inc., Model 3010) and 1.50 L min^{-1} drawn by the CFDC. The activated fraction was calculated by taking the ratio of the ice crystal number concentration to the total particle number concentration measured with the CPC.

For comparison with other IN instruments measuring in the immersion mode, we follow *Sullivan et al*. (2010a and 2010b) and a number of other papers from the CSU group in processing aerosol at $RH_w \approx 105$ %, with the understanding that higher active fractions of mineral dusts have been noted in processing up to about 110% RH_w (*Petters et al*., 2009; *DeMott et al*., 2011). We did not raise RH_w to these higher levels in these studies so that we could avoid any influence of droplet breakthrough. We do now report that for representative atmospheric mineral dusts, activation at 105% RH_w likely underestimates the active fraction

measured at 109% RH_w by the CFDC by a factor of 3 across a broad temperature range (*DeMott et al*. 2014).

Particle losses in upstream tubing, the aerosol impactor, and the inlet manifold of the CFDC have been previously estimated as 30% of total condensation nuclei when sampling ambient air (*Rogers et al*. 2001), but only 10% for aerosols in the 100 to 800 nm size range based on laboratory tests (*Prenni et al*. 2009). We did not correct for such losses in the ice nuclei data for 500 nm particles reported for the CFDC.

Experimental uncertainties: The thermodynamic conditions in the CFDC are inferred based on measurements of chamber pressure, wall temperatures and flow rates. Results are reported for the calculated average aerosol lamina position. The solution for the lamina position, and thus its temperature and supersaturation, requires numerical solution (*Rogers*, 1988), thus making the calculation of uncertainty in the conditions more complex than propagation of error. *Richardson* (2009) used Monte-Carlo methods to estimate the uncertainty in reported lamina temperature and supersaturation, assuming the typical 1 °C temperature variation along the length of the CFDC cylindrical walls. On this basis, temperature uncertainty is ± 0.5 °C at the reported CFDC processing temperature, independent of processing temperature. Supersaturation uncertainty was found by *Richardson* (2009) to depend inversely on temperature. This uncertainty may be approximated by the relation ΔRH_w (%) = 21.8 - 0.08 T (in Kelvin). Thus, ΔRH_w uncertainty is ± 1.6, 2 and 2.4 % at -20, -25, and -30 °C, respectively. This temperature uncertainty propagates into and n_s uncertainty of ± 60% at any temperature. This dominates over the variation in N_{ice} at any temperature when N_{ice} is determined for statistically meaningful sample periods, as reported.

ElectroDynamic Balance (EDB) levitator

The EDB setup was used for investigation of the contact and immersion freezing of levitated supercooled water droplets colliding with the illite particles. The setup used for the contact freezing experiments is described in detail by (*Hoffmann et al*., 2013a and 2013b) and therefore only briefly explained here. The centerpiece of the setup is an electrodynamic balance (EDB) for levitating charged water microdroplets. The droplets with diameter of 90 µm are produced by a piezoelectric injector (GeSIM model A010-006 SPIP, cylindrical housing) and charged via induction to the value of 1 pC (*Rzesanke et al*., 2012). The aerosol is generated by a fluidized bed generator operated with synthetic air followed by a multistage impactor to eliminate the super micron particles from the aerosol flow. Specifically, the multi-

orifice rotating stage cascade impactor (LPI-ROT 25/0018, HAUKE) operated with five impactor stages (largest cut-off diameter 2 µm) was used as described in *Hoffmann et al.* (2013b). Only particles of the desired electrical mobility diameter (750, 550 and 320 nm, as preselected by Differential Mobility Analyzer, TSI Inc., Model 3081) were allowed to enter EDB. After EDB, the particle number concentration was counted by an Ultrafine Condensation Particle Counter (UCPC, TSI Inc., Model 3776).

To perform immersion freezing experiments we have modified the setup in the following way. The supercooled water droplet was exposed to the flow of the aerosol particles only for a limited time t_1. During this time the droplet, if not frozen via contact nucleation mechanism, has collected average number of particles equal to the product of collision rate (calculated theoretically) and the time t_1. After that, the aerosol particles were removed from the flow by switching on the electrostatic precipitator installed just in front of EDB. For $t > t_1$ the droplet can only freeze via the immersion freezing pathway induced by the particles it has already collected during $t < t_1$.

To compare contact and immersion freezing results we calculate the ice nucleation active surface-site density, n_s, which is given by the following equations:

$$t < t_1(\text{contact mode}): n_s(T) = -\frac{\ln(1-f_{ice}(T))}{S_{IN} n_c t} = \frac{e_c}{S_{IN}} \quad \text{(Eqn. S5)}$$

$$t > t_1(\text{immersion mode}): n_s(T) = -\frac{\ln(1-f^*_{ice}(T))}{S_{IN} n_c t_1 t} \quad \text{(Eqn. S6)}$$

where f_{ice} is the frozen fraction after time t, e_c is the probability of freezing on a single contact, n_c is a collision rate, S_{IN} is surface area of a single ice-nucleating particle, f^*_{ice} is a fraction of droplets frozen heterogeneously after the aerosol flow was switched off.

Experimental uncertainties: The temperature uncertainty is $T \pm 0.2$ °C, and the uncertainty of the freezing probability is $e_c \pm 35\%$. The uncertainty for n_s depends on the uncertainty of the BET surface. Assuming a BET uncertainty of 10-20%, the uncertainty is n_s ± 50-69%.

Fast Ice Nucleus CHamber (FINCH)

FINCH is an online instrument in which aerosol particles are activated to ice crystals under different freezing temperatures and supersaturations. It consists of a chamber (stainless steel tube, 80 cm in length, 8.6 cm inner diameter) for which the wall can be cooled down to temperatures between 0 and -65 °C. Inside the chamber a specific supersaturation and temperature is reached by mixing the sample flow of ambient aerosol with a warm moist and a cold dry airflow (*Bundke et al*., 2008). By changing the flow rates and/or temperatures of the individual airflows the chamber supersaturation and freezing temperature can be varied relatively quickly. Ice-nucleating particles entering the chamber are activated and grow to sizes of a few micrometers. At the end of the growth tube they are counted in an optical particle counter (OPC) similar to the detector described in *Bundke et al*. (2010) (405 nm wavelength laser with a power of 100 mW). It is able to distinguish between water droplets and ice crystals by analyzing the polarization ratio of the scattered circular polarized light (P44/P11 ratio of the scattering matrix; *Hu et al*., 2003) and detects the auto-fluorescence following from excitation of the grown particles with UV light, which is an indication for biological particle material.

The presented FINCH illite NX dataset was obtained during a joint campaign with LACIS at the Leibniz Institute for Tropospheric Research (TROPOS) facility. Therefore the aerosol generation is identical as described for the LACIS experiments (see below). Size-selected illite NX particles of 500 nm in diameter were fed into FINCH, which was operated at a saturation ratio above water saturation and at temperatures between -21 and -28 °C. The frozen fraction, α, was calculated by division of the N_{ice} detected by FINCH at a certain freezing temperature and the number concentration of all particles, which was measured in parallel to FINCH by a CPC (TSI Inc., Model 3010).

Experimental uncertainties: The FINCH uncertainties for the freezing temperature are in the range of ± 1.5 °C and ± 30% for n_s. A potential systematic over-estimation of the freezing temperature due to imperfect mixing of the individual airflows are a matter of current investigations.

FRankfurt Ice Deposition freezinG Experiment (FRIDGE) diffusion cell

FRIDGE is an isothermal static vacuum vapor diffusion chamber that freezes droplets with immersed particles on a cold stage (S1.1; immersion mode operation) or nucleates ice on dry particles deposited on a substrate (S1.2; default mode operation).

Dry particle measurements: The default mode operation of FRIDGE provided data at -18 and -25 °C (a total of ten data points with five points at each temperature). INPs were collected from the dry illite NX particles in AIDA by electrostatic precipitation of the particles onto silicon wafers of 45 mm diameter. After sampling the wafers were placed on the cold table in the FRIDGE isothermal chamber (~500 mL volume; *Klein et al*., 2010), which was then evacuated. Upon inflation of water vapor into the chamber ice crystals grew on the INP, were photographed by a CCD camera, and were counted automatically for around 100 s. It is assumed that one ice crystal represents one INP active at the selected temperature and vapor pressure. Crystals can be evaporated by evacuation of the chamber, and the measurement can be repeated at another temperature and/or supersaturation. The cold stage temperature can be regulated from 0 to -35 °C.

Experimental uncertainties: FRIDGE measurement uncertainties are $T \pm 0.2$ °C and $n_s \pm 40\%$ at -20 °C. The n_s error may become lower with decreasing temperature.

Leipzig Aerosol Cloud Interaction Simulator (LACIS)

LACIS was used in its immersion freezing mode (*Hartmann et al*., 2011) to study immersion freezing efficiency of illite NX particles. LACIS measurements were performed on size segregated particles. Particle generation was done using a similar setup as e.g. described in *Wex et al*. (2014). In short, illite NX particles were made airborne using a fluidized bed. Subsequently, particles larger than those which should be examined were removed from the aerosol using a micro orifice uniform deposition impactor (MOUDI, MSP Corporation, USA, Model 100R) and a cyclone. Downstream, a neutralizer established a bipolar equilibrium charge distribution on the particles. Then particles were size-selected by a DMA (Type Vienna Hauke medium; aerosol to sheath air flow ratio of 1:10), and selected particle sizes were 300, 500 and 700 nm. The aerosol was then provided for further analysis.

The before mentioned removal of larger particles was done to minimize the number of multiply charged particles that pass the DMA, and measurements with a UHSAS (Ultra-High Sensitivity Aerosol Spectrometer, DMT) behind the DMA were done to confirm that the number of multiply charged particles could be neglected.

Size-selected aerosol particles were also fed into a CPC (TSI Inc., Model 3010), and into LACIS. LACIS is a flow tube, consisting of 7 sections where each is 1m long. Each section can be temperature controlled separately. Temperatures can go down to -40 °C. Before entering the flow tube, by use of a humidifier (Perma Pure, PH-30T-24KS), the sheath air stream is hydrated such that droplets form on the aerosol particles upon cooling, i.e. while passing through the flow tube. The droplets can subsequently freeze, depending on the nature of the immersed aerosol particle and the adjusted temperature. At the LACIS outlet, a home-built optical particle spectrometer (*Clauss et al*., 2013) is used to determine if the arriving hydrometeors are liquid droples or frozen ice crystals. This information then is used to derive a frozen fraction, α.

Experimental uncertainties: The temperature uncertainty is $T \pm 0.3$ K, the uncertainty of the measured α is on average ± 27.4%. The uncertainty in n_s was calculated accounting for this measurement uncertainty and for the uncertainty related to the width of the transfer function in the DMA, which was assumed to be 5%. The resulting uncertainty in n_s derived from LACIS data is 28%.

Meteorological Research Institute Dynamic Controlled Expansion Cloud-simulation Chamber (MRI-DCECC)

The DCECC at Meteorological Research Institute (MRI) in Tsukuba, Japan (*Tajiri et al*., 2013) was used to investigate immersion freezing properties of dry illite NX particles. The DCECC can simulate quasi-adiabatic expansions by synchronously controlling air pressure and inner wall temperature of the chamber vessel. MRI-DCECC warrants experiments with atmospherically relevant droplet sizes as well as controllable droplet onset temperature ($T_{\mathrm{droplet,onset}}$) and supersaturation conditions resulting in freezing of particles in water droplets. Dry illite NX particles were aerosolized by a rotating brush generator (PALAS, RBG1000) and injected into the ventilated 1.4 m^3 chamber vessel. All experiments were performed by employing a constant cooling rate of about -3 ˚C min^{-1} (equivalent to the updraft rate of about 5.0 m s^{-1}) from initial gas temperature typically about 5 ˚C. The DCECC is equipped with

various devices, such as an SMPS, a welas-OPC, an APS and a CPC, for sensing cloud formation and measuring size distributions and shapes of aerosol and cloud particles from 0.01 to several hundred micrometers in size. As these instruments were also employed at AIDA-CECC, the procedures to calculate the total ice number and total geometric surface were also consistent with AIDA measurements.

Experimental uncertainties: The temperature uncertainty in MRI-DCECC is $T \pm 1.0$ °C for the evacuation rate corresponding to 5.0 m s^{-1}. The 40% uncertainty for n_s was derived from the errors in the measurements of N_{ice} by a welas (20%; *Möhler et al*., 2006) and surface area estimation (34%). More specifically, the uncertainty for surface area estimation was derived from the relative standard deviation of the 10 s time-averaged welas surface measurements for approximately 5 min prior to expansion experiments (i.e., MRI02_131001a, MRI02_131003b and MRI02_131004).

Portable Ice Nucleation Chamber (PINC)

PINC operation principle is based on the Continuous Flow Diffusion Chamber (*Rogers*, 1988). Two flat parallel plates (568 x 300 mm) whose inner walls coated with ice before each experiment are temperature controlled so as to apply a temperature gradient between the ice layers leading to a supersaturation with respect to ice and water. This allows ice crystals to form and grow on ice nuclei in the water sub-saturated (RH_w < 100 %) and supersaturated (RH_w > 100 %) regimes thus inferring deposition and condensation freezing respectively. Any water drops that may form will evaporate in the evaporation section downstream of the freezing chamber. Upstream of PINC, aerosol particles are counted with a CPC after flowing through an impactor with a D_{50} cutoff at 0.91 µm aerodynamic diameter (*Chou et al*., 2011). The ice crystals are counted with an OPC at the exit of PINC and are distinguished from the small, unactivated aerosol particles by their size. For the data collected in this work, we counted all particles in size bins above 2 µm to be ice particles since the illite NX particles we sampled were 500 and 1000 nm in diameter. Measurements conducted for 3 min before each sample and one minute after a sample were averaged in order to determine the background signal in the OPC. These values were then subtracted from the IN concentrations obtained during sample measurement to correct for the background. Further details on the PINC design and operation are described in *Chou et al*. (2011) and *Kanji et al*. (2013).

Polydisperse illite NX particles that were suspended in the 4 m^3 volume aerosol buffer chamber were size-selected using a DMA and counted using a CPC after which they were sampled by PINC. The activated fraction is calculated by taking the ratio of the ice crystal number concentration to the total particle number concentration measured with the CPC. Particles with diameters 500 and 1000 nm were size-selected using the Maxi-DMA developed at the TROPOS and described in more detail elsewhere (*Raddatz et al*., 2013).

For comparison with other IN counters measuring in immersion mode, only IN data taken by PINC at $RH_w \geq 104$ % and below the RH_w at which droplets survive past the evaporation section ($RH_{w,ds}$), are presented. For each temperature, RH was scanned continuously from RH_{ice} = 100 % up to $RH_{w,ds}$. $RH_{w,ds}$ lies for T = -20 °C at 105 % and at -38 °C at 109 %.

Particle losses in the tubing and the impactor upstream of PINC were accounted for by a particle loss curve determined for kaolinite particles with a mobility diameter between 500 – 950 nm. As such the data for 500 and 1000 nm particles have been corrected for losses through the impactor of 25 and 60% respectively.

At lower temperatures, the results show reasonable agreement with AIDA and LACIS measurements, however at higher temperatures (-25 °C) we find that for the 1000 nm particle we underestimate the n_s compared to LACIS for example. The reason for this is that we do not have enough residence time in the growth and nucleation section of PINC (residence time of 4-5 s) to fully activate the particles into droplets and as such underestimate the activated fraction in immersion mode. The way to compensate for this would be to sample at higher RH_w (as we do for lower temperatures), but at higher temperatures we are limited by the water drop survival line (RH_w = 105%) so we cannot compensate for the short residence time by taking data points at higher RH_w. As such, data taken for immersion freezing at higher temperatures could mean that we are underestimating immersion freezing, or rather be reporting deposition nucleation or condensation freezing.

Experimental uncertainties: Temperature uncertainties are on the order of ± 0.1 ˚C resulting in a relative uncertainty of ± 2% in RH. The temperature uncertainty results in a variation across the sample lamina of ± 0.4 ˚C. Uncertainty in N_{ice} (From OPC) is 10% and surface area estimate is about 25% resulting in an uncertainty in n_s of ± 27%.

627 **PNNL Compact Ice Chamber (PNNL-CIC)**

628

629 Heterogeneous ice nucleation properties of illite NX dust particles generated by the
630 small-scale powder disc-disperser (SSPD, TSI, Model 3433) were investigated using ice
631 nucleation chamber located at Atmospheric Measurement Laboratory, an atmospheric
632 sciences laboratory at Pacific Northwest National Laboratory (PNNL), WA., USA. The
633 working principle of PNNL compact ice chamber (PNNL-CIC) has been described in the
634 literature (*Stetzer et al*., 2008; *Friedman et al*., 2011; *Kulkarni et al*., 2012); its design and
635 experimental details are as follows. PNNL-CIC is a continuous flow diffusion chamber
636 consisting of two flat, vertical parallel aluminum plates that are cooled and covered with a
637 layer of ice. The chamber also has an evaporation section attached at the bottom of the
638 chamber to remove water droplets. The chamber design ensures that aerosols are exposed to
639 constant temperature and RH_{ice} over the length of the chamber. Saturation vapor pressures
640 over ice and water are calculated using formulations published by *Murphy and Koop* (2005).
641 The chamber wall temperatures are controlled by using two external cooling baths (Lauda
642 Brinkmann Inc.), and temperature data are logged using the National Instrument CompactRIO
643 programmable automation controller (cRIO-9114 combined with cRIO-9022). The chamber
644 plates are temperature controlled independently to develop a linear temperature gradient
645 across them, which according to the principle of thermal gradient diffusion theory, produces a
646 supersaturation profile between the plates (e.g., *Rogers et al*., 1988). Recently we modified
647 the evaporation section design, such that this section now has separate cooling bath and its
648 temperature is independently controlled. Temperature of the evaporation section is typically
649 maintained at ~ -32 °C. At the beginning of the experiment, the chamber walls are coated with
650 an ~0.5 mm thick ice layer, and the temperature gradient is set at zero, which creates ice-
651 saturation conditions inside the chamber (RH_{ice} = 100 %), Then, the refrigeration system cools
652 one plate and warms the other to increase the RH_{ice}. The total flow used is 11 L min^{-1}; sheath
653 and sample flows used were 10 and 1 L min^{-1}, respectively, which limits the aerosol residence
654 time to ~12 s within the CIC. Ice nucleates on the aerosol particles and the newly formed ice
655 crystal grows to a size greater than the original aerosol size, and ice crystals >3 μm exiting the
656 chamber are counted with an OPC (CLiMET, model CI-3100). The ice active fraction was
657 calculated as the ratio of number of ice crystals measured by the OPC to the condensation
658 nuclei available for nucleation. Background ice nuclei concentrations were calculated to
659 estimate the lower detection limit of an α. The lower detection limit of α was <0.01 %. To

660 make sure our background IN concentrations are less than 0.01 %, we restrict our
661 experimental time to less than 3 hours.

662 **Experimental uncertainties:** Temperature uncertainty is ~ ± 0.3 ˚C. For n_s the
663 uncertainty arises from N_{ice} measurement and surface area estimation. The resulting error is ~
664 ± one order of magnitude at any $n_s(T)$ space.

665

666 **Zurich Ice Nucleation Chamber with Immersion Mode Cooling chAmber (IMCA-ZINC)**

667

668 ZINC is a parallel plate CFDC type chamber developed by *Stetzer et al*. (2008)
669 following the design described in the work of *Rogers* (1988). The chamber inner-walls are
670 coated with ice prior to experiments. Under equilibrium conditions, linear temperature and
671 vapor pressure gradients are established between the warmer and colder walls creating
672 supersaturated conditions with respect to ice or water in the chamber volume. The two
673 chamber walls are separately temperature-controlled by two cryostats (Lauda RP890).
674 Independent temperature control of the two walls enables experiments at relative humidity
675 conditions ranging from ice saturation until several hundred per cent of water saturation. An
676 evaporation section, where both walls are kept at the same temperature to create ice saturated
677 but water-sub-saturated conditions, is able to evaporate potentially formed droplets, before
678 being sampled by an OPC. Deposition mode experiments are conducted by scanning through
679 relative humidity space while keeping the experimental temperature constant by increasing the
680 temperature gradient between the two wall plates. The streamline of the injected illite NX
681 particles (generated by a combination of a TSI fluidized bed, a series of URG cyclone
682 impactors and a TSI DMA; *Welti et al*., 2009) is maintained at approximately the center
683 position between the ice coated walls by two layers of particle-free sheath air. At the exit of
684 ZINC, ice crystals are detected and distinguished from inactivated particles by size using an
685 OPC (Climet Cl-3100). The particle concentration introduced into the experiment is detected
686 with a butanol-CPC (TSI 3010).

687 The IMCA chamber was developed by *Lüönd et al*. (2010) as a vertical extension to
688 ZINC and has the same parallel plate geometry. The walls are layered with continuously
689 wetted filter papers and temperature controlled. Similar to ZINC, a horizontal temperature
690 gradient is applied to create supersaturation with respect to water between the walls. When
691 entering IMCA, particles are exposed to 120% saturation with respect to water at 40 °C to

trigger droplet formation and growth. Subsequently, a vertical temperature gradient is established to cool the formed droplets down to the experimental temperatures prevailing in ZINC. For immersion freezing experiments ZINC is held at water saturated conditions to prevent evaporation or droplet growth. Droplets and ice crystals are detected in line before entering ZINC's evaporation section using the Ice Optical DEpolarization detector (IODE) described in *Nicolet et al*. (2010). IMCA-ZINC combination mimics an atmospheric pathway where particles are activated as cloud droplets at temperatures above 0 °C, subsequently cooled and exposed to sub-zero temperatures at which freezing can occur.

Experimental uncertainties: Temperature uncertainty is ± 0.4 ˚C. The uncertainties in $n_s(T)$ are propagated from the uncertainties in IODE and the surface area (± 25%).

S2. Supplementary Figures

An X-ray diffraction measurement was performed by a Panalytical X`Pert Pro device (fixed divergence, 40 kV, 30 mA, $CuK_a$ exication). For data analysis the X`Pert Pro software was applied. While we successfully identified several different forms of orthoclase ($KAlSi_3O_8$) with some Na inclusion, we cannot specify the type of K-feldspar polymorphs (e.g., microcline). Therefore, we define the feldspar as orthoclase or sanidine in the present study.

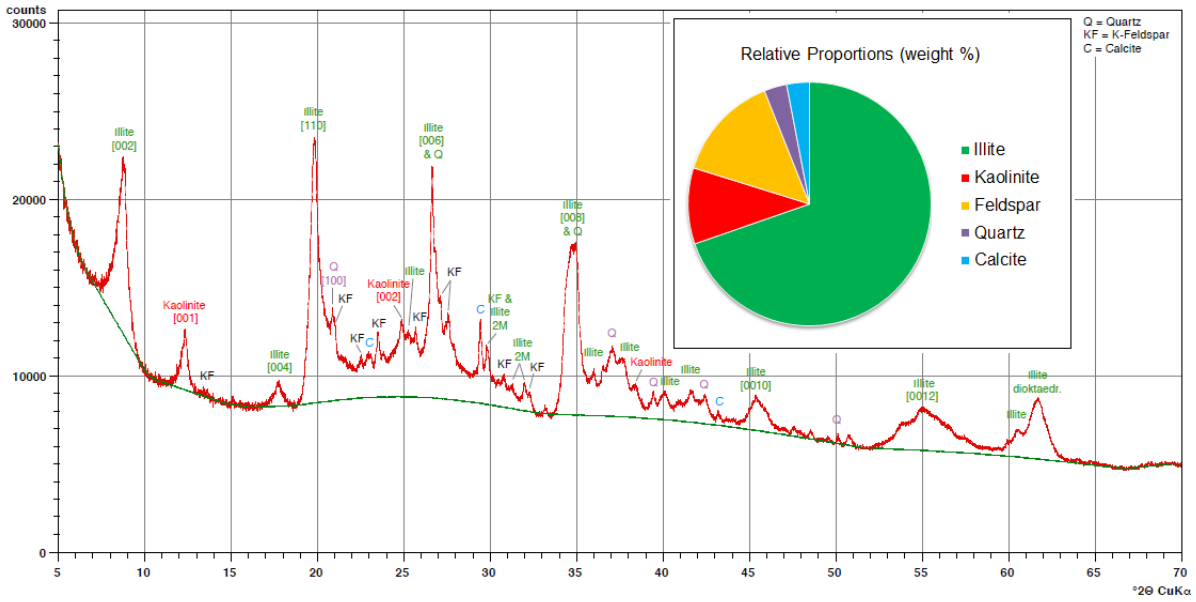

Figure S1. X-ray diffraction spectrum of the illite NX sample. The pie chart reflects the wt% presented in Table 2 (*this study*).

Spectra of $n_s(T)$ (Figs. 4 and 5) can be converted to $n_m(T)$ spectra using Eqn. 4. Spectra of $n_m(T)$ are presented in Fig. S2. Illite NX is insoluble and is a non-swelling dust, so $n_m(T)$ may not correctly represent its immersion freezing efficiency (*Murray et al.*, 2012). However, we note that this IN mass reflects the most direct representation of suspension measurements since conversion of α into $n_{m,\mathrm{sus}}(T)$ requires only one value, which is SSA (Eqn. 4).

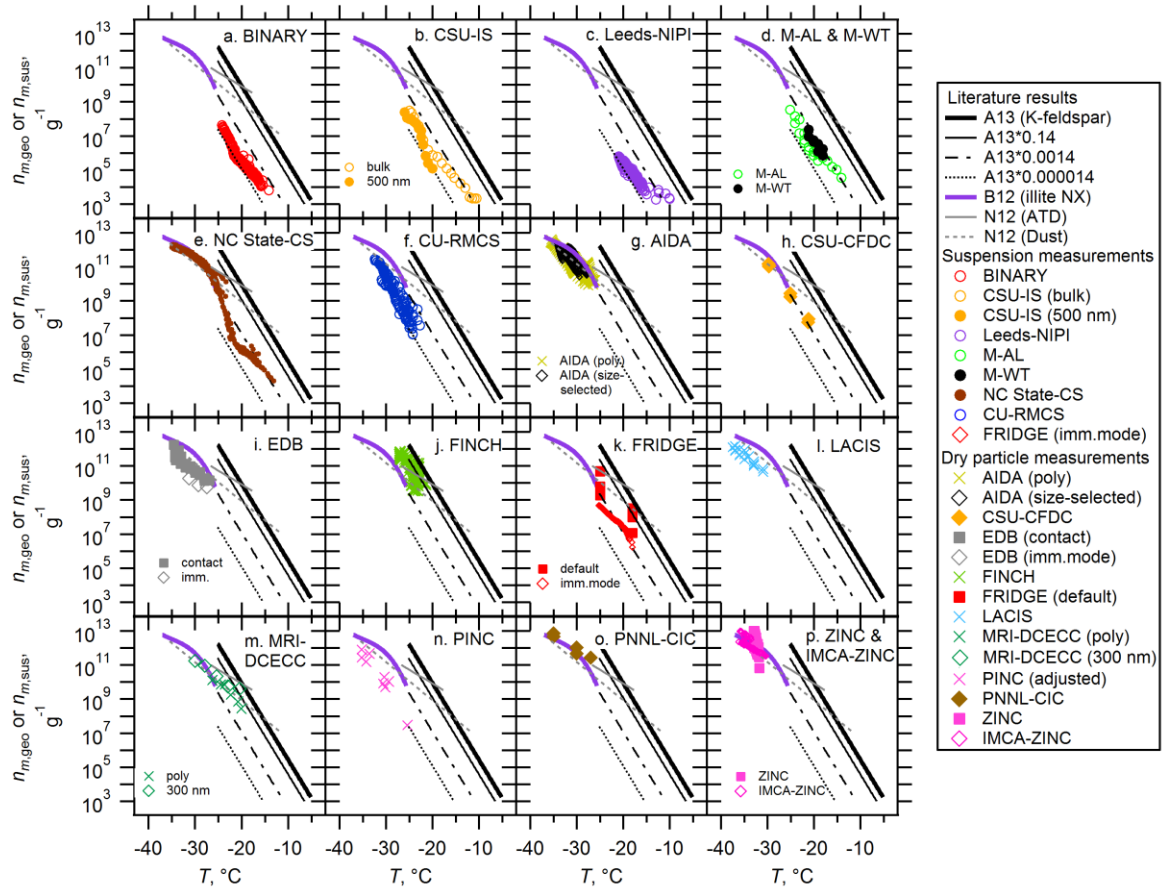

Figure S2. Inter-comparison of seventeen instruments with $n_{m,\mathrm{geo}}$ or $n_{m,\mathrm{sus}}$ (for dry-dispersed particle and suspension measurements, respectively). Note that M-AL and M-WT results are presented in single panel (d). In (k), FRIDGE results of default (solid square) and imm.mode (open diamond) are presented. Both ZINC (solid square) and IMCA-ZINC (open diamond) data are shown in (p). Reference immersion freezing $n_s(T)$ spectra for illite NX (B12), K-feldspar (A13), ATD and desert dusts (Dust) (N12) are also shown (See Sect. 3.2).

The linear space n_s average as presented in Fig. 8 may bias the fit to higher n_s values. Therefore, we present T-binned $n_{s,BET}(T)$ and $n_{s,geo}(T)$ spectra averaged in the 'log space' in Fig. S3a and b, respectively. In a similar way to the presentation in Fig. 8, panels i, ii and iii of Fig. S3 show T-binned data averaged in the log space of all seventeen instruments, all suspension type measurements, and all measurements that involved dry particles, respectively, while panel iv shows a comparison between suspension and dry-particle measurements. To be comparable with Fig. 8, the data from 'EDB (contact)' and 'ZINC' (*Welti et al.*, 2009) were not used to generate T-binned data. As can be seen in both Fig. S3 and Fig. 8, there seems a different trend between suspension and dry-dispersed particle measurements for this mineral dust. Thus, the choice of averaging procedure does not influence our data interpretation of the observed deviation (i.e., n_s from dry-dispersed methods > n_s from suspension methods) in this study.

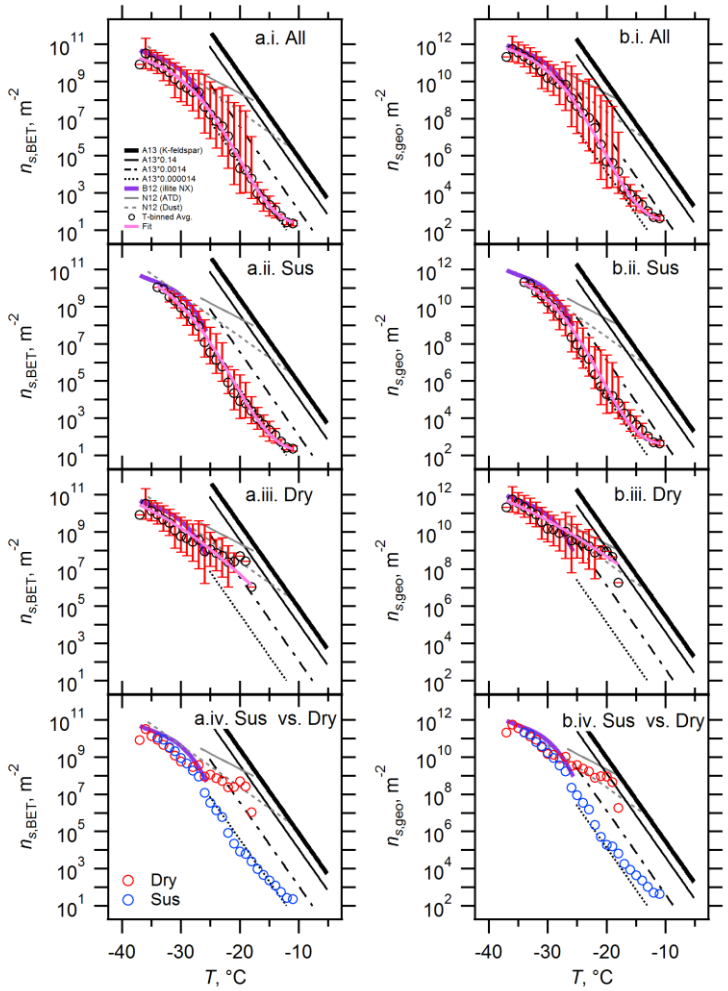

Figure S3. T-binned spectra based on $n_{s,geo}$ (a) and $n_{s,BET}$ (b). T-binned data (i.e., average in the log space with 1 ˚C bins for -37 ˚C < T < -11 ˚C) of $n_s(T)$ spectra are presented for (i) All interpolated dataset (All), (ii) Suspension measurements (Sus), (iii) Dry-dispersed particle measurements (Dry), and (iv) comparison between Sus and Dry. Red sticks represent maxima (positive direction) and minima (negative direction). Literature results (B12, A13, and N12) are also shown.

Figures S4 depicts the n_s diversity in $\log(n_{s,ind.})/\log(n_{s,fit})$, which represents the ratio of the individual measurements ($n_{s,ind.}$) to the log fit line to either all data [All (log)], the suspension data [Sus (log)] or the dry-dispersed particle data [Dry (log)] as $n_{s,fit}$. The interpolated T-binned data (i.e., interpolated data points in Figs. 4 and 5) are used for $n_{s,ind.}$. The fit in the log space, which is derived from the parameters summarized in Table 3, is used as a denominator to avoid a bias of sudden jump of the reference value at certain temperatures where the number of available data changes. As shown in the figure, data deviation (i.e., scatter from the Avg. $\log(n_{s,ind.})/\log(n_{s,fit})$ = 1 line) can be seen in both suspension measurements and dry aerosol measurements. This deviation is observed with all the $n_{s,fit}$ cases [All (log), Sus (log) and Dry (log)]. Additionally, the scatter of individual non-T-binned data and the validity of interpolations are presented in Figs. S5-S8. In specific, these four figures (Figs. S5-S8) complement panels a.ii and a.iii, panels b.ii and b.iii, panels a.iv anda.v and panels b.iv and b.v. from Fig. S4, respectively, in greater detail.

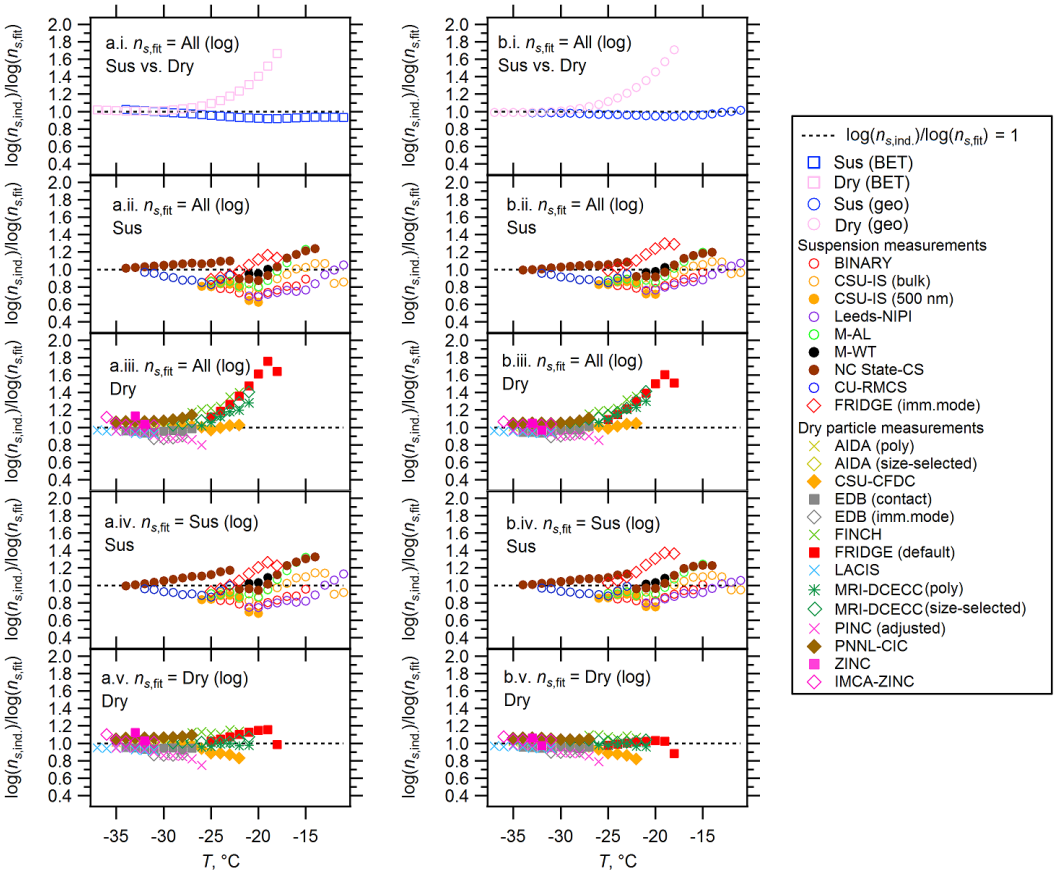

Figure S4. T-binned ratios of the interpolated individual measurements to the fit of the data, $\log(n_{s,ind.})/\log(n_{s,fit})$, based on the BET (a) and geometric (b) surface area, across the temperature range covered for all the measurement techniques used in the present study (i.e., 1 ˚C bins for -37 ˚C < T < -11 ˚C). T-binned $\log(n_{s,ind.})/\log(n_{s,fit})$ are presented for (i) ratios of the log fit to suspension measurements [Sus (log)] or dry-dispersed particle measurements [Dry (log)] to the log fit to all the data [All (log)], (ii) ratios of the individual suspension measurements to All (log), (iii) ratios of the individual dry-dispersed particle measurements to All (log), (iv) ratios of the individual suspension measurements to Sus (log) and (v) ratios of the individual dry-dispersed particle measurements to Dry (log). The black dotted line represents $\log(n_{s,ind.})/\log(n_{s,fit})$ = 1.

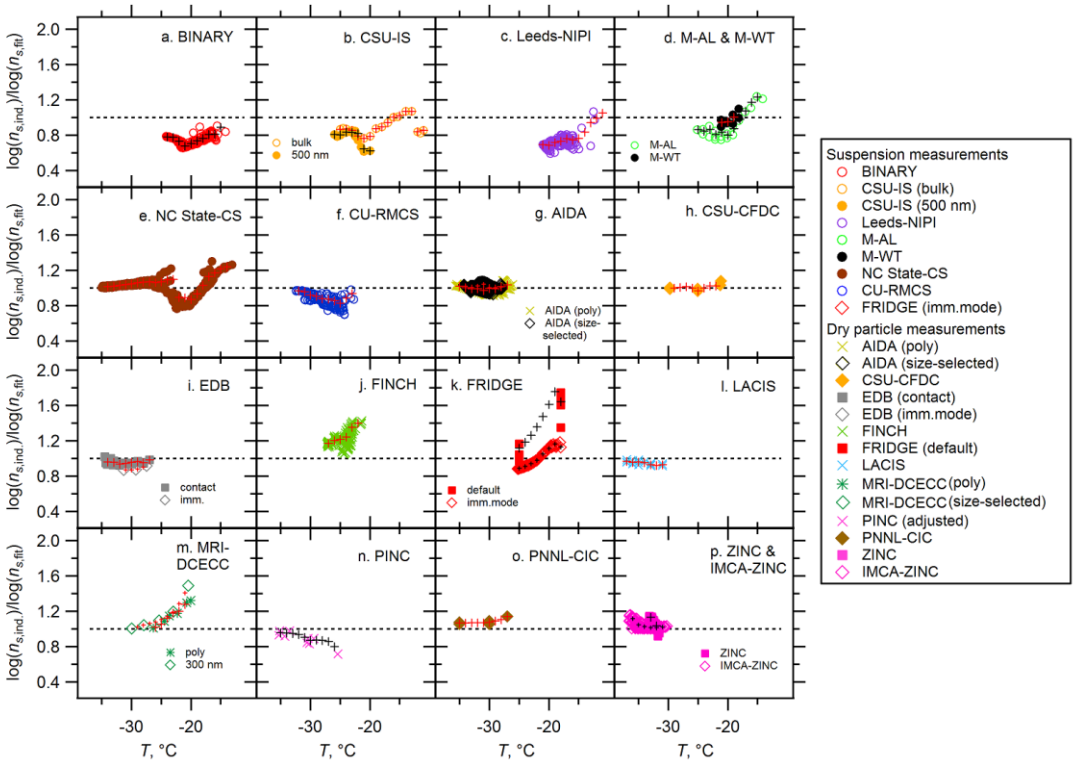

Figure S5. Ratios of the individual measurements to the log fit to all the data [All (log)], $\log(n_{s,ind.})/\log(n_{s,fit})$, based on the BET surface area ($n_{s,ind.} = n_{s,BET}$). Black or red cross markers represent *T*-binned ratios of the interpolated individual measurements to All (log) in comparison to the non-*T*-binned ratios. The black dotted line represents $\log(n_{s,ind.})/\log(n_{s,fit}) = 1$.

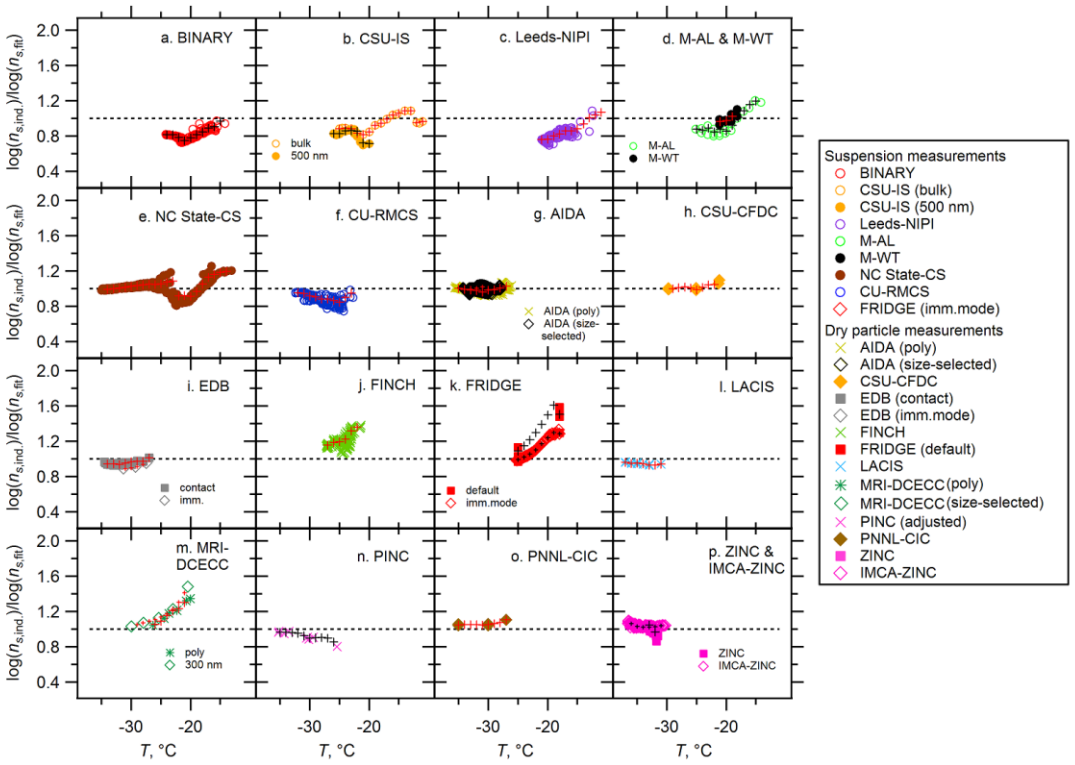

Figure S6. Ratios of the individual measurements to the log fit to all the data [All (log)], $\log(n_{s,ind.})/\log(n_{s,fit})$, based on the geometric surface area ($n_{s,ind.} = n_{s,geo}$). Black or red cross markers represent *T*-binned ratios of the interpolated individual measurements to All (log) in comparison to the non-*T*-binned ratios. The black dotted line represents $\log(n_{s,ind.})/\log(n_{s,fit}) = 1$.

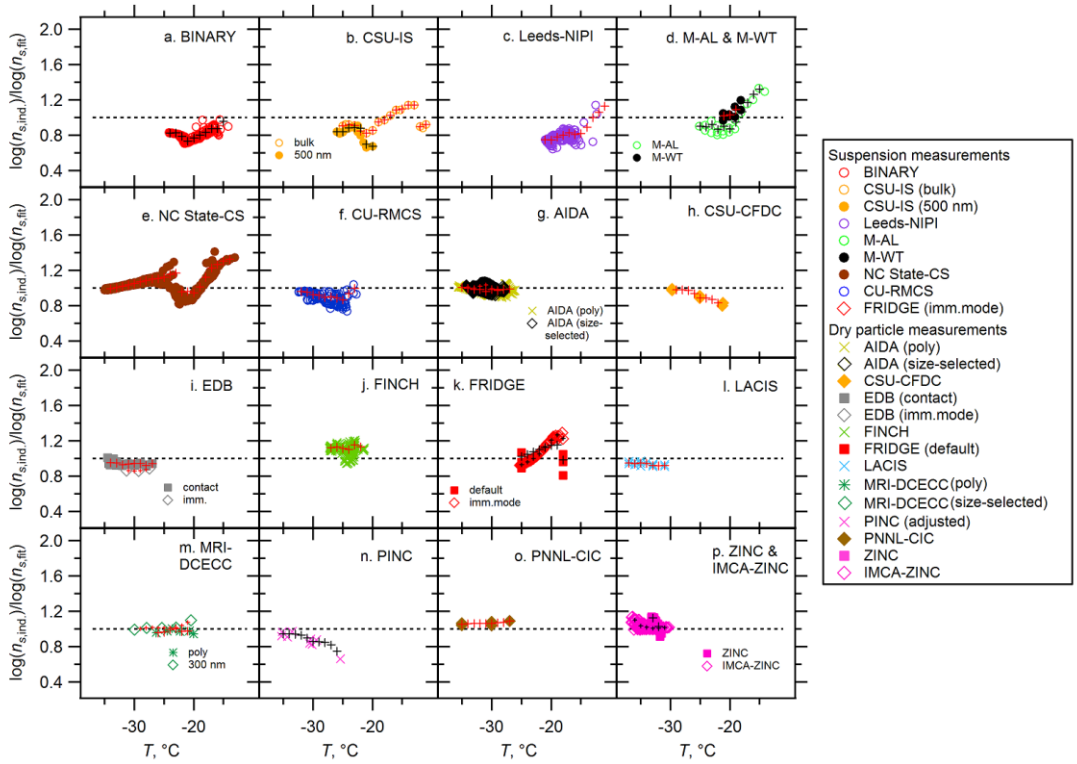

Figure S7. Ratios of the individual measurements to the log fit to suspension measurements [Sus (log)] or dry-dispersed particle measurements [Dry (log)], $\log(n_{s,ind.})/\log(n_{s,fit})$, based on the BET surface area ($n_{s,ind.} = n_{s,BET}$). Black or red cross markers represent *T*-binned ratios of the interpolated individual measurements to Sus (log) or Dry (log) in comparison to the non-*T*-binned ratios. The black dotted line represents $\log(n_{s,ind.})/\log(n_{s,fit}) = 1$.

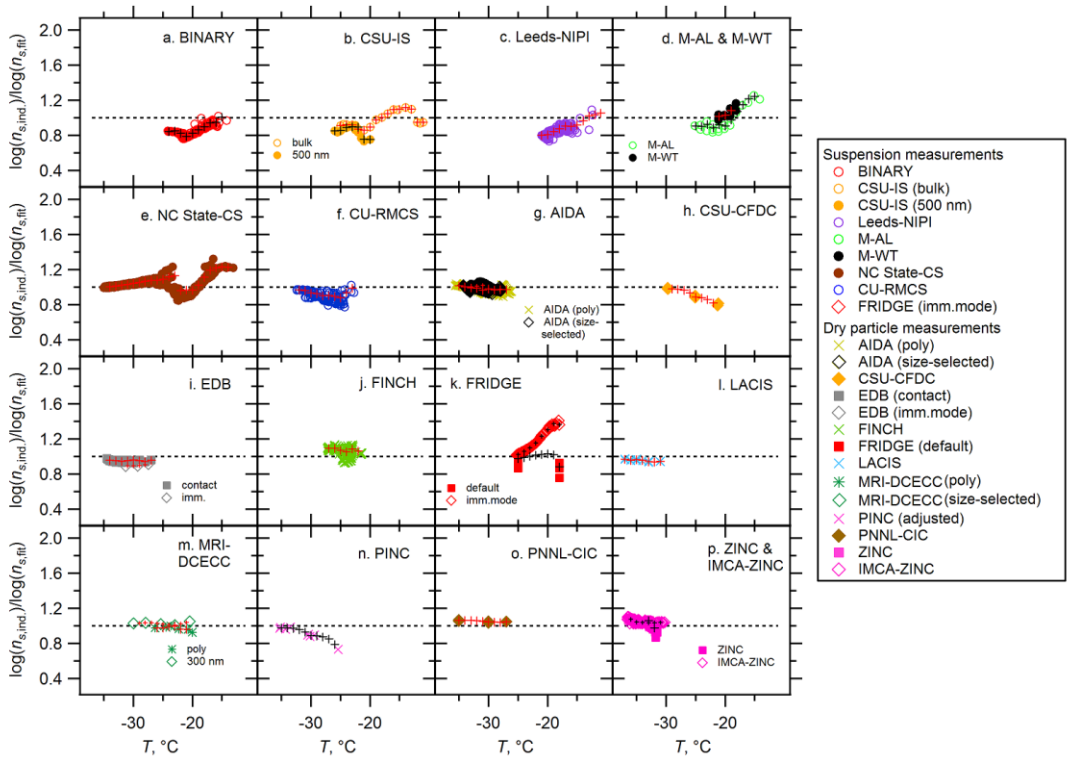

Figure S8. Ratios of the individual measurements to the log fit to suspension measurements [Sus (log)] or dry-dispersed particle measurements [Dry (log)], $\log(n_{s,ind.})/\log(n_{s,fit})$, based on the geometric surface area ($n_{s,ind.} = n_{s,geo}$). Black or red cross markers represent *T*-binned ratios of the interpolated individual measurements to Sus (log) or Dry (log) in comparison to the non-*T*-binned ratios. The black dotted line represents $\log(n_{s,ind.})/\log(n_{s,fit}) = 1$.

S3. Supplementary Table

A combination of four different methods for particle dispersion (rotating brush, flask dispersion, fluidized bed, or disc-dispersion method) and four types of DMA [commercially available one from TSI (Model 3081), Type Vienna Hauke medium (*Knutson and Whitby*, 1975) or custom built Maxi-DMA from TROPOS (*Raddatz et al*., 2013)] was employed for particle generation of illite NX samples. Further, most of the dry dispersion techniques used upstream impactors to filter out large agglomerated particles and safeguard against counting these large particles as INPs. The different types of dispersion methods, impactors and size segregating instruments used in the present work are listed below.

Table S1. Summary of methods used for dry particle generation.

Instrument	Dispersion method	Size selecting instrument	Impactor type
AIDA*	Rotating brush	TSI DMA 3081	Cyclone impactors (D_{50} 1 µm and 5 µm)
CSU-CFDC	Flask dispersion	TSI DMA 3081	Dual single-jet impactors (cutpoint of 1.5 and 2.4 µm)
EDB*	Fluidized bed	TSI DMA 3081	Multistage impactor (cutpoint of 2 µm)
FINCH*	Fluidized bed	DMA, type Vienna Hauke medium	MOUDI and cyclone impactors
FRIDGE (default)*	Rotating brush	TSI DMA 3081	Cyclone impactors (D_{50} 1 µm and 5 µm)
LACIS*	Fluidized bed	DMA, type Vienna Hauke medium	MOUDI and cyclone impactors
MRI-DCECC	Rotating brush	TSI DMA 3081	Cyclone impactors (D_{50} of 2.5 µm and 1.0 µm)
PINC	Rotating brush	TROPOS Maxi-DMA	Impactor (D_{50} at 0.91 µm)
PNNL-CIC	Rotating disc dispersion	TSI DMA 3081	Cyclone impactor (D_{50} ~1 µm)
IMCA-ZINC	Fluidized bed	TSI DMA 3081	Cyclone impactors (D_{50} 3 µm and 1 µm)

*Instruments of INUIT project partners.

S4. List of Abbreviations, Acronyms and Symbols (Alphabetical Order)

AIDA:	Aerosol Interaction and Dynamics in the Atmosphere
All (lin):	multiple exponential fit to *T*-binned ensemble n_s dataset fitted in the linear space
All (log):	multiple exponential fit to *T*-binned ensemble n_s dataset fitted in the log space
All_{max}:	multiple exponential fit to *T*-binned ensemble maximum n_s values
All_{min}:	multiple exponential fit to *T*-binned ensemble minimum n_s values
APS:	aerodynamic particle sizer
ATD:	Arizona Test Dust
A13:	Atkinson's parameterization
BET:	Brunauer, Emmett, and Teller
BINARY:	Bielefeld Ice Nucleation ARraY
B12:	Broadley's parameterization
CEC:	Cation Exchange Capacity
CECC:	controlled expansion cloud-simulation chamber
CFDC:	continuous flow diffusion chamber
$c_{impurities}(T)$:	concentration of impurities per unit volume water at temperature *T*
$c_{IN}(T)$:	concentration of INP per unit volume water at temperature *T*
CNT:	classical nucleation theory
CPC:	condensation particle counter
CSU-IS:	Colorado State University Ice Spectrometer
CSU-CFDC:	Colorado State University Continuous Flow Diffusion Chamber
CU-RMCS:	University of Colorado Raman microscope cold stage
DCECC:	Dynamic Controlled Expansion Cloud-simulation Chamber
DFG:	Deutsche Forschungsgemeinschaft (German Research Society)
$\Delta\log(n_s)/\Delta T$:	slope of $n_s(T)$ spectrum
DLS:	dynamic light scattering
DMA:	differential mobility analyzer
DSF:	dynamic shape factor
D:	average median diameter
Dry (lin):	multiple exponential fit to *T*-binned dry-dispersed particle n_s subset fitted in the linear space
Dry (log):	multiple exponential fit to *T*-binned dry-dispersed particle n_s subset fitted in the log space
D_{thresh}:	droplet-ice threshold diameter
D_{ve}:	volume equivalent midpoint diameter of individual particle
D_{50}:	cut size with a 50% mass of particles
D_{95}:	cut size with a 95% mass of particles
e_c:	probability of freezing on a single contact
EDB:	ElectroDynamic Balance
EDX:	energy dispersive X-ray
FINCH:	Fast Ice Nucleus CHamber
FRIDGE:	FRankfurt Ice Deposition freezinG Experiment
f:	proportion of droplets not frozen
f_{ice}:	frozen fraction after time *t*
f^*_{ice}:	fraction of droplets frozen
$f_{unfrozen}$:	fraction of unfrozen drops at each particular temperature

$Hor_{Max-Min}$: horizontal T deviation between maxima and minima in $n_s(T)$ spectrum
IC: ion chromatography
ICIS-2007: international ice nucleation workshop in 2007
illite NX: commercially available NX Nanopowder illite-rich dust from Arginotec
IMCA-ZINC: Zurich Ice Nucleation Chamber with Immersion Mode Cooling-chAmber
IN ice nucleation
INP: ice-nucleating particle
INUIT: Ice Nuclei research UnIT
IODE: Ice Optical DEpolarization detector
K-feldspar: potassium-rich feldspar
$K'(T)$: cumulative INP concentration at a temperature T
LACIS: Leipzig Aerosol Cloud Interaction Simulator
Leeds-NIPI: Leeds Nucleation by Immersed Particles Instrument
$\log(n_{s,ind.})/\log(n_{s,fit})$:
ratios of the individual measurements to the fit of the data
M-AL: Mainz Acoustic Levitator
M-WT: Mainz vertical Wind Tunnel
min: minute
MRI-DCECC: Meteorological Research Institute DCECC
M_{total}: total mass concentration of particles
M_{ve}: volume equivalent mass of individual particle
n_c: collision rate
NC State-CS: North Carolina State cold stage
N_{ae}: number concentration of aerosols
$N_{droplet}$: number concentration of droplets
N_{ice}: number concentration of ice crystals
$n_{m,geo}$: geometric mass-based ice-nucleating mass
$n_{m,sus}$: ice-nucleating mass derived from suspension measurements
n_s: IN active surface-site density
$n_{s,average}$: average n_s
$n_{s,BET}$: BET surface-inferred n_s
$n_{s,ind.}$: individual n_s measurements
$n_{s,fit}$: fit of all the $n_{s,ind.}$ data across the measured temperature range
$n_{s,geo:}$ geometric size based n_s
$n_{s,max}$: maximum n_s
$n_{s,min}$: minimum n_s
$N(T)$: number of frozen droplets at temperature T
N_{total}: total number concentration of particles
N_0: total number of droplets
N12: Niemand's parameterization
OPC: optical particle counter
OPS: optical particle sizer
PCR: polymerase chain reaction
PDF: probability density function
PDMS: polydimethylsiloxane
PINC: Portable Ice Nucleation Chamber
PNNL-CIC: Pacific Northwest National Laboratory Compact Ice Chamber
r: correlation coefficient
RH_{ice}: relative humidity with respect to ice
RH_w: relative humidity with respect to water
$RH_{w,ds}$: RH_w at which droplets survive past the evaporation section

s: second
SBM: soccer ball model
SIMONE: German acronym of *Streulicht-intensitätsmessungen zum optischen Nachweis von Eispartikeln*, which translates to the scattering intensity measurement for the optical detection of ice
S_{IN}: surface area of a single ice-nucleating particle
SMPS: scanning mobility particle sizer
SSA: specific surface area
SSPD: small-scale powder disc-disperser
S_{total}: total surface area concentration of particles
Sus (lin): multiple exponential fit to *T*-binned suspension n_s subset fitted in the linear space
Sus (log): multiple exponential fit to *T*-binned suspension n_s subset fitted in the log space
S_{ve}: volume equivalent surface area of individual particle
t: time
T: temperature
T-binned Lin. Avg.: multiple exponential distribution fit to the *T*-binned average data in the linear space
T-binned Log. Avg: multiple exponential distribution fit to the *T*-binned average data in the log space
T-binned Max.: fit to the *T*-binned maxima in the linear space
T-binned Min.: fit to the *T*-binned minima in the linear space
TDL: tunable diode laser
$T_{drop}(t)$: drop surface temperature
$T_{droplet,onset}$: droplet onset temperature
TROPOS: Leibniz Institute for Tropospheric Research
UHSAS: Ultra-High Sensitivity Aerosol Spectrometer
V: droplet volume
V_{drop}: median drop volume of the population
$Ver_{Max-Min}$: vertical n_s deviation between maxima and minima in $n_s(T)$ spectrum
w: mass ratio of dust and water (g dust/g water)
wt%: weight percent
x: volume of water used to wash the particles from the filter
XRD: X-ray diffraction
y: volume of air sampled through the filter
α: ice activated fraction (= N_{ice}/N_{total})
θ: specific surface area measured by BET technique
θ_{N2}: specific surface area measured by BET technique with nitrogen gas
θ_{H2O}: specific surface area measured by BET technique with water vapor
ρ: particle density of illite NX
ρ_w: density of water (0.9971 g H_2O/m^3 H_2O)
χ: dynamic shape factor

Additional information

Additional supplementary information is available in the online version of the paper. A publically accessible data base is available at http://imk-aaf-s1.imk-aaf.kit.edu/inuit/. Correspondence and requests (including readme files and access information to the database) for materials should be addressed to N. Hiranuma (seong.moon@kit.edu).

References

Agresti, A. and Coull, B. A.: Approximate is better than "exact" for interval estimation of binomial proportions. Am. Stat., 52, 119–126, doi:10.2307/2685469, 1998.

Ardon-Dryer, K. and Levin, Z.: Ground-based measurements of immersion freezing in the eastern Mediterranean, Atmos. Chem. Phys., 14, 5217–5231, doi:10.5194/acp-14-5217-2014, 2014.

Atkinson, J. D., Murray, B. J., Woodhouse, M. T., Carslaw, K., Whale, T. F., Baustian, K., Dobbie, S., O'Sullivan, D., and Malkin, T. L.: Nature, 498, 355–358, doi:10.1038/nature12278, 2013.

Baustian, K. J., Wise, M. E., and Tolbert, M. A.: Depositional ice nucleation on solid ammonium sulfate and glutaric acid particles, Atmos. Chem. Phys., 10, 2307–2317, doi:10.5194/acp-10-2307-2010, 2010.

Benz, S., Megahed, K., Möhler, O., Saathoff, H., Wagner, R., and Schurath, U.: T-dependent rate measurements of homogeneous ice nucleation in cloud droplets using a large atmospheric simulation chamber, J. Photoch. Photobio. A, 176, 208–217, doi:10.1016/j.jphotochem.2005.08.026, 2005.

Broadley, S. L., Murray, B. J., Herbert, R. J., Atkinson, J. D., Dobbie, S., Malkin, T. L., Condliffe, E., and Neve, L.: Immersion mode heterogeneous ice nucleation by an illite rich powder representative of atmospheric mineral dust, Atmos. Chem. Phys., 12, 287–307, doi:10.5194/acp-12-287-2012, 2012.

Budke, C. and Koop, T.: BINARY: an optical freezing array for assessing temperature and time dependence of heterogeneous ice nucleation, Atmos. Meas. Tech. Discuss., 7, 9137–9172, doi:10.5194/amtd-7-9137-2014, 2014.

Bundke, U., Nillius, B., Jaenicke, R., Wetter, T., Klein, H., and Bingemer, H.: The fast ice nucleus chamber FINCH, Atmos. Res., 90, 180–186, doi:10.1016/j.atmosres.2008.02.008, 2008.

Bundke, U., Reimann, B., Nillius, B., Jaenicke, R., and Bingemer, H.: Development of a Bioaerosol single particle detector (BIO IN) for the Fast Ice Nucleus CHamber FINCH, Atmos. Meas. Tech., 3, 263–271, doi:10.5194/amt-3-263-2010, 2010.

Chou, C., Stetzer, O.,Weingartner, E., Jurányi, Z., Kanji, Z. A., and Lohmann, U.: Ice nuclei properties within a Saharan dust event at the Jungfraujoch in the Swiss Alps, Atmos. Chem. Phys., 11, 4725–4738, doi:10.5194/acp-11-4725-2011, 2011.

Clauss, T., Kiselev, A., Hartmann, S., Augustin, S., Pfeifer, S., Niedermeier, D., Wex, H., and Stratmann, F.: Application of linear polarized light for the discrimination of frozen and liquid droplets in ice nucleation experiments, Atmos. Meas. Tech., 6, 1041–1052, doi:10.5194/amt-6-1041-2013, 2013.

DeMott, P. J. and Coauthors: Resurgence in ice nuclei measurement research, B. Am. Meteorol. Soc., 92, 1623–1635, doi:http://dx.doi.org/10.1175/2011BAMS3119.1, 2011.

DeMott, P. J., Prenni, A. J., McMeeking, G. R., Sullivan, R. C., Petters, M. D., Tobo, Y., Niemand, M., Möhler, O., Snider, J. R., Wang, Z., and Kreidenweis, S. M.: Integrating laboratory and field data to quantify the immersion freezing ice nucleation activity of mineral dust particles, Atmos. Chem. Phys. Discuss., 14, 17359–17400, doi:10.5194/acpd-14-17359-2014, 2014.

Diehl, K., Mitra, S. K., Szakáll, M., Blohn, N. v., Borrmann, S., and Pruppacher, H.R.: Chapter 2. Wind Tunnels: Aerodynamics, Models, and Experiments. In: The Mainz Vertical Wind Tunnel Facility: A Review of 25 Years of Laboratory Experiments on Cloud Physics and Chemistry [Pereira, J. D. (eds.)], Nova Science Publishers, Inc., Hauppauge, NY, USA, 2011.

Diehl, K., Debertshäuser, M., Eppers, O., Schmithüsen, H., Mitra, S.K., and Borrmann, S.: Particle-area dependence of mineral dust in the immersion mode: investigations with freely suspended drops in an acoustic levitator. Atmos. Chem. Phys., 14, 12343–12355, doi:10.5194/acp-14-12343-2014, 2014.

Eidhammer, T., DeMott, P. J., Prenni, A. J., Petters, M. D., Twohy, C. H., Rogers, D. C., Stith, J., Heymsfield, A., Wang, Z., Haimov, S., French, J., Pratt, K., Prather, K., Murphy, S., Seinfeld, J., Subramanian, R., and Kreidenweis, S. M.: Ice initiation by aerosol particles: Measured and predicted ice nuclei concentrations versus measured ice crystal concentrations in an orographic wave cloud. J. Atmos. Sci., 67, 2417–2436. doi: 10.1175/2010JAS3266.1, 2010.

Fahey, D. W., Gao, R.-S., Möhler, O., Saathoff, H., Schiller, C., Ebert, V., Krämer, M., Peter, T., Amarouche, N., Avallone, L. M., Bauer, R., Bozóki, Z., Christensen, L. E., Davis, S. M., Durry, G., Dyroff, C., Herman, R. L., Hunsmann, S., Khaykin, S. M., Mackrodt, P., Meyer, J., Smith, J. B., Spelten, N., Troy, R. F., Vömel, H., Wagner, S., and Wienhold, F. G.: The AquaVIT-1 intercomparison of atmospheric water vapor measurement techniques, Atmos. Meas. Tech. Discuss., 7, 3159–3251, doi:10.5194/amtd-7-3159-2014, 2014.

Friedman, B., Kulkarni, G., Beránek, J., Zelenyuk, A., Thornton, J. A., and Cziczo, D. J.: Ice nucleation and droplet formation by bare and coated soot particles, J. Geophys. Res., 116, D17203, doi:10.1029/2011JD015999, 2011.

Hader, J. D., Wright, T. P., and Petters, M. D.: Contribution of pollen to atmospheric ice nuclei concentrations, Atmos. Chem. Phys., 14, 5433–5449, doi:10.5194/acp-14-5433-2014, 2014.

Hartmann, S., Niedermeier, D., Voigtländer, J., Clauss, T., Shaw, R. A., Wex, H., Kiselev, A., and Stratmann, F.: Homogeneous and heterogeneous ice nucleation at LACIS: operating principle and theoretical studies, Atmos. Chem. Phys., 11, 1753–1767, doi:10.5194/acp-11-1753-2011, 2011.

Herbert, R. J., Murray, B. J., Whale, T. F., Dobbie, S. J., and Atkinson, J. D.: Representing time-dependent freezing behaviour in immersion mode ice nucleation, Atmos. Chem. Phys., 14, 8501–8520, doi:10.5194/acp-14-8501-2014, 2014.

Hiranuma, N., Paukert, M., Steinke, I., Zhang, K., Kulkarni, G., Hoose, C., Schnaiter, M., Saathoff, H., and Möhler, O.: A comprehensive parameterization of heterogeneous ice nucleation of dust surrogate: laboratory study with hematite particles and its application to atmospheric models, Atmos. Chem. Phys., 14, 13145–13158, doi:10.5194/acp-14-13145-2014, 2014a.

Hiranuma, N., Hoffmann, N., Kiselev, A., Dreyer, A., Zhang, K., Kulkarni, G., Koop, T., and Möhler, O.: Influence of surface morphology on the immersion mode ice nucleation efficiency of hematite particles, Atmos. Chem. Phys., 14, 2315–2324, doi:10.5194/acp-14-2315-2014, 2014b.

Hoffmann, N., Duft, D., Kiselev, A., and Leisner, T.: Contact freezing efficiency of mineral dust aerosols studied in an electrodynamic balance: quantitative size and temperature dependence for illite particles, Faraday Discuss., 165, 383–390, doi:10.1039/C3FD00033H, 2013a.

Hoffmann, N., Kiselev, A., Rzesanke, D., Duft, D., and Leisner, T.: Experimental quantification of contact freezing in an electrodynamic balance, Atmos. Meas. Tech., 6, 2373–2382, doi:10.5194/amt-6-2373-2013, 2013b.

Hu, Y.-X., Yang, P., Lin, B., Gibson, G., Hostetler, C.: Discriminating between spherical and non-spherical scatterers with lidar using circular polarization: a theoretical study. J. Quant. Spectrosc. Radiat. Transfer, 79–80, 757–764, doi:10.1016/S0022-4073(02)00320-5, 2003.

Kanji, Z. A., Welti, A., Chou, C., Stetzer, O., and Lohmann, U.: Laboratory studies of immersion and deposition mode ice nucleation of ozone aged mineral dust particles, Atmos. Chem. Phys., 13, 9097–9118, doi:10.5194/acp-13-9097-2013, 2013.

Klein, H., Haunold, W., Bundke, U., Nillius, B., Wetter, T., Schallenberg, S., and Bingemer, H.: A new method for sampling of atmospheric ice nuclei with subsequent analysis in a static diffusion chamber, Atmos. Res., 96, 218–224, doi:10.1016/j.atmosres.2009.08.002, 2010.

Knutson, E. O., and Whitby, K. T.: Aerosol classification by electric mobility: apparatus, theory, and applications. Aerosol Sci., 6, 6, 443–451, doi:10.1016/0021-8502(75)90060-9, 1975.

Kulkarni, G., Fan, J., Comstock, J. M., Liu, X., and Ovchinnikov, M.: Laboratory measurements and model sensitivity studies of dust deposition ice nucleation, Atmos. Chem. Phys., 12, 7295–7308, doi:10.5194/acp-12-7295-2012, 2012.

Langham, E. J. and Mason, B. J.: The heterogeneous and homogeneous nucleation of supercooled water. Proceedings of the Royal Society A: Mathematical, Physical and Engineering Sciences, 247, 1251, 493–504. doi:10.1098/rspa.1958.0207, 1958.

Lüönd, F., Stetzer, O., Welti, A., and Lohmann, U.: Experimental study on the ice nucleation ability of size-selected kaolinite particles in the immersion mode, J. Geophys. Res., 115, D14201, doi:10.1029/2009JD012959, 2010.

Möhler, O., Stetzer, O., Schaefers, S., Linke, C., Schnaiter, M., Tiede, R., Saathoff, H., Krämer, M., Mangold, A., Budz, P., Zink, P., Schreiner, J., Mauersberger, K., Haag, W., Kärcher, B., and Schurath, U.: Experimental investigation of homogeneous freezing of

sulphuric acid particles in the aerosol chamber AIDA, Atmos. Chem. Phys., 3, 211–223, doi:10.5194/acp-3-211-2003, 2003.

Möhler, O., Field, P. R., Connolly, P., Benz, S., Saathoff, H., Schnaiter, M., Wagner, R., Cotton, R., Krämer, M., Mangold, A., and Heymsfield, A. J.: Efficiency of the deposition mode ice nucleation on mineral dust particles, Atmos. Chem. Phys., 6, 3007–3021, doi:10.5194/acp-6-3007-2006, 2006.

Murphy, D. M., and Koop, T.: Review of the vapour pressures of ice and supercooled water for atmospheric applications, Q. J. R. Meteorol. Soc., 131, 1539–1565, doi:10.1256/qj.04.94, 2005.

Murray, B. J., Broadley, S. L., Wilson, T. W., Atkinson, J. D., and Wills, R. H.: Heterogeneous freezing of water droplets containing kaolinite particles, Atmos. Chem. Phys., 11, 4191–4207, doi:10.5194/acp-11-4191-2011, 2011.

Murray, B. J., O'Sullivan, D., Atkinson, J. D., and Webb, M. E.: Ice nucleation by particles immersed in supercooled cloud droplets, Chem. Soc. Rev., 41, 6519–6554, doi:10.1039/c2cs35200a, 2012.

Nicolet, M., Stetzer, O., Lüönd, F., Möhler, O., and Lohmann, U.: Single ice crystal measurements during nucleation experiments with the depolarization detector IODE, Atmos. Chem. Phys., 10, 313–325, doi:10.5194/acp-10-313-2010, 2010.

O'Sullivan, D., Murray, B. J., Malkin, T. L., Whale, T. F., Umo, N. S., Atkinson, J. D., Price, H. C., Baustian, K. J., Browse, J., and Webb, M. E.: Ice nucleation by fertile soil dusts: relative importance of mineral and biogenic components, Atmos. Chem. Phys., 14, 1853–1867, doi:10.5194/acp-14-1853-2014, 2014.

Petters, M. D., Parsons, M. T., Prenni, A. J., DeMott, P. J., Kreidenweis, S. M., Carrico, C. M., Sullivan, A. P., McMeeking, G. R., Levin, E., Wold, C. E., Collett, J. L. Jr., and Moosmüller, H.: Ice nuclei emissions from biomass burning, J. Geophys. Res., 114, D07209, doi:10.1029/2008JD011532, 2009.

Prenni, A. J., DeMott, P. J., Rogers, D. C., Kreidenweis, S. M., McFarquhar, G. M., Zhang, G., and Poellot, M. R.: Ice nuclei characteristics from M-PACE and their relation to ice formation in clouds, Tellus, 61B, 436–448, doi:10.1111/j.1600-0889.2009.00415.x, 2009.

Raddatz, M., Wiedensohler, A., Wex, H., and Stratmann, F.: Size selection of sub- and super-micron clay mineral kaolinite particles using a custom-built Maxi-DMA, AIP Conference Proceedings, 1527, 457–460, 2013.

Richardson, M.: Making real time measurements of ice nuclei concentrations at upper tropospheric temperatures: Extending the capabilities of the continuous flow diffusion chamber, DISSERTATION thesis, Colorado State Univ., Fort Collins, CO, USA, 268 pp, 2009.

Rzesanke, D., Nadolny, J., Duft, D., Muller, R., Kiselev, A., and Leisner, T.: On the role of surface charges for homogeneous freezing of supercooled water microdroplets, Phys. Chem. Chem. Phys., 14, 9359–9363, doi:10.1039/c2cp23653b, 2012.

Rogers, D. C.: Development of a continuous flow thermal gradient diffusion chamber for ice nucleation studies, Atmos. Res., 22, 149–181, doi:10.1016/0169-8095(88)90005-1, 1988.

Rogers, D. C., DeMott, P. J., Kreidenweis, S. M., and Chen, Y.: A continuous-flow diffusion chamber for airborne measurements of ice nuclei, J. Atmos. Oceanic Technol., 18, 725–741, doi:http://dx.doi.org/10.1175/1520-0426(2001)018<0725:ACFDCF>2.0.CO;2, 2001.

Schill, G. P. and Tolbert, M. A.: Heterogeneous ice nucleation on phase-separated organic-sulfate particles: effect of liquid vs. glassy coatings, Atmos. Chem. Phys., 13, 4681–4695, doi:10.5194/acp-13-4681-2013, 2013.

Schnaiter, M., Büttner, S., Möhler, O., Skrotzki, J., Vragel, M., and Wagner, R.: Influence of particle size and shape on the backscattering linear depolarisation ratio of small ice crystals – cloud chamber measurements in the context of contrail and cirrus microphysics, Atmos. Chem. Phys., 12, 10465–10484, doi:10.5194/acp-12-10465-2012, 2012.

Steinke, I., Möhler, O., Kiselev, A., Niemand, M., Saathoff, H., Schnaiter, M., Skrotzki, J., Hoose, C., and Leisner, T.: Ice nucleation properties of fine ash particles from the Eyjafjallajökull eruption in April 2010, Atmos. Chem. Phys., 11, 12945–12958, doi:10.5194/acp-11-12945-2011, 2011.

Stetzer, O., Baschek, B., Luond, F., and Lohmann, U.: The Zurich Ice Nucleation Chamber (ZINC) – A new instrument to investigate atmospheric ice formation, Aerosol Sci. Technol., 42, 64–74, doi:10.1080/02786820701787944, 2008.

Sullivan, R. C., Petters, M. D., DeMott, P. J., Kreidenweis, S. M., Wex, H., Niedermeier, D., Hartmann, S., Clauss, T., Stratmann, F., Reitz, P., Schneider, J., and Sierau, B.: Irreversible loss of ice nucleation active sites in mineral dust particles caused by sulphuric acid condensation, Atmos. Chem. Phys., 10, 11471–11487, doi:10.5194/acp-10-11471-2010, 2010a.

Sullivan, R. C., Miñambres, L., DeMott, P. J., Prenni, A. J., Carrico, C. M., Levin, E. J. T., and Kreidenweis, S. M.: Chemical processing does not always impair heterogeneous ice nucleation of mineral dust particles, Geophys. Res. Lett., 37, L24805, doi:10.1029/2010GL045540, 2010b.

Szakáll, M., Diehl, K., Mitra, S. K., and Borrmann, S.: A wind tunnel study on the shape, oscillation, and internal circulation of large raindrops with sizes between 2.5 and 7.5 mm, J. Atmos. Sci., 66, 755–765, doi:http://dx.doi.org/10.1175/2008JAS2777.1, 2009.

Tajiri, T., Yamashita, K., Murakami, M., Orikasa, N., Saito, A., Kusunoki, K., and Lilie, L.: A novel adiabatic-expansion-type cloud simulation chamber. J. Meteor. Soc. Japan, 91, 5, 687–704, doi:http://dx.doi.org/10.2151/jmsj.2013-509, 2013.

Tobo, Y., DeMott, P. J., Hill, T. C. J., Prenni, A. J., Swoboda-Colberg, N. G., Franc, G. D., and Kreidenweis, S. M.: Organic matter matters for ice nuclei of agricultural soil origin, Atmos. Chem. Phys. Discuss., 14, 9705–9728, doi:10.5194/acpd-14-9705-2014, 2014.

Vali, G.: Quantitative evaluation of experimental results an the heterogeneous freezing nucleation of supercooled liquids. J. Atmos. Sci., 28, 402–409. doi:http://dx.doi.org/10.1175/1520-0469(1971)028<0402:QEOERA>2.0.CO;2, 1971.

Welti, A., Lüönd, F., Stetzer, O., and Lohmann, U.: Influence of particle size on the ice nucleating ability of mineral dusts, Atmos. Chem. Phys., 9, 6705–6715, doi:10.5194/acp-9-6705-2009, 2009.

Wex, H., DeMott, P. J., Tobo, Y., Hartmann, S., Rösch, M., Clauss, T., Tomsche, L., Niedermeier, D., and Stratmann, F.: Kaolinite particles as ice nuclei: learning from the use of different kaolinite samples and different coatings, Atmos. Chem. Phys., 14, 5529–5546, doi:10.5194/acp-14-5529-2014, 2014.

Wright, T. P. and Petters, M. D.: The role of time in heterogeneous freezing nucleation, J. Geophys. Res. Atmos., 118, 3731–3743, doi:10.1002/jgrd.50365, 2013.